Universitetet i Stavanger

FACULTY OF SCIENCE AND TECHNOLOGY

MASTER'S THESIS

Study programme/specialisation: Erasmus 2017	Spring / Autumn semester, 20.17. X Open/Confidential
Author: Antonio Manuel Sutil Ortiz 242362	..... (signature of author)
Programme coordinator: Kjersti Engan Supervisor(s): Kristian Thorsen	
Title of master's thesis: SINGLE-PHASE INVERTER WITH ACTIVE RIPPLE ENERGY STORAGE.	
Credits: 30 ECTS	
Keywords: single-phase inverter, bidirectional converter, PWM, high power density, ripple energy.	Number of pages: 106 + supplemental material/other: ..... Stavanger, 14 / 12 / 2017 date/year

SINGLE-PHASE INVERTER WITH ACTIVE RIPPLE ENERGY STORAGE.

Master Thesis.
Automatization and Signal Processing Master Degree.

Masteroppgave Informasjonsteknologi.
Automatisering og Signalbehandling.

Universitetet i Stavanger

Author: Antonio Manuel Sutil Ortiz.
Supervisor: Kristian Thorsen.

Stavanger, Norway, December 2017.

Acknowledgment.

I would like to thank my supervisor Phd. Kristian Thorsen for the following and support throughout the project. His observations and comments helped me to establish the overall direction of the work. He has been a source of knowledge helping me greatly.

Special thank goes also to the Universitetet i Stavanger, Norway, for giving me the opportunity to develop this thesis in their university and in fact on other country than my own. They provided me the material required and allowed me to use their facilities.

Moreover, I want to thank the Universitat Politècnica de Valencia for letting me take part of an exchange program. I could gain the big knowledge of a new culture.

Last, but not least, I would like to acknowledge the love, support and motivation I received from my girlfriend, Cristina, as well as from my family.

Antonio M. Sutil.

Stavanger, Norway. December 2017.

Abstract.

It is well known that conventional energy sources such as coal, oil, and natural gas are decreasing and a growing problem of environmental pollution. The renewable energy sources are becoming the best alternative for a clean and inexhaustible energy source, and solar energy is one of the most popular energy sources. Solar energy has gained more and more attention because of its advantages such as abundance, pollution free, renewability and low maintenance.

The solar energy is usually obtained from photovoltaic (PV) cell which transform the solar irradiance into direct current (DC), that is electric energy. Since the majority of the electric devices and the main grid, require AC (alternate current) a power converter is needed to convert the DC electricity coming from the PV cell into AC electricity. The most used electronic converter for that is an inverter.

Inverters contains semiconductor switches that are often controlled using the pulse width modulation technique, which yields second-order harmonic currents and corresponding ripple voltages on the DC bus. This double line frequency on the DC bus affect the performance of the photovoltaic system. Bulky DC link electrolytic capacitors are typically employed as transient energy buffer to decouple, or smooth out, the pulsating ac power from constant dc power.

However, the use of electrolytic capacitor leads to temperature and aging concerns, and this also result in a low power density. A novel active power decoupling method proposed to add a bidirectional buck and boost converter that can store the ripple energy in its inductor and capacitor. This method can effectively reduce the energy storage in the DC link capacitor.

This thesis deals with the design of such as bidirectional DC-DC converter and an inverter. The theoretical work mode of the bidirectional converter together with an inverter is studied.

The power stages, inverter and bidirectional converter are studied in steady state to dimension the components. These stages are also modelled in their small signal equivalent model to find their transfer functions need to design the control loops.

Different control strategies are studied and implemented to achieve the independent controls of the inverter and DC-DC converter. By using LTspice, the simulation results have verified the proposed power decoupling method.

Key words: single-phase inverter, bidirectional converter, PWM, high power density, ripple energy.

Resumen.

Es bien conocido que las fuentes de energía convencionales como el carbón, petróleo y gas natural están disminuyendo y volviéndose un problema de contaminación ambiental. Las fuentes de energías renovables están llegando a ser la mejor alternativa para a una fuente de energía limpia e inagotable y la energía solar es una de la más popular fuente de energía. La energía solar ha ganado más y más atención por sus ventajas, tales como, abundancia, libre de polución, renovabilidad y poco mantenimiento.

La energía solar es normalmente obtenida de una célula fotovoltaica (FV) la cual transforma la irradiancia solar en corriente continua (CC), es decir, en energía eléctrica. Como la mayoría de los dispositivos electrónicos y la red requieren corriente alterna (CA) un convertidor de potencia es necesitado para convertir la electricidad continua proveniente de la célula fotovoltaica en electricidad alterna. El dispositivo más usado para esto es un inversor.

Los inversores contienen conmutadores semiconductores que son a menudo controlados usando la técnica de modulación por ancho de pulso la cual produce un armónico de segundo orden en la corriente que da a lugar un rizado en el voltaje del bus de continua. Esta frecuencia de dos veces la frecuencia de línea en el bus de continua afecta el rendimiento del sistema fotovoltaico. Grandes condensadores electrolíticos son típicamente usados como buffer de energía transitoria para desacoplar, o suavizar, la potencia alterna de la potencia continua.

Sin embargo, el uso de condensadores electrolíticos da lugar a problemas de temperatura y degeneración y estos además resultan en una baja densidad de potencia. Un método novedoso propone añadir un convertidor elevador reductor, bidireccional, que almacene la energía de rizado en sus inductor y capacitor. Este método puede reducir eficazmente la energía almacenada en el condensador usado en el DC link.

Esta tesis trata sobre el diseño de un convertidor CC-CC bidireccional y un inversor. El modo de operación teórico del convertidor bidireccional junto con un inversor es estudiado.

Las etapas de potencia, inversor y convertidor bidireccional son estudiadas en estado estacionario para dimensionar los componentes. Estas etapas son también modeladas en su modelo equivalente en pequeña señal para encontrar sus funciones de transferencia necesarias para el diseño de los lazos de control.

Diferentes estrategias de control son estudiadas e implementadas para conseguir el control del inversor y del convertidor de continua. Usando LTspice, los resultados de las simulaciones han verificado el método propuesto de desacoplo de potencia.

Palabras clave: Inversor monofásico, convertidor bidireccional, PWM, alta densidad de potencia, energía de rizado.

Contents.

List of Figures.

List of Tables.

Chapter 1.

Introduction.

Chapter 1. Introduction.

1.1. Introduction.

Chapter 1 gives a general background and the purpose of this thesis. Section 1.2 gives brief idea about the purpose of this work and motivation. The state of the literature is reviewed in section 1.3. The work herein is considered a standalone PV system, a grid-connected PV system, PV modelling, DC-DC converters, active filters and decoupling circuits. These different parts are further introduced and discussed in section 1.4. Section 1.5 describes the objectives and the contribution to the research work. Finally, the chapter concludes with the organization of this thesis in Section 1.6.

1.2. Background and Motivation.

In recent years, with the rapid penetration of distributed renewable energy sources (such as solar photovoltaic and wind power) into the traditional power system, it is imagined that a mixture of AC and emerging DC power systems will make out the future form of our power network and power supplies. In addition, the development of DC power stages increases the need for efficient converters that can transform power from DC to AC and from AC to DC. Some well-known power electronic engineers like professor Robert Erickson estimates that by 2030, 80% of all electrical energy will be processed by power electronics.

On the whole, the use of renewable energy is a challenge to reduce the CO_2 emission and offer sustainable clean and affordable energy. Energy saving is one of the best cost-effective solution. But the worldwide energy demand is increasing, and energy saving alone does not tackle the problem. For that issue, renewable energy is a good option because it gives a green and clean energy, free of CO_2 emission.

Renewable energy is defined as energy that comes from resources which are naturally generated like sunlight, wind, rain, tides, waves and geothermal heat. In recent years, the development of renewable energy sources has become a global priority which have given rise to intensive research on renewable energy technologies such as PV, hydroelectric, wind, geothermal, and tidal systems.

Production of PV modules is growing by approximately 25% per year [1], and the implementation of PV systems on buildings and interconnection to utility networks are rapidly increasing and become major programs of developed countries like Japan, U.S.A and Europe. PV systems have been used for over 50 years in various specialized applications and grid-connected PV systems have been in use for over 20 years. At the end of 2016, worldwide installed PV capacity increased to more than 300 gigawatts (GW) [1]. The global PV market grew significantly, to at least 74,4 GW in 2016. With non-reporting countries, this number could grow up to 75,4 GW, compared to 50 GW in 2015. This represents a 50% growth year-on-year. Worldwide, maximum PV systems are utility connected where large amount of PV capacity is involved. But for remote areas, which are isolated from utility grid, standalone operation is the best option. An evolution of the PV installations can be seen in figure 1.1 from the International Energy Agency [1].

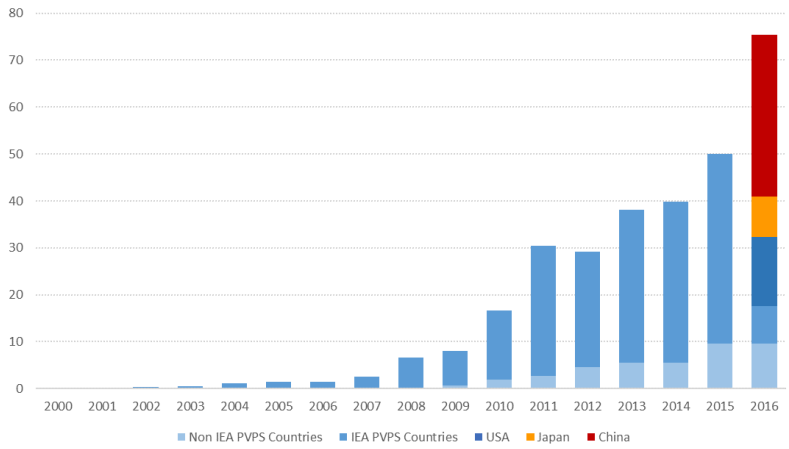

Figure 1. 1. Evolution of annual PV installations in GW.

1.3. Literature Review.

The solar energy is converter into electrical energy by the solar cells. The PV systems are like any other electrical power generating system, but the equipment used for PV system is different than that used for conventional electro-mechanical generating systems.

Although other topologies are also used which consist of only one stage like the transformerless PV inverters, two stage systems are most used in a two stage PV system where a DC-DC converter is connected between the PV modules and the DC-AC inverter [2]. In that way the output voltage of the PV system and the input voltage of the inverter need not be the same.

The DC-DC converter perform the maximum power point tracking (MPPT) algorithm for a PV string and it is connected in the middle, between the PV modules and the DC-AC inverter [3].

DC-AC inverter is then a voltage sourced inverter which handles the output current regulation and DC bus voltage regulation when is connected to the grid or also AC voltage and output current regulation when it works in standalone mode [4], [5].

The inverter must control the output current in each mode of operation. There are three major output current control techniques for the single phase VSI: hysteresis band, predictive, and sinusoidal pulse width modulation (SPWM) control [6] [7].

The inverter is in this work controlled by SPWM because the hysteresis controllers normally have an error band within a fixed range [7]. On another hand the predictive control needs complicated calculations and requires a very accurate knowledge of the system parameters although it offers a potential to achieve precise current control with minimum distortions [8].

The SPWM control is the most extended technique for SMPS (switch mode power supply) and is easy to implement [9]. This method of SPWM control uses a proportional-integral (PI) compensator in the feedback loop to regulate the output current. Though, while PI compensators have excellent performances on regulating DC quantities, many researchers have also explored the use of proportional-resonant (PR) [10].

However, in this thesis we use PI and PID compensators and implements the current controller using SPWM control theory. The current control is usually developed with an

outer loop which control the AC voltage [4], [10] or the DC voltage [11]. Both of them are developed in this thesis.

The selection of the DC link capacitor is a big challenge when one design an inverter, even a rectifier. The capacitor must support a twice line frequency energy ripple.

Because of the DC-link contains power pulsation large electrolytic capacitors are connected to the DC-link in order to absorb this power pulsation and decrease the DC link voltage ripple.

Although most PV module manufactures offer 25 warranty years on 80% of the initial efficiency and five years warranty on materials and workmanship [3], electrolytic capacitors with large capacitance can not be used in PV applications because of their short lifetime [12].

Furthermore, the DC link capacitor cause usually a large converter volume and low power density. For space application, for example, where the solar energy is the only energy available to use, the global volume of the energy supply system will dramatically increase. The usual choice for this function is the aluminium electrolytic (AE) capacitor, which offers low cost and a high energy density, partially offsetting the overall increase in the power converter volume. However, this type of capacitors is also known for having a somewhat short lifetime, which is unacceptable in many applications [13].

There are several techniques to reduce the size of the DC-link capacitor by adding an auxiliary circuit. There are different configurations for this circuit in the literature [14], [15] some of them are shown in figure 1.2.

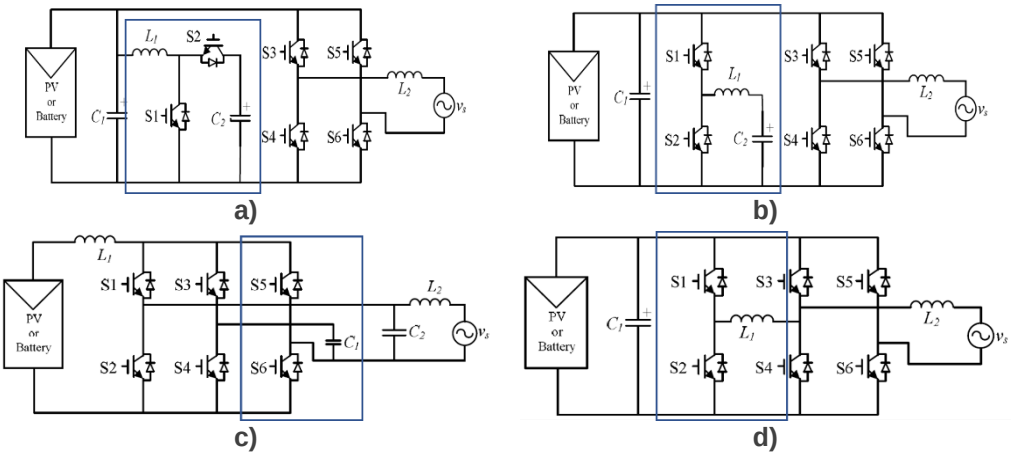

Figure 1. 2. Auxiliary circuits to reduce the voltage ripple in DC link capacitor [39].

The topology shows in figure 1.2. c) and d) store the energy ripple in an only electronic components, capacitor and inductor respectively. Whereas the circuit shown in figure a) and b) work as a bidirectional buck and boost. The topology used in this project is the one shown in figure 1.2 b) where a bidirectional DC-DC converter decuple the DC link voltage ripple. This circuit allow improve the inverter in the future by using only the two additional switches and converting the single-phase inverter in a three-phase inverter [16].

To control the bidirectional converter some techniques are used in the literature like direct control of the instantaneous power in the energy storage device in a closed-loop, such that it matches the ripple power generated by the AC/DC converter [17]. Other

strategies consist in a direct regulation of the instantaneous DC-link voltage in a closed-loop [18]. Full review of different control strategies can be seen in [14].

More control ways are found to deal with the bidirectional DC-DC converter, where this is study as two independent converters a buck and a boost converter [19].

In this research the circuit is study as bidirectional converter follow the references [20] and [21]. Two different control loops are designed, one which keep a stable DC link voltage and another one which control the inductor current.

1.4. PV System of the thesis and its parts.

In both operation modes of the PV system, standalone mode or grid connected mode, an inverter is used. This power stage converts the DC energy coming from the PV cell or panel into AC current to feed the load in standalone mode or to inject the energy in the grid. So, it does not matter the application in the AC side since an inverter is the most used electronic converter because of the majority of the load are AC load. The simple circuit configuration of a full bridge single phase inverter is shown in figure 1.3. Where V_{AB} is a AC voltage but its waveform is not sinusoidal. Typically pulse width modulation is used to control the switches which are usually IGBT o MOSFET if the inverter power is less than 1KV.

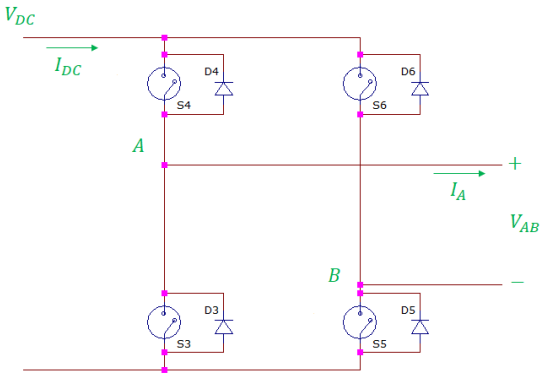

Figure 1. 3. Single-Phase inverter.

In addition, due to the output voltage is not sinusoidal because it is switched, a low pass filter is used, most of the time a LC or LCL filter is the best options used by the electronical engineer [2], [3], [10] and [22]. In this thesis a LCL filter is designed to alleviate the output harmonic. A LCL filter with a damping resistor is shown in figure 1.4.

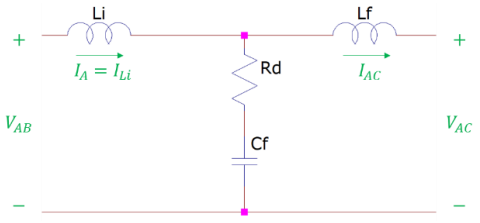

Figure 1. 4. LCL inverter filter.

Unlike large scale rural solar farms, residential PV modules require the inverters to be small, low-power and single-phase units. One of the challenges when designing single phase VSIs (Voltage Source Inverter) for PV application is the selection of the DC-link capacitor. Although a analytical justification is developed in chapter 2 the instantaneous output power of a single-phase inverter is graphically shown in figure 1.5.

AC output power of an inverter is product of the current and voltage is sinusoidal waveform which is not the same as the DC input power. Because of that a power with double fundamental frequency is caused in the DC capacitor. The waveform of the power and output current and voltage are figure 1.5. Note that the amplitude is not relevant in this moment.

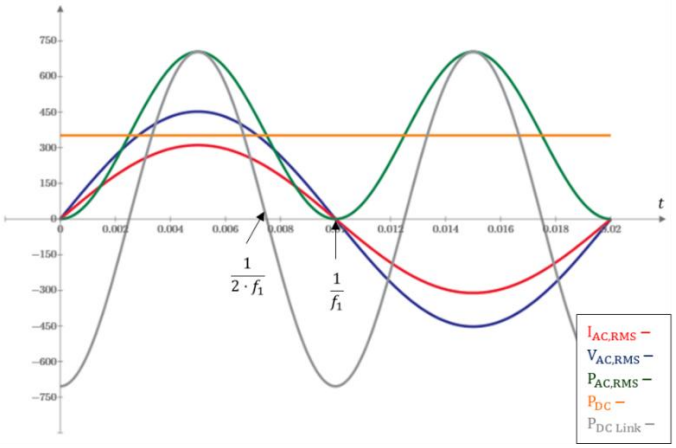

Figure 1. 5. Power balance in an inverter.

This power contains a constant and a double-line frequency component. Therefore, the DC-link contains power pulsation with twice the grid frequency. Often, large electrolytic capacitors are connected to the DC-link to absorb this power pulsation so that the DC-link voltage ripple can be kept small. However, electrolytic capacitors with large capacitance (1.6mF for 15KW) are not ideal to use in PV applications because of their big dimension and price (167.5cm^3 and 20€ for an electrolytic capacitor of 1.6mF).

Many techniques were proposed to reduce the size of the DC-link capacitor while maintaining a good inverter power quality so that a more reliable film type capacitor can be used [14], [15]. In this thesis a bidirectional DC-DC converter is used to reduce the DC link voltage ripple, this converter work as a buck or boost depending of the energy flux. The converted is shown in figure 1.6.

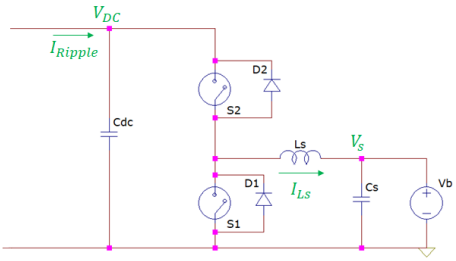

Figure 1. 6. Bidirectional DC-DC converter.

This method uses an auxiliary circuit to circulate the double-line frequency ripple power. Figure 1.6 is an example where the bidirectional DC/DC converter is used as a decoupling circuit. The decoupling capacitor, C_S is allowed to contain a large ripple component. In addition to the fact that an auxiliary circuit would increase the energy loss and the complexity of the system.

This challenging technique to reduce the DC-link voltage ripple is the primary motivation of the work in this thesis. The thesis will therefore focus on designing a single-phase inverter in standalone mode and in grid connected mode plus a bidirectional DC-DC converter which is used to reduce the voltage ripple in the DC-link.

The foci of this work are on the control of the inverter and the bidirectional DC-DC converter. This challenge involves the reduction of the size of the DC-link capacitor in order to use a long-life film capacitor.

1.5. Objectives and Contribution of the Thesis.

A high power-density inverter leads to the following thesis's objectives:

- Ensure that the voltage on the DC side and the voltage in the AC side of the VSI and the output current are well regulated by choosing appropriate inverter topology, the output filter configuration and proper control methods.
- To supply power to local load at a regulated voltage by suppressing the transient that may occur in PV system due to source or load variation.
- To store electrical energy in an auxiliary circuit when the dc link voltage ripple is over the average value and to delivery this when is under the average value.
- To design a filter to the output voltage and current which can deliver a quality current and voltage waveform.

The primary objective of this work is to model, control and analyse a photovoltaic inverter plus a bidirectional DC-DC. Some of the noticeable points of this thesis are:

- Description of a PV system and its components.
- Steady state analysis of both power stages, the inverter and the DC-DC converter
- Modelling of an inverter and a DC-DC buck and boost converter.
- Modelling a PV string working its MPP.
- Implementation of average current control strategy for single phase voltage source inverter.
- Implementation of input voltage and inductor current control strategy for a bidirectional converter.
- Stability analysis of the system by using different method to tune a regulator.

1.6. Thesis Organization.

This project is organized in the following chapters:

Chapter 2. Provides a brief description about the PV system, its power stages, the performance of this and the PV modelling.

Chapter 3. Based on a steady state analysis the components like inductors, capacitors and resistors are chosen here.

Chapter 4. Deals with the small signal modelling and implementation of all the control strategies and their stability analysis.

Chapter 5. Contains all the simulation results and its discussion under several parameter variations.

Chapter 6. The conclusion about the system and the future research scope are written here.

Chapter 2.

Power Stage Topology and Operation Principle.

Chapter 2. Power Stage Topologies and Operation Principles.

2.1. Introduction.

Before looking into the aboard specific value of the components and the control of the photovoltaic (PV) system, it is necessary to study the performance of the system in steady state. That means to analyse the circuit with fixed input, i.e. constant input voltage, disturbances and duty cycle of internal switches. Since the system consist of four subsystem each section corresponds to a different power stage.

The following section 2.2 gives brief introduction to the photovoltaic systems and the involved power stages. Section 2.3 define the PV source, the configuration as panel or array, the voltage-current waveform and the desired point of operation, and its modelling. Section 2.4 gives a fundamental description of the single-phase inverter and sinusoidal pulse width modulation. One of the main contributions of this thesis is the use of a bidirectional buck and boost converter to mitigate ripple in the DC-link. This converter is used together with an auxiliary battery/capacitor charging and discharging. Section 2.6 described the details about the bidirectional buck-boost converter and its working.

The main power stages of this thesis are shown in figure 2.1. Although the system is connected to the grid when the system is working in standalone it has the same subsystems which are described below:

- PV solar panel: The energy source
- Inverter: Transforms DC current from the PV panel into AC current.
- DC-DC converter: Used as active power decoupling.
- LCL filter: Needed to filter current harmonics.
- Control stage: The brain of the system that keeps all the stages working property, and which also ensuring stability against disturbances.

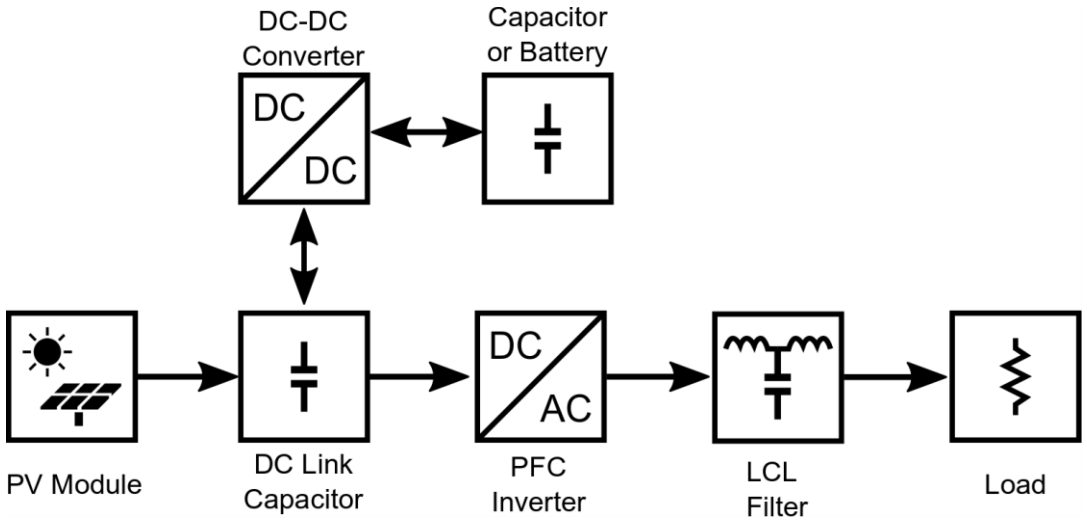

Figure 2. 1. Main power stages of this thesis.

2.2. Photovoltaic Systems.

The photovoltaic cell converts solar energy into electrical energy. When sunlight strikes the surface of a PV cell, an electrical field (created by the material used) provides

momentum and direction to light-stimulated electrons, resulting in a flow of current when the solar cell is connected to an electrical load [23].

PV systems are like any other electrical power generating systems; Although the equipment used is different than what is used for conventional electromechanical generators. The principles of operation and interfacing with other electrical systems remain the same.

A typical PV installation consist of a number of interfaces, or subparts, that convert, conduct, control, distribute, and store the electric energy produced by the PV array [9].

Figure 2.2 shows a typical PV system with a DC converter, which is used to track the MPP and to control the charge in a battery, and an inverter used to supply a AC load or to inject current to the grid.

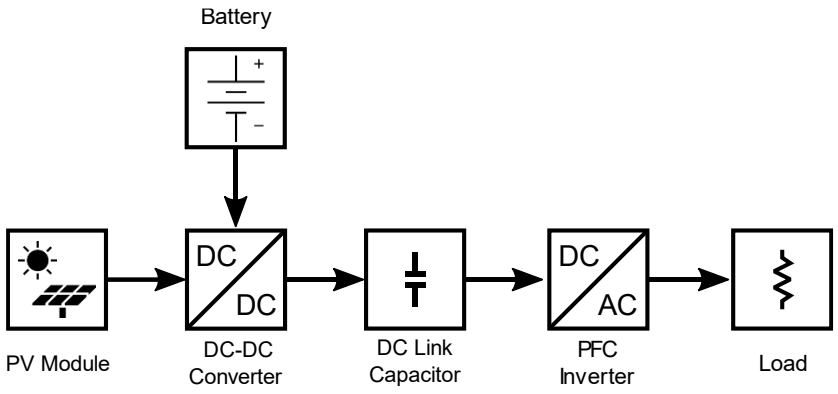

Figure 2. 2. PV system with ac load or connected to the grid.

Depending on the application of the system, the required equipment is a DC-DC power converter, a DC-AC power inverter, battery bank, etc. Essentially, depending of which, where and how the load is, the system will need convert the energy to supply this load and consequently the converters, inverters and storage devices will be defined. However, a DC-DC converter which tracks the maximum power point of the panel is used most of the time. Similarly, when an inverter is used a filter is needed to get a sinusoidal waveform. Even though in this thesis, the DC-DC converter it is not used for MPP tracking, the following schemes will include it. On another hand the control stage is not shown because this is not an electric converter, this ensure property work of each power converter.

Looking at figure 2.2, we can see an AC load, but also a DC load which is the battery. It is possible to classify the PV system in 2 main types, grid tied and stand-alone PV system. In addiction there are hybrid systems, although these are included into stand-alone system [24].

2.2.1. Grid tied PV System.

A grid-tied system or a grid connected system is a solar installation that is directly connected to an electric utility grid. The main device of these systems is the inverter which must ensure that electrical energy is exchanged between the PV-system and the grid in a proper way that minimize noise and harmonics. Grid connected systems rarely have battery storage since the objective of these installations are provide energy to the grid and no energy to supply any specific load. When the solar panels do not supply any energy, simply no energy is injected to the grid. Furthermore, a grid tied PV system normally deals with very high power, so it is tough to store this much of power in battery.

The size of grid tied PV systems range from power plant with MW capacity to small residential systems. Figure 2.3. shows the mains power stages of a grid connected system.

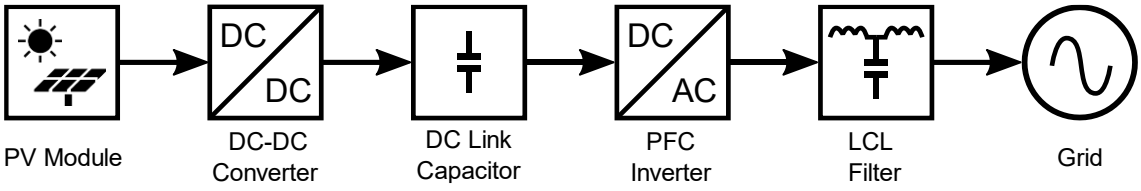

Figure 2. 3. Grid tied PV system.

2.2.2. Stand-Alone PV System.

Stand-alone PV systems are designed to operate independent of the electric utility grid, and are generally designed and sized to supply a certain DC and/or AC electrical loads. These types of systems may be powered by a PV array only, or may use wind, engine-generator, or utility power, as an auxiliary power source in what is called a PV-hybrid system.

Non-Hybrid systems provide only solar energy, and this typically need storage capacity to supply the load during the night. Because of that, it is common to use a battery as storage method. An example of a stand-alone PV system is shown in figure 2.4.

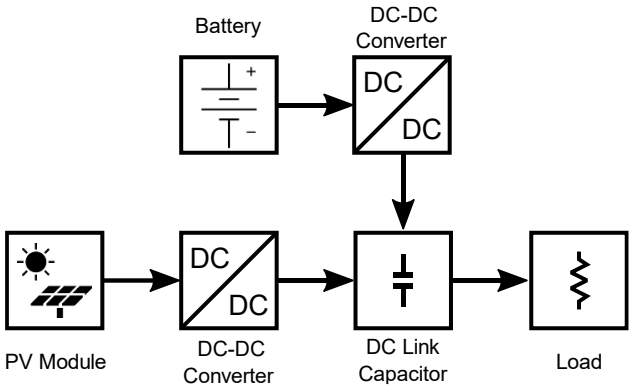

Figure 2. 4. Scheme of stand-alone PV system.

2.3. Photovoltaic Source.

A PV cell produce current from light because of the photovoltaic effect. The electric power depends on the light radiation. The cell is made up with Silicon, Boron (B) and Gallium (Ga).

Generally, a PV source can consist of several cells as a module, a commercial module, or a group of modules which is called PV array.

A single cell measures 10x10 cm and it supply a voltage of approximately 0.5 volts. The delivered power depends of the irradiancy over its surface. Generally, PV cells are connected electrically in series and/or parallel to produce higher voltages and currents respectively. Normally, a panel is formed for a normalized configuration of cells. Likewise, a PV array consist of any number of PV modules and panels to generate a specific power range.

The most commercial format of a PV source is a panel, so in this project a panel is used as energy source. However, a part of the real device, the equivalent circuit for simulation is derived as a current source.

2.3.1. Photovoltaic module.

In order to get real energy source a commercial photovoltaic module is chosen as energy source.

The module use in this project is the JW-S100 from the company Jiawei. It is a panel of monocrystalline cells, 100 W, [25]. Table 2.1 show all the specification for this panel.

Maximum Power ($\mathbf{P_{max}}$)	100 W
Voltage at P_{max} ($\mathbf{V_{MP}}$)	17.9 V
Open Circuit Voltage ($\mathbf{V_{OC}}$)	21.6 V
Short Circuit Current ($\mathbf{I_{SC}}$)	6.15 A
Maximum System Voltage	70 V
Power Temperature Coefficients	-0.38 %/°C
Voltage Temperature Coefficients	-60.8 mV/°C
Current Temperature Coefficients	3.5 mA/°C

Table 2. 1. JW-S100 PV panel specifications.

Since the focus of this projects is the inverter and DC-DC converter the chosen PV panel is used just to have a realistic voltage and current values.

2.3.2. PV Equivalent Circuit.

An equivalent circuit of the PV panel is needed so that we can model and simulate the system before to build a prototype. The circuit in Figure 2.5 shows a common circuit model for PV cells or arrays found in the literature. Where I_{PV} is the photovoltaic current and R_s and R_p are the series and parallel resistances, respectively [27].

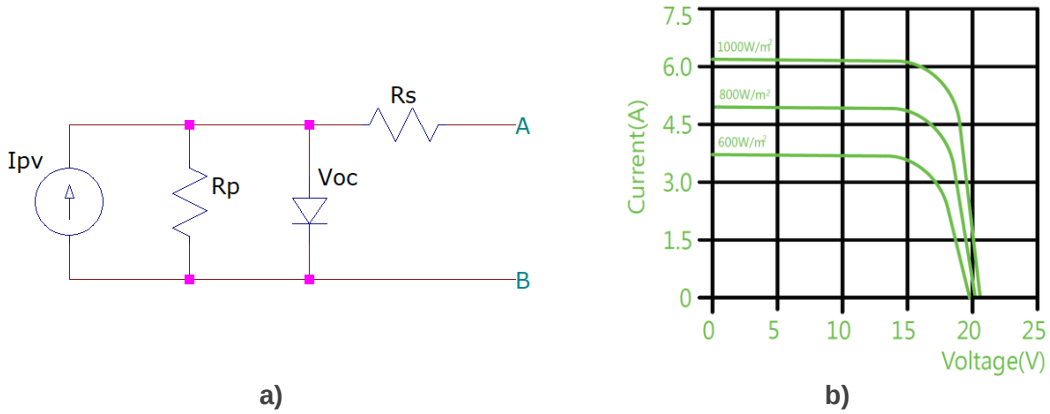

a) **b)**

Figure 2. 5. a) PV Equivalent circuit, b) UV charateristic curve.

The characteristic VI curve of a solar panel is shown in figure 2.5 b), since a MPPT algorithm is not implemented we will suppose the photovoltaic cell work as a constant current source with a constant voltage value. However experimental testing, a physical constant power source can be used instead of a photovoltaic panel. So, the final circuit used for simulation is as shown in figure 2.6

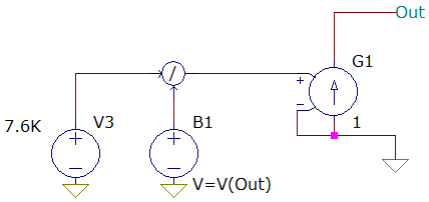

Figure 2. 6. Equivalent circuit used as a input enery source.

We suppose 20 panels connected in series as a string and 3 strings in parallel which form the array with 400V and 19A. Form figure 2.5 where the current source G1 is dependence of the power (7.6 KW) and the output voltage V(out). Thus, for the voltage settled in Out, the DC bus voltage ("out" on figure 2.5) will receive the current according to the nominal power, 7.6KW.

2.4. Full Bridge Inverter.

Basically, an inverter is a power electronic circuit which converts a DC input in a AC output. A clearly justification of the energy flux direction could be found in [9].

There are plenty of applications where DC-AC current conversions are needed. Examples include AC-motor drivers, battery powered uninterruptible power supplies, photovoltaic application, etc. A grid connected inverter is uses in this project to deliver the current from the solar panel (DC energy) to the grid (AC energy).

2.4.1 Inverters Characteristics and Classifications.

There are several ways to categorize inverters, in this project these are classified according to their circuit and behavior characteristic. Although it will be detailed explained, table 3.1 shows a common way to characterize the inverters.

Input DC source	VSI	CSI
Output AC load phases	Single Phase	Three Phase
Number of switches	Full Bridge	Half Bridge
Output waveforms	Sinusoidal Wave	Square Wave
PWM technique	Bipolar	Unipolar

Table 2. 2. Characteristic classifications of inverters.

A. Input source.

There are two mains group of inverters depending on if the input current or voltage is kept constant:

1. *Single phase current source inverter (CSI).*

In this inverter the input is a DC current source. Since this type of inverter is mostly only used for very high-power ac motor drives, they are not appropriate for this application.

2. *Single phase voltage source inverter (VSI).*

A VSI, in opposite, was a constant DC voltage source input. The voltage is kept constant by connecting a capacitor in parallel to the input voltage. The AC side current is fixed up by the load.

B. Output AC load phases.

Depending on the number of phases of the AC the load, there are several types of device. The most common configurations of VSI are:

1. *Single-phase inverters.*
2. *Three-phase inverters.*

Figure 2.7 shows a schematic of their basic schematic.

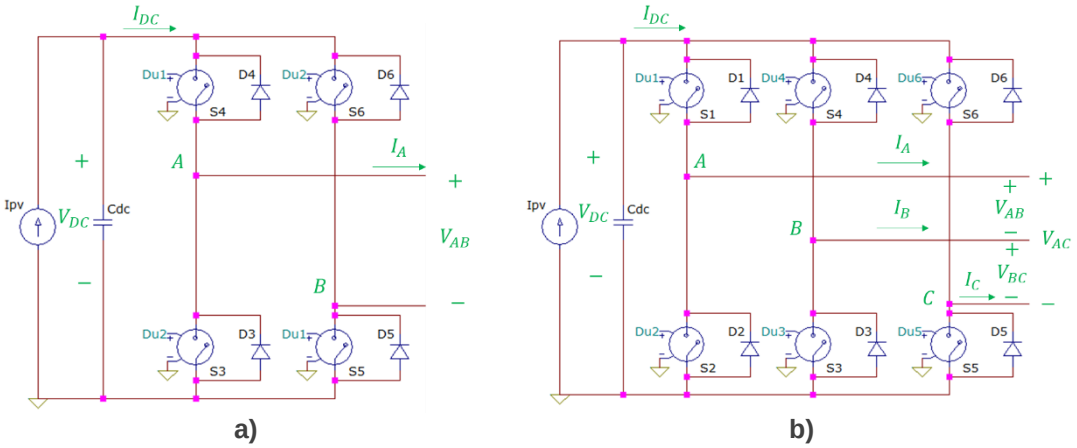

Figure 2. 7. a) Single phase inverter and b) three phase inverter.

A single-phase inverter has been chosen in this application since it is the most used configuration for low power inverters.

C. Number of switches.

Since a single-phase inverter have only two phases it is possible to divide the single-phase inverters according to the number of switches. Thus, the two topologies are:

1. *Half-Bridge Inverters.*

In these inverters the only leg is used, the other leg is replaced by two equal capacitors connected in series across the dc input. The junction of these two capacitors is the medium voltage point. A scheme of half-bridge inverters is shown in figure 2.8.

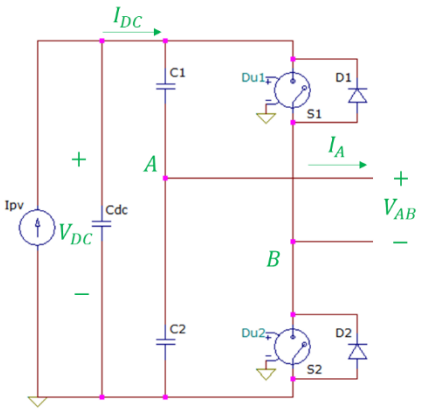

Figure 2. 8. Hal-Bridge inverter with DC-Link capacitor.

Although, it seems the cheapest options since only two switches are needed, a half-bridge is not the best choice for this application since the switches must support twice output voltage during $t_{ON}$and it makes the switching losses become very high [27].

2. Full-Bridge Inverters.

A full bridge inverter is shown in figure 2.7 a), this inverter has two legs (the switches couple in the same branch) and 4 switches in total. It is commonly used in high power applications.

Because of the numerous possibilities to control the energy (output/input voltage, current, etc.), the big input and output voltage range and the performance a full-bridge inverter is the topology used for this project, although a complex control is needed.

2.4.2. Full-Bridge Inverters topology.

In the previous section the circuit configuration of a full-bridge inverter was introduced, and we will now look into how it functions. Depending of a duty cycle the inverter's switch operates to invert the DC inputs. For instance, when S4 and S5 is driving the output V_{AB} is V_{DC} (green arrows describe the current flux) unlike when S3 and S6 drive, V_{AB} is $-V_{DC}$ (red arrows describe the current flux).

The switches must also satisfy two main rules, on the one hand, two switches of a same branch can not drive at the same time, if this happen, the input will be in short circuit and on the other hand, the opposite situation, two switches in a leg can not be OFF at the same time since the inductors (LCL filter) at the output side will be in open circuit.

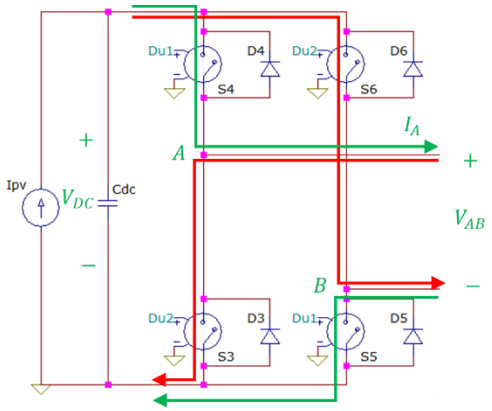

Figure 2. 9. Full-Bridge inverters plus LCL low pass filter and DC link capacitor

Seeing that, it seems like the output voltage is a square wave. However, a sinusoidal wave can be also obtained, depending on the control technique (duty signal) used.

So, the inverters control techniques can be divided in:

Square wave inverters.

In these inverters the output ac voltage has a waveform like a square waveform. Here the input dc voltage is controlled in order to control the magnitude of the output ac voltage, and therefore the inverter has to control only the frequency of the output voltage. The switching frequency of this inverter is so much lower than the pulse width modulated inverters.

Pulse width modulated inverters.

This is the most typical technique, here the inverter switches at high frequency, so in principle, these produce a square wave, only that its frequency is so high that it can be easily filtered to become a sine.

The input DC voltage is transformed in a sine wave at output ac voltage. So, the inverter controls the magnitude and the frequency of the output by PWM (Pulse Width Modulation). Although it will be described in point 2.4.3. basically, the PWM is obtained comparing a sinusoidal wave with a triangular wave.

There is other kind of inverters where the two characteristics of above inverters are combined. The technique is called voltage cancelation and only work with single phase inverters. The output voltage is like a square waveform.

2.4.3. SPWM Inverters.

The Sinusoidal Pulse Width Modulation (SPWM) is a technique used in most of the inverter switching system. Here, a sinusoidal control signal ($V_{control}$ signal) is compared with a triangular carrier signal ($V_{carrier}$) in order to detect the intersection between both signals.

The PWM signal is 1 when the control signal is larger than carrier signal (the correspondently switches are ON) and vice versa. The ON time of a switch couple is the variable called duty cycle (D). Neglecting the amplitude values, figure 2.10 illustrates the technique.

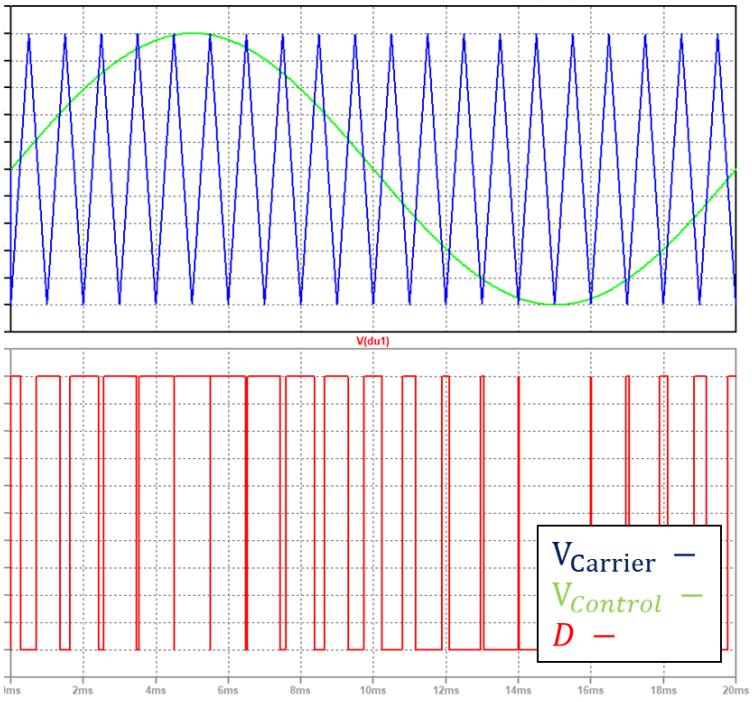

Figure 2. 10. SPWM Technique

There is also other way to generate the duty cycle signal with two opposites sinusoidal control signals, see figure 2.11. So, depending of the number of control signals the modulation is called:

A. Bipolar: one sinusoidal signal is used. The inverter output voltage is either at $+V_{DC}$ or $-V_{DC}$. Figure 2.11 a).

B. Unipolar: Two opposites sinusoidal signals are compared with a triangular signal. The inverter output voltage is at $+V_{DC}$ or 0 for the positive part of a sine, of at 0 or $-V_{DC}$ for the negative part of a sine. Figure 2.11 b).

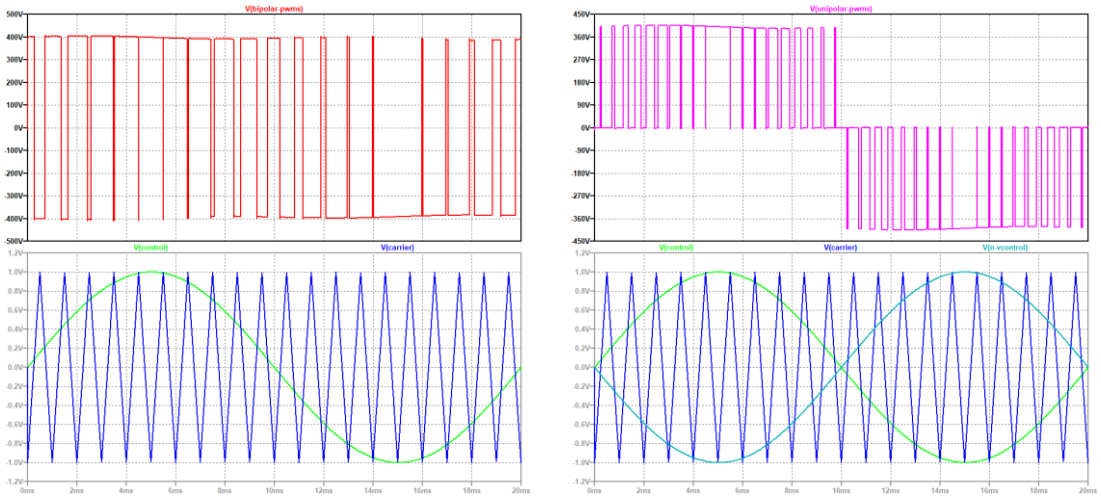

a) b)

Figure 2. 11. Sinusoidal PWMs. a) Bipolar PWM, b) Unipolar PWM

Note that the name come from the number of potentials at the output voltage and do not from the number of control signals used.

Table 2.3 describe the switching states according the control signals.

		Bipolar				Unipolar			
		S3	S4	S5	S6	S3	S4	S5	S6
1 $V_{Control}$	$V_{Carrier} < V_{Control}$	OFF	ON	ON	OFF	ON	OFF	-	-
	$V_{Carrier} > V_{Control}$	ON	OFF	OFF	ON	OFF	ON	-	-
2 $V_{Control}$	$V_{Carrier} < -V_{Control}$	-	-	-	-	-	-	OFF	ON
	$V_{Carrier} > -V_{Control}$	-	-	-	-	-	-	ON	OFF

Table 2. 3. Switch States. Unipolar and Bipolar modulations.

The bipolar modulation is not used in this thesis because of the following disadvantages:

- The DC side current becomes higher due to elevated frequency.
- A complex control is needed to correctly control the zero crossing.

A detailed description of the unipolar modulation can be found on the chapter 8 of the book [9].

Looking to the power balance, the inverter itself is not able to store energy, so the instantaneous power input (photovoltaic input) must equal the instantaneous power output.

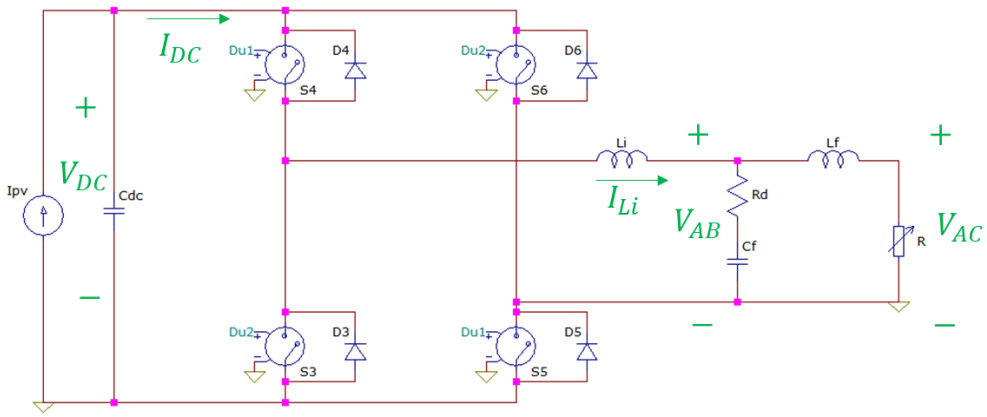

Figure 2. 12. Full bridge inverter with AC sinusoidal load.

If the load is an AC load, such as an AC motor or the grid (on grid connecter inverter) the output current is also sinusoidal, and this could lag V_{AB}. From the circuit on figure 2.12 the voltage and current on the AC side are expressed in equation 2.1 where ω_{load} is the fundamental frequency of the AC load:

$$V_{AB} = \sqrt{2} \cdot V_{AB,RMS} \cdot \sin(\omega_1 \cdot t) \quad (2.1)$$

$$I_{load} = \sqrt{2} \cdot I_{load,RMS} \cdot \sin(\omega_1 \cdot t - \varphi) \quad (2.2)$$

As the inverter itself has no energy stored elements, the instantaneous power input must equal the instantaneous power output. So, it is means:

$$P_{in} = V_{AB} \cdot I_{load} \quad (2.3)$$

$$P_{in} = \left[\sqrt{2} \cdot V_{AB,RMS} \cdot \sin \omega_1 \cdot t\right] \cdot \left[\sqrt{2} \cdot I_{load,RMS} \cdot \sin(\omega_1 \cdot t - \varphi)\right] \quad (2.4)$$

Using trigonometric property, one can get:

$$P_{in} = V_{AB,RMS} \cdot I_{load,RMS} \cdot \cos \varphi - V_{AB,RMS} \cdot I_{load,RMS} \cdot \cos(2 \cdot \omega_1 \cdot t - \varphi) \quad (2.5)$$

From equation 2.5, the input power has two terms, a DC term minus a second order harmonic component (twice the fundamental frequency of the output inverter voltage).

$$P_{DC} = V_{AB,RMS} \cdot I_{load,RMS} \cdot \cos \varphi \quad (2.6)$$

$$P_{ripple} = V_{AB,RMS} \cdot I_{load,RMS} \cdot \cos(2 \cdot \omega_1 \cdot t - \varphi) \quad (2.7)$$

The second order harmonic components come from the ac side current and it produce a voltage ripple in the input capacitor C_{DC}. That is other reason why a DC link capacitor is needed.

2.5. LCL Output Filter.

The use of renewable energy source is rapidly increasing in the modern distribution networks because of the disadvantages of the non-renewable energy sources. But renewable energy sources need inverters for interfacing with the utility grid. The switching frequency of these inverters is very high and this may introduce high order harmonics that can interfere with neighborhood EMI (Electromagnetic interference) sensitive loads or equipment which are connected to the grid.

On another hand, the output voltage between two branches (V_{AB}) is a square waveform with high frequency (See figure 2.11 b) for red waveform). This voltage can not be applied directly to a load because it could damage it. Therefore, a filter is necessary between the bridge and the load.

A third order LCL filter is shown in figure 2.13 a), this is used to transforms the output square waveform in a sinusoidal waveform, but also to decrease the harmonics in the spectrum of the output voltage. The main characteristic of the selected filter are that this attenuates at -60db/decade after the resonant frequency and it produce few reactive power.

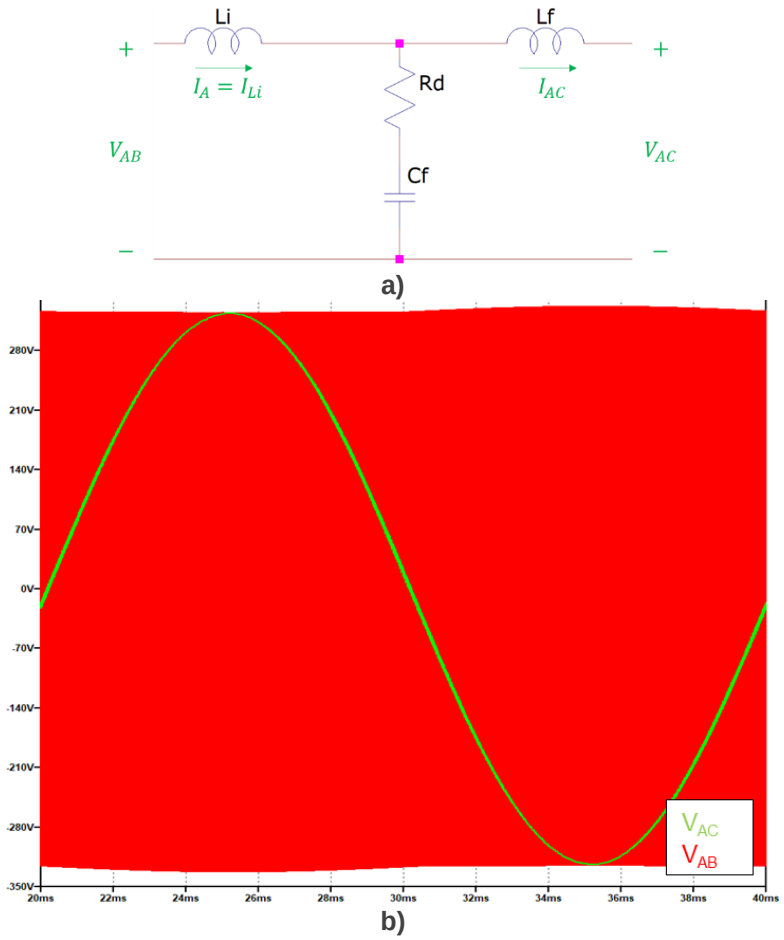

Figure 2. 13. a) LCL Low pass filter b) Input and Output voltage waveforms of a LCL filter.

In figure 2.14 the output voltage spectrum is shown before and after to filter it. Note that the main harmonics are located at multiples of the switching frequency (70KHz in this simulation). The harmonic magnitude depends of the duty ratio and the capacitors and inductor values of the filter. Because of these values will be developed in chapter 3 the harmonics magnitudes of figure 2.14 are not consider. Moreover, a derivation of the harmonics magnitude based into the duty ratio and the frequency location of these can be found in [9].

In addition, figure 2.14 b) shows the behavior of the output LCL filter which work as a low pass filter.

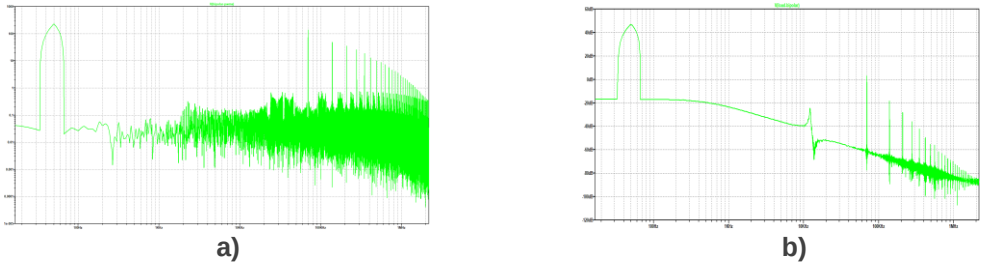

Figure 2. 14. Output voltage spectrum. a)Without filer, b)With a LCL filter

2.6. Bidirectional DC-DC Converter.

The bidirectional dc-dc converter has become a promising option for many power related systems, including hybrid vehicles, fuel cell vehicles, renewable energy systems and as active filters [28]. It not only converts an input DC voltage to an output DC voltage of different value, but can also work to mitigate ripple keeping a stable voltage in one of the two sides (normally in high voltage side).

The bidirectional converter in this project is used to keep a constant voltage in DC-Link and to minimalize the ripple due to the PFC inverter. The bidirectional converter is connected to the DC bus and this shares the DC capacitor with the inverter.

In a bidirectional DC-DC converter power can flow in both directions; it thus allows one to decrease or increase the output voltage. Consequently, the converter work as a unidirectional converter in each mode of operation depending of the energy flux direction and in this way the converter can be described as a single DC-DC converter depending on the operation mode.

Basically, DC-DC converters can be divided into two categories depending on the Galvanic isolation between the input and output side [9]. Table 2.4 shows the main DC-DC converters:

Non-Isolated	**1 Coil**	Buck (Step Down)
		Boost (Step Up)
		Buck-Boost
	>1 Coil	Cúk
		Sepic
		Zeta
Isolated	**Unidirectional Core Excitation**	Flayback
		Forward
	Bidirectional Core Excitation	Push-Pull
		Half Bridge
		Full Bridge

Table 2. 4. Types of DC-DC converters

For the present bidirectional dc-dc converter a non-isolated boost and buck converter is chosen because it only works primarily as a ripple mitigator and the output is only used to store energy in a capacitor and no galvanic isolation is needed.

The basic non-isolated one coil converter (in table 2.4) do not have the inherent property of the bidirectional power flow due to the presence of a diode. This limitation in the conventional Boost and Buck converter circuits can be removed by introducing a second switch (with anti-parallel diode across them) allowing current conduction in both directions for bidirectional power flow in accordance with the controlled switching operation. This bidirectional buck and boost circuit can be seen in figure 2.15.

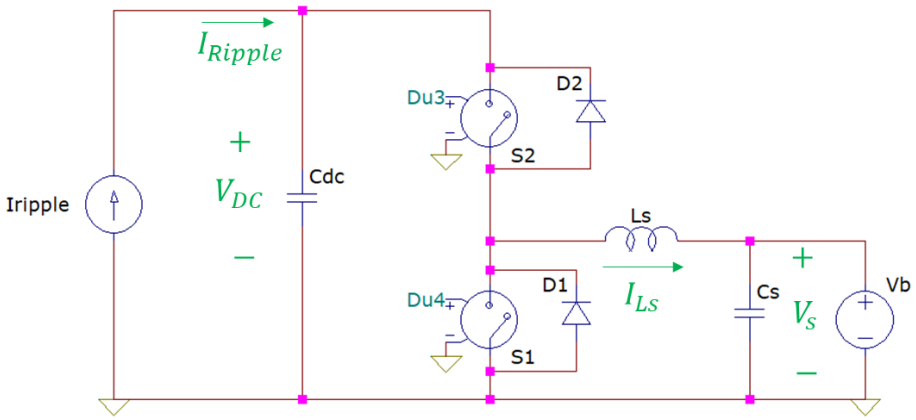

Figure 2. 15. Bidirectional Buck and Boost

The converter has two switches, S1 and S2 with both with anti-parallel diodes D1 and D2. The mode of operation depends of which switch is used. The S1 switch set the Boost mode, so the voltage in V_{DC} is increasing (energy moved from V_S side to V_{DC} side), on the contrary, the S2 switch set the Buck mode and the voltage in V_{DC} is decreasing (energy moved from V_{DC} side to V_S side). Although the operation modes can be also see in figure 2.16, a more detailed behaviour of the bidirectional DC-DC is explained below where the converter is divided into the two modes of operations.

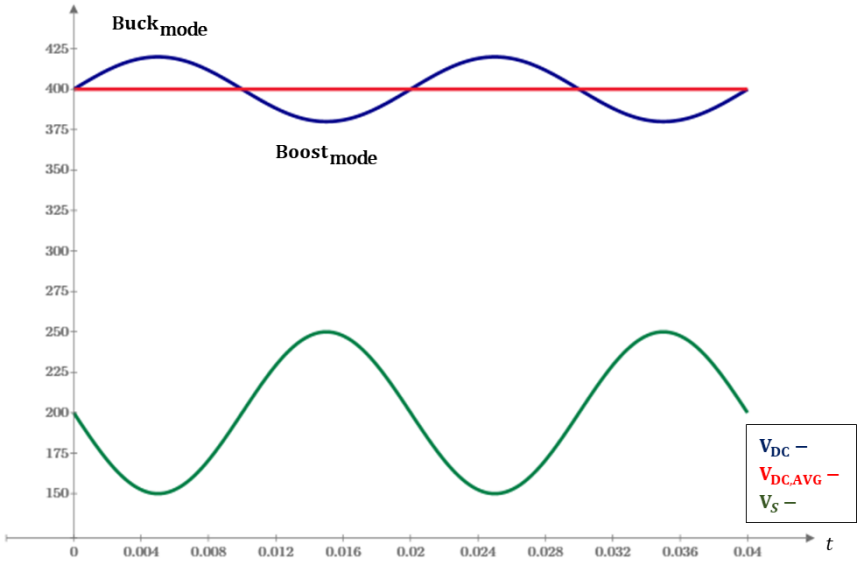

Figure 2. 16. V_{DC} Voltage and opertation modes of the bidirectional DC-DC converter.

2.6.2. Boost Mode.

In this mode, the switch S2 is off all the time whereas S1 and diode D2 enter into conduction depending on the duty cycle.

In order to simply the analysis, in Boost mode the input current come from the inductor L_S and capacitor C_S. Thus, the capacitor, C_{DC} absorb this current and increase the DC-link voltage.

Due to ON and OFF state in the S2, there are two states:

State 1. S1 ON, D2 OFF.

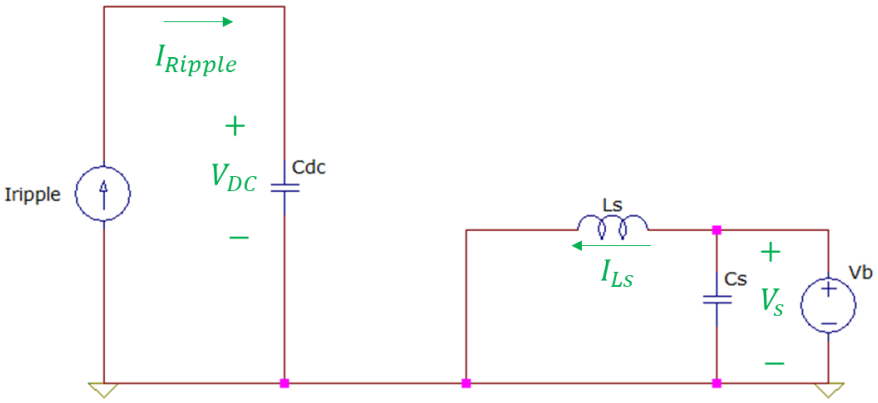

Figure 2. 17. ON State S1. Boost operation mode.

Referring to figure 2.17 when S1 is ON its $R_{DS(ON)}$ presents a low drain-to-source resistance and in consequence, it has a small voltage drop of V_{DS} [29]. Although R_{DS} and V_{DS} are not consider in the calculus since these values depend of the switch chosen.

The difference between input voltage V_S and a small voltage drop across the DC resistance of the inductor (equal to I_{Ls}×R_{Ls}) is the voltage applied over the inductor L_s. As equation 2.8 describe:

$$V_{Ls(t_{ON})} = V_S - I_{Ls} \cdot R_{Ls} \tag{2.8}$$

The diode D2 is OFF during this time, because its reverse biased, the inductor current, I_{Ls}, flows from the input source, V_S, through S1 to ground. Thus, during the ON state, the voltage across the inductor is constant, as consequence, the inductor current increases linearly according to the equation 2.9.

$$\Delta I_{Ls}(+) = \frac{V_S - I_{Ls} \cdot R_{Ls}}{L_s} \cdot D \cdot T_S \tag{2.9}$$

Likewise, the DC capacitor current is delivered to the inverter, so the DC voltage decrease. During the S1 ON state the slope of the voltage waveform in C_{DC} capacitor is:

$$\Delta V_{DC}(-) = \frac{-V_{DC}}{Z_{in} \cdot C_{DC}} \cdot D \cdot T_S \tag{2.10}$$

Where Z_{in} is the inverter impedance and D de duty signal which is complementary for the switch S2.

- State 2. S1 OFF, D2 ON.

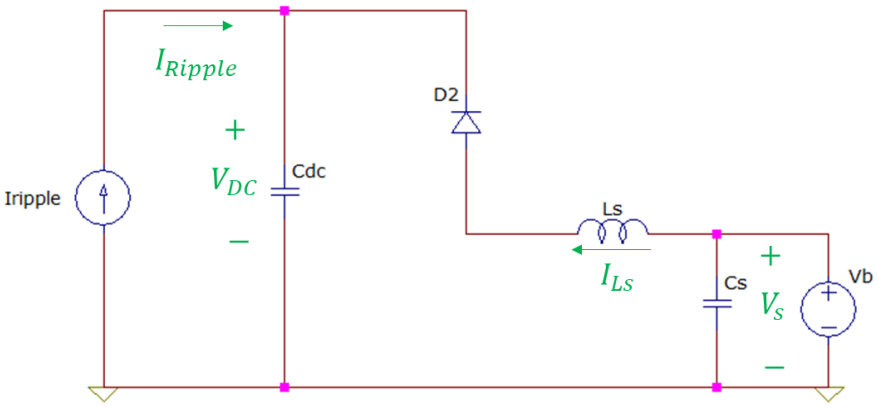

Figure 2. 18. OFF State S1. Boost operation mode.

Opposite to the previous state, when S1 is OFF, it presents a high drain-to-source impedance. Consequently, the voltage across the inductor reverses polarity until D2 becomes forward biased and turns ON.

During t_{ON}, the inductor voltage applied to the inductor, V_L remains the same as before plus DC voltage, V_{DC} and plus the diode (D2) forward voltage, V_{D2}. Neglecting the V_{D2}, the equation of the voltage in this state is:

$$V_{Ls(t_{OFF})} = V_S - I_{Ls} \cdot R_{Ls} - V_{DC} \quad \textbf{(2.11)}$$

The inductor current, I_{Ls}, now flows from the input source, V_S, through D2 to the DC capacitor and inverter. Maintaining the same polarity convention as the ON state, this applied voltage is negative (or opposite in polarity from the applied voltage during the on time). Hence, the inductor current decreases during the off time. The amount of decrease is given by:

$$\Delta I_{Ls}(-) = \frac{I_{Ls} \cdot R_{Ls} + V_{DC} - V_S}{L_s} \cdot (1 - D) \cdot T_S \quad \textbf{(2.12)}$$

Analogy, the output DC voltage ripple peak magnitude can be derived. Thus, for the S1 OFF state the increase of the voltage waveform in C_{DC} capacitor is:

$$\Delta V_{DC}(+) = \frac{I_{Ls}}{C_{DC}} - \frac{V_{DC}}{Z_{in} \cdot C_{DC}} \cdot (1 - D) \cdot T_S \quad \textbf{(2.13)}$$

2.6.3. Buck Mode.

Contrary to the previous mode, in the Buck mode the switch S2 and diode D1 are working according the duty cycle.

In addition, in this mode of operation the bidirectional converter must store energy from the DC side because of its excess. As consequence the DC side can be approximated as a constant voltage source and a impedance connected to the right side of C_S which store the surpass input energy.

As well as the Boost mode there are two states depending of ON or OFF state on switch S2:

- State 1, S2 ON, D1 OFF.

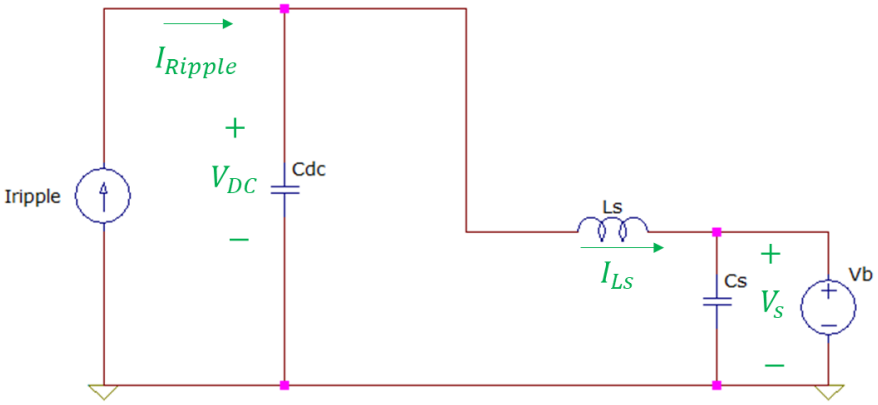

Figure 2. 19. ON State S2. Buck operation mode.

Analog to the Boost mode, when the S2 is ON the current flow through its $R_{DS(ON)}$, and through the inductor. There is also a voltage across the dc resistance of the inductor, R_{Ls}, and the voltage V_{DC} and V_S are in the same mesh. Thus, considering figure 2.19 the inductor voltage, V_{Ls} is:

$$V_{Ls(t_{ON})} = V_{DC} - I_{Ls} \cdot R_{Ls} - V_S \quad \textbf{(2.14)}$$

The inductor current, I_{Ls}, flows from the DC side through S2 and to the C_S capacitor and battery unit V_b. Because of the constant applied voltage, the inductor current increases linearly. The equation which describe the amount of increase is:

$$\Delta I_{Ls}(+) = \frac{V_{DC} - I_{Ls} \cdot R_{Ls} - V_S}{L_s} \cdot D \cdot T_S \quad \textbf{(2.15)}$$

- State 1, S2 OFF, D1 ON.

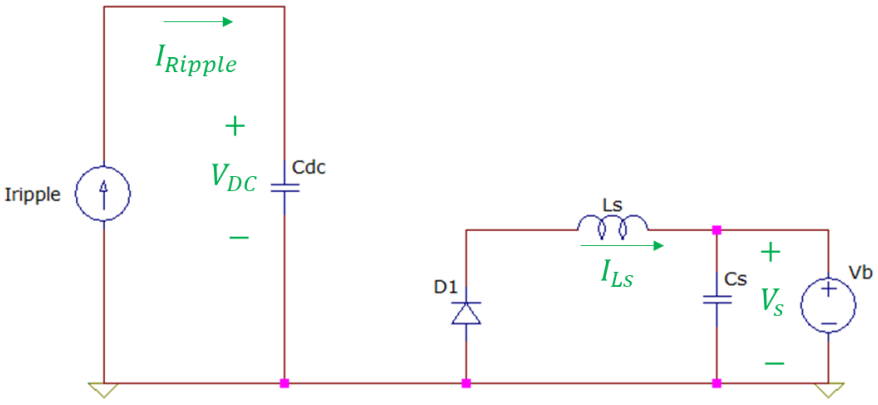

Figure 2. 20. OFF State S2. Buck operation mode.

Referring to Figure 2.20, when S2 is OFF, the voltage across the inductor reverses polarity until D1 becomes forward biased and turns ON.
Them, the voltage over the inductor can be derived as:

$$V_{Ls(t_{OFF})} = -V_S - I_{Ls} \cdot R_{Ls} \quad \textbf{(2.16)}$$

When diode, D1 is conducting, the inductor current flows from ground through D1 and to the output capacitor, C_S, and series resistors combination. So, maintaining our same polarity convention, this applied voltage is opposite in polarity from the applied voltage during the ON time, hence the voltage over the inductor decrease. The amount of decrease is given by the equation 2.17

$$\Delta I_L(-) = \frac{V_S - I_{Ls} \cdot R_{Ls}}{L_s} \cdot (1 - D) \cdot T_S \quad (2.17)$$

As the capacitor is connected directly to the inductor and to the output impedance, the voltage over C_S capacitor increase when the inductor current is higher than the output impedance current and decrease when the inductor current is lower than the output impedance current. Therefore, the amount of decrease or increase must be exactly the same at the end of each period. The amount of voltage ripple in C_S is expressed in equation 2.18:

$$\Delta V_s = \frac{\Delta I_L}{8 \cdot C_S} \cdot T_s \quad (2.18)$$

The voltage ripple in V_s will be developed in section 3.3 of chapter 3.

Finally, it can be seen how the inductor current change the direction depending of the operation mode, for instance, if the I_L in Boost mode is chosen as a positive, the I_L in Buck mode will be negative, or in opposite direction. The follow figure from [20] shows the inductor current waveform when the bidirectional converter changes the mode of operations.

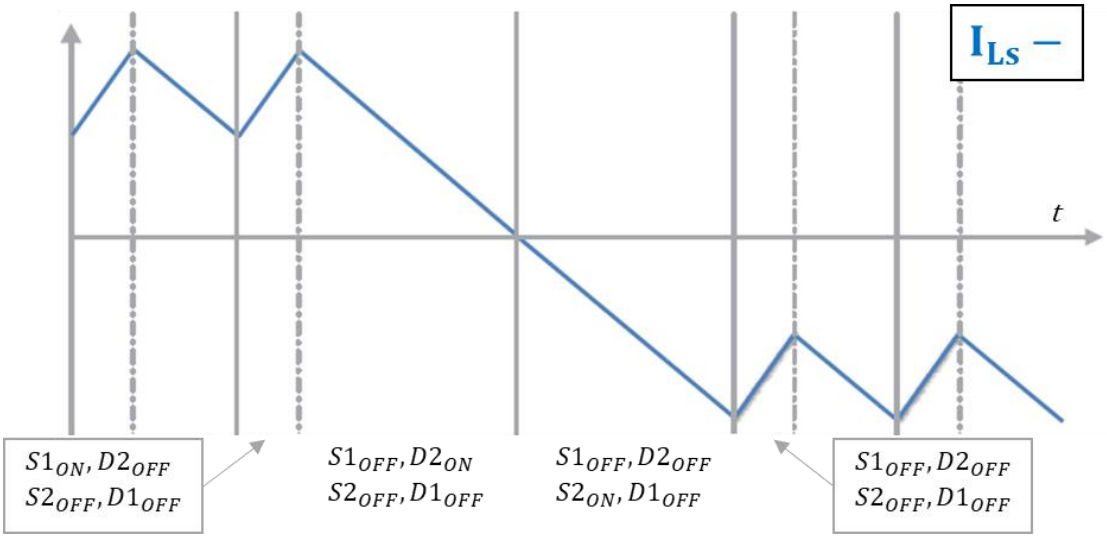

Figure 2. 21. Inductor current waveform when the mode of operation change.

Chapter 3.

Components Selection.

Chapter 3. Components Selection.

3.1. Introduction.

Although many times the value of some components are determined by the power supply specifications, the main objective of this section is to derive the electrical requirements and applied stresses of each components used in the power stages of this thesis.

As it was explained in chapter 2, there are two power stages plus a LCL filter, the power stages are a single-phase inverter and a bidirectional converter. In this chapter the components used in each power stage and in the filter, are dimensions.

Firstly, the DC capacitor is designed since the inverter itself does not have more storage components than this capacitor. We will design the capacitor for both power stages because of the DC link capacitor is shared with both power stages.

The bidirectional converter is a combination of two known DC converters, buck and boost. Even though the converter works independently in either mode (or direction), the components are the same. The chosen components must therefore assure the correct performance of both operations directions.

The behaviour of the Buck-Boost converter is described in chapter 2 where it is noted that the storage components (inductors and capacitors) have an important role in the operation mode of the converter. These can change the mode of operation depending on their values. In this section the values of the inductance and capacitance are discussed to assure the continuous conduction mode (CCM).

Secondly the value of the inductances, capacitance and damping resistor is calculated for the LCL output filter in order to mitigate the main harmonic.

A part of the capacitances and inductances other values will be calculated, such as equivalent series resistances (ESR) of capacitors, DC resistance of inductors (DCR), etc. However, we will start with the inductance and capacitor since their values condition the others. The components are dimensioned according to the inverter specifications collected in table 3.1

Parameter	Magnitude
$V_{AC,RMS}$	230 V
$I_{AC,RMS}$	32 A
F_{AC}	50 Hz
P_{in}	7.6 kW
$V_{DC\ Link}$	400 V
V_s	200 V
F_{sw}	70 KHz

Table 3. 1. Inverter Specifications.

Although some basics analytical equations are calculated below to dimension the components, the final value of this are chosen studying the performance of the converter by simulations.

3.2. DC link Capacitor, C_{DC}.

The input capacitor is placed after the PV current source, its aim is to keep a stable voltage in the input and to damp the voltage ripple resulting from a pulsating current that appears on the DC side of the inverter. The frequency of this current is twice the output frequency.

The value of the DC capacitor can be calculated from two different ways depending of the converter. We will calculate first the capacitor attending to the behaviour of the DC-DC converter, then the capacitor will be dimension according to the inverter power flux and finally a new method based on [30] will be presented to dimension the capacitor for both power stages.

3.2.1. Calculus for DC-DC converter.

First of all, let assume only the bidirectional converter with constant voltage in both sides. When the converter is working as a boost, it is especially important since the DC capacitor must to store energy during ON state of switch, S1 and then supply the load when the S1 is in OFF state. The bidirectional converter working as a Boost can be seen in figure 3.1.

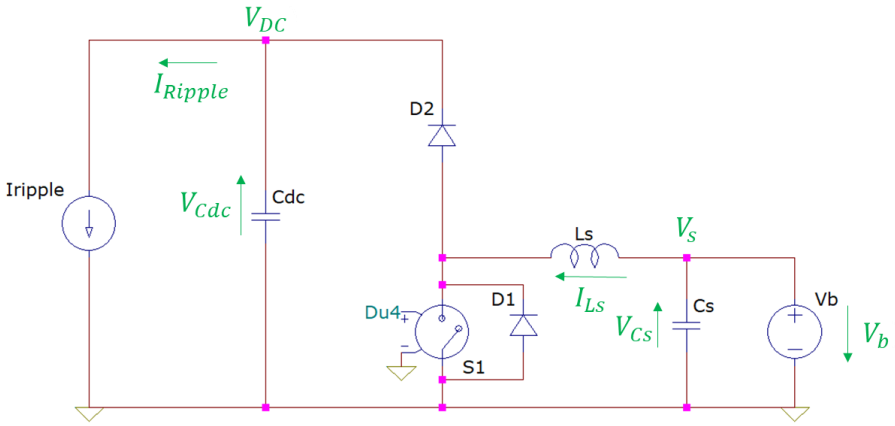

Figure 3. 1. Boost converter equivalent circuit.

Clearly, the amount of voltage in the input capacitor depend of the duty cycle as the following two equations shown:

$$\Delta V_{DC}(-) = \frac{-V_{DC}}{\frac{V_{DC}}{I_{ripple}} \cdot C_{DC}} \cdot D \cdot T_S \tag{3.1}$$

$$\Delta V_{DC}(+) = \frac{I_{DC,ripple}}{C_{DC}} - \frac{-V_{DC}}{\frac{V_{DC}}{I_{ripple}} \cdot C_{DC}} \cdot (1 - D) \cdot T_S \tag{3.2}$$

The above equations are also sketched in follow figure where it is noted that the load current is maximum during the beginning of t_{ON} state, when capacitor current is minimum, as well as maximum DC voltage. The capacitor value should be dimensions then, using the maximum DC current or minimum V_S, voltage. The boost converter waveform can be seen in figure 3.2.

As mentioned previously the duty value is required. The duty cycle ratio is deducted in equation 3.3:

$$D = D_{u4} = 1 - \frac{V_{s,min}}{V_{DC}} = 1 - \frac{200}{400} = 0.5 \tag{3.3}$$

Finally, the capacitor can be deducted from 3.1 admitting a 5% as the maximum voltage ripple:

$$C_{DC} = \frac{I_{ripple}}{\Delta V_{DC}} \cdot D \cdot T_S = \frac{\frac{7.6KW}{400V}}{0.05 \cdot 400V \cdot 70KHz} \cdot 0.5 = 6.8\mu F \tag{3.4}$$

Although a solar panel (the current source) can not be feed we assume that the converter will deliver the needed current until keep the DC voltage at 400V, when can assume, then, resistive load for this analysis since the DC capacitor will be compared. So, in the equation 3.4 we use the nominal current.

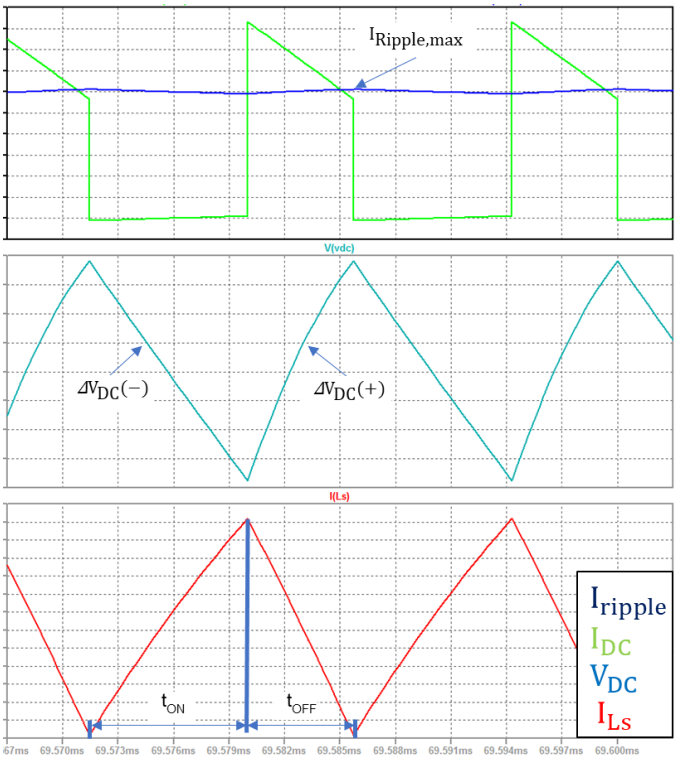

Figure 3. 2. DC Capacitor waveforms in Boost mode.

3.2.2. Calculus for Inverter.

The DC link capacitor can also be obtained considering the voltage ripple of double line frequency. It can be expressed as the equation 3.5.

$$C_{DC} = \frac{I_{ripple}}{\Delta V_{DC} \cdot \omega_1} = \frac{\frac{7.6KW}{400V}}{0.05 \cdot 400V \cdot 2 \cdot \pi \cdot 50Hz} = 3mF \quad (3.5)$$

3.2.3. Active Filter Capacitor Calculation.

Both method offered a big different capacitor magnitude, some authors have developing a new analysis to set the capacitance value of the DC link capacitor [30].

From equations 2.7 of the chapter 2 we can obtain the energy ripple by integrating the power ripple, so the energy ripple is:

$$E_{ripple} = \int_0^t P_{ripple}(t) \cdot dt + 0 \cdot dt \quad (3.6)$$

The powers, P_{AC}, P_{DC}, P_{ripple} and the energy ripple, E_{ripple} are plot in figure 3.3.

On another hand, the energy ripple will be stored in the auxiliary capacitor, C_s and/or in a battery, if we consider the energy store in a capacitor, the equation 3.7 can be written:

$$E_{Cs}(t) = \frac{1}{2} \cdot C_s \cdot V_s^2 \quad (3.7)$$

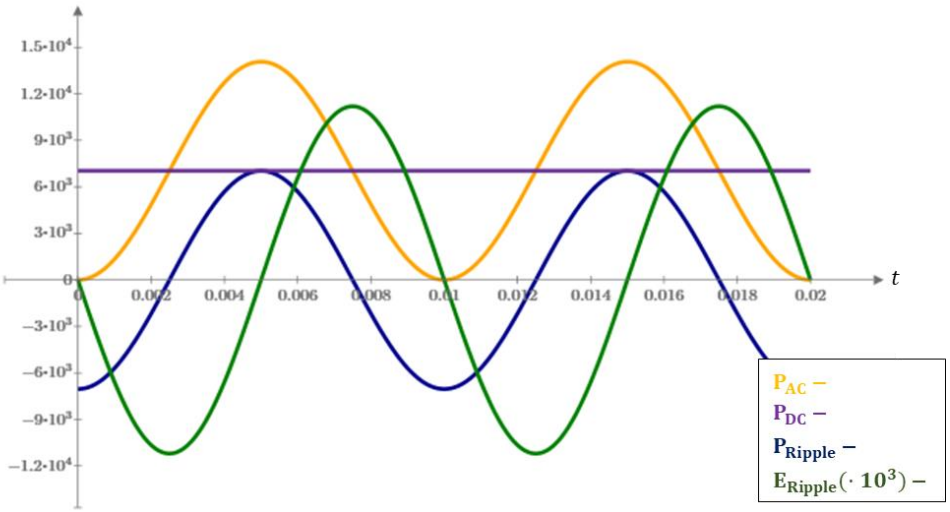

Figure 3. 3. Powers and energy ripple waveforms.

Now it is possible to relate the equation 3.6 and 3.7 since the auxiliary capacitor is supposed to store the energy ripple.

$$V_s(t) = \sqrt[2]{2 \cdot \frac{E_{ripple} + E_0}{C_s}} \tag{3.8}$$

So, based on the initial value of the energy ripple which coming from the constant term of the integral. One can plot the voltage V_s as function of E_0 for one desired value of the C_s capacitor, the waveforms are shown in figure 3.4 for a $C_s = 160\mu F$

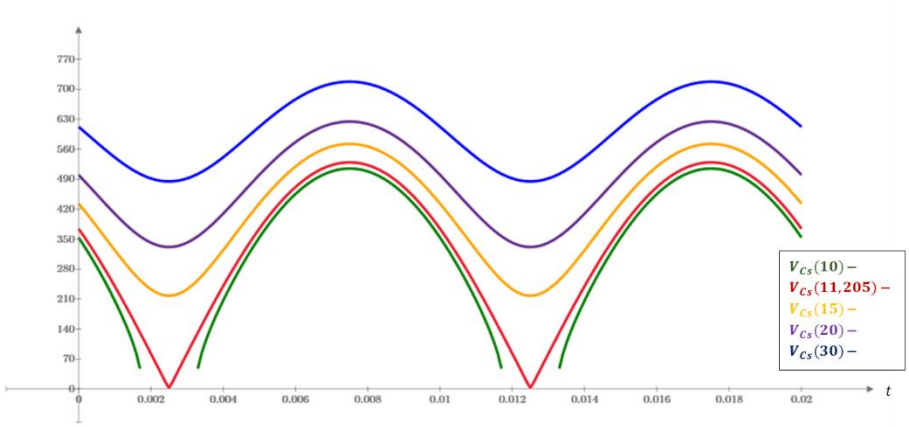

Figure 3. 4. V_s as funtion of E_{ripple}.

Similarly, the current can be expressed as the equation 3.8:

$$I_{Cs}(t) = C_s \cdot \frac{dV_s(t)}{dt} \tag{3.9}$$

The current for the same energy values as the voltage is plot in figure 3.5.

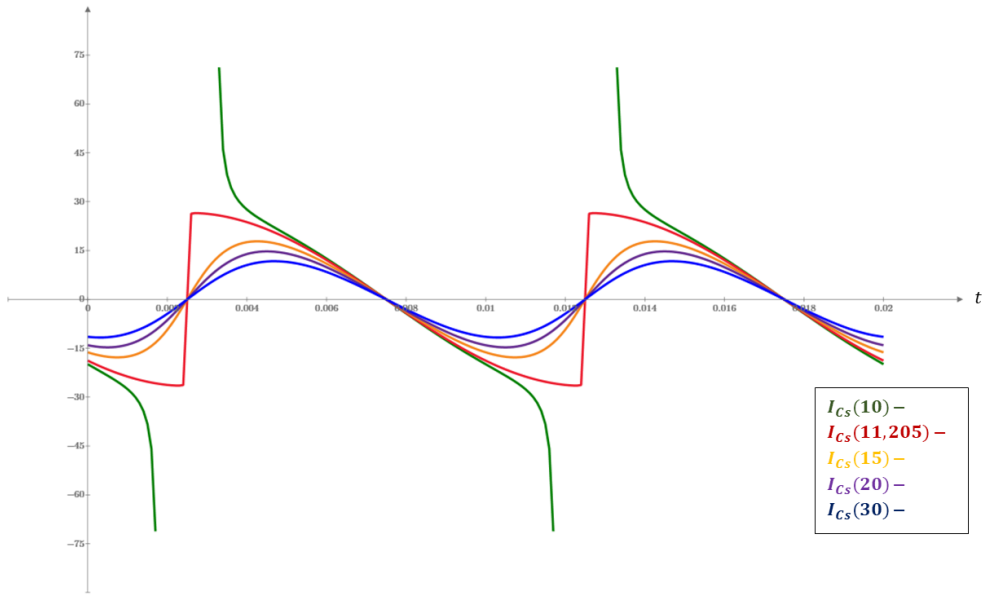

Figure 3. 5. I_s as funtion of E_{ripple}.

From figure 3.4 and 3.5 one can see how depending of the energy store in the auxilary device (a capacitor) the average calue of the voltage change and more over the ripple increase when energy store decrease since the capacitor can charge and discharge.

Based on that whith the math software like matlab one can choose both capacitor according to the amount of voltage ripple is allow in each one.

3.2.4. RMS Current, $I_{Cdc,RMS}$.

Accordingly, power dissipation in the capacitor, excessive temperature can seriously shorten the expected life of a capacitor. The RMS value of the current ripple flowing through output capacitor is calculated from the equation 3.10 wich is developed in [31].

$$\mathrm{I_{Cdc,RMS}} = \sqrt{2} \cdot \mathrm{I_{AC,RMS}} \cdot \sqrt{\frac{1}{8} \cdot [4 - \mathrm{m_a^2} \cdot (1 + 2 \cdot \cos(\varphi)^2)]} = 22{,}7\mathrm{A} \qquad \textbf{(3.10)}$$

Where m_a is the modulation index and φ is equal to zero when the inverter work as power factor corrector.

3.2.5. Equivalent Series Resistance, R_{Cdc}.

The equivalent series resistance (ESR) will also limit the ripple, ΔV_{DC}, voltage. However, the ESR in the capacitor will dissipate power. Since the capacitance of the DC link capacitor is chosen initially $3\mathrm{mF}$, this limit the range of product available because the capacitance is bigger than the most commercial capacitor. The ESR of the DC link capacitor is chosen based on the commercial capacitor.

$$\mathrm{Rc_{,DC}} \geq \frac{\Delta \mathrm{V_{DC}}}{\frac{\mathrm{P_{R,DC}}}{\mathrm{V_{RDC}}}};\ \mathrm{R_{DC}} = 0.06\Omega \qquad \textbf{(3.11)}$$

3.3. Inductor, L_S.

The choice of the inductor L_S is critical for the operation mode of the converter and consequently for the control. Continuous conduction mode is set to dimensions the inductor.

The analysis will be developed from buck converter operation as shown in figure 3.6 (Since this direction of operation is more stressed for the inductor because this to delivery his current to capacitor and battery). After that, the inductor value is checked with the boost mode operation to justify the chosen value.

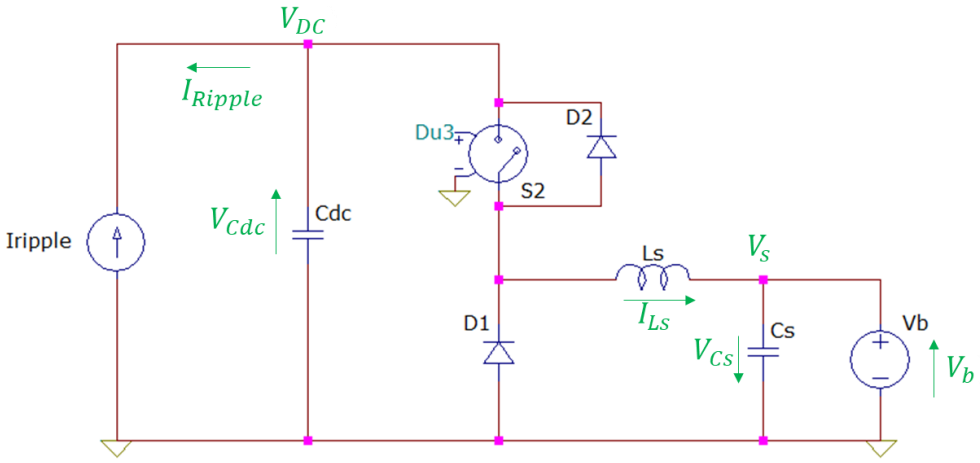

Figure 3. 6. Buck operation mode.

The waveforms of the circuit can be seen in figure 3.7. The inductor current rise and fall during t_{ON} and t_{OFF} respectively, hence the inductor current I_{Ls} has two states, $\Delta I_{Ls}(+)$ during t_{ON} and $\Delta I_{Ls}(-)$during t_{OFF}.

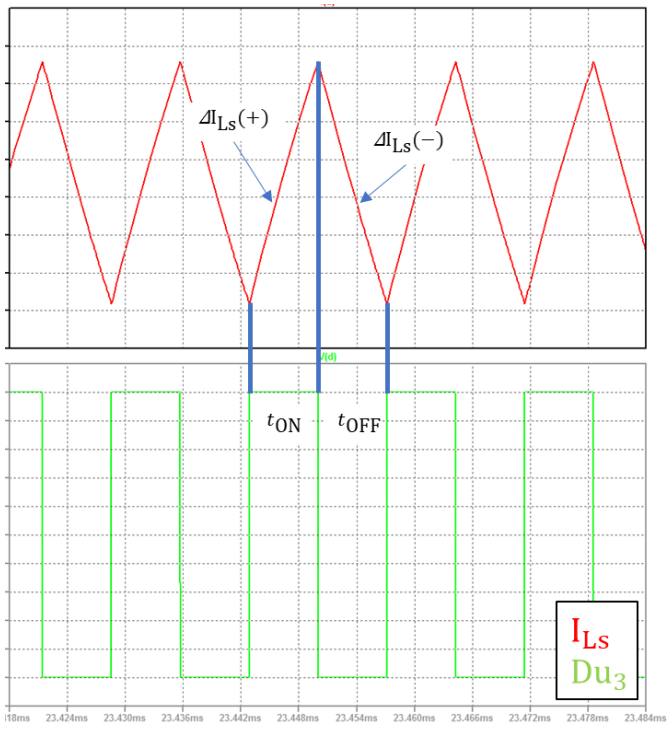

Figure 3. 7. Current Ripple through L_s.

The current increase and decrease are derived are shown again in equations 3.12 and 3.13. Where the increase of the current, $\Delta I_L(+)$, depend of the input voltage V_{DC} and the output voltage V_S, and the decrease of the current, $\Delta I_L(-)$, depend only of the input voltage V_{DC}.

$$\Delta I_L(+) = \frac{V_{DC} - V_S}{L_S} \cdot D \cdot T_S \quad \textbf{(3.12)}$$

$$\Delta I_L(-) = \frac{V_S}{L_S} \cdot (1 - D) \cdot T_S \quad \textbf{(3.13)}$$

From above equations D is the same as Du_3, this is the duty cycle. Because of the ON and OFF states there are two states in the inductor current and these must be equal during each switching period for CCM. Therefore $\Delta I_L(+)$ must be the same as $\Delta I_L(-)$.

If the above equations are expressed as function of V_S and solved for ΔI_L we get [33]:

$$\Delta I_L = I_{L\_PP} = \frac{V_{DC}}{L_S} \cdot D \cdot (1 - D) \cdot T_S \quad \textbf{(3.14)}$$

Note that ΔI_L is also the peak-to-peak value of the inductor current, I_{L_PP}.

It is possible to find the duty cycle for maximum I_{L_PP} by plotting this equation (3.13), shown in figure 3.8. The blue curve shown I_{L_PP} for different duty cycle values. The duty cycle for the maximum ripple current is 0.5.

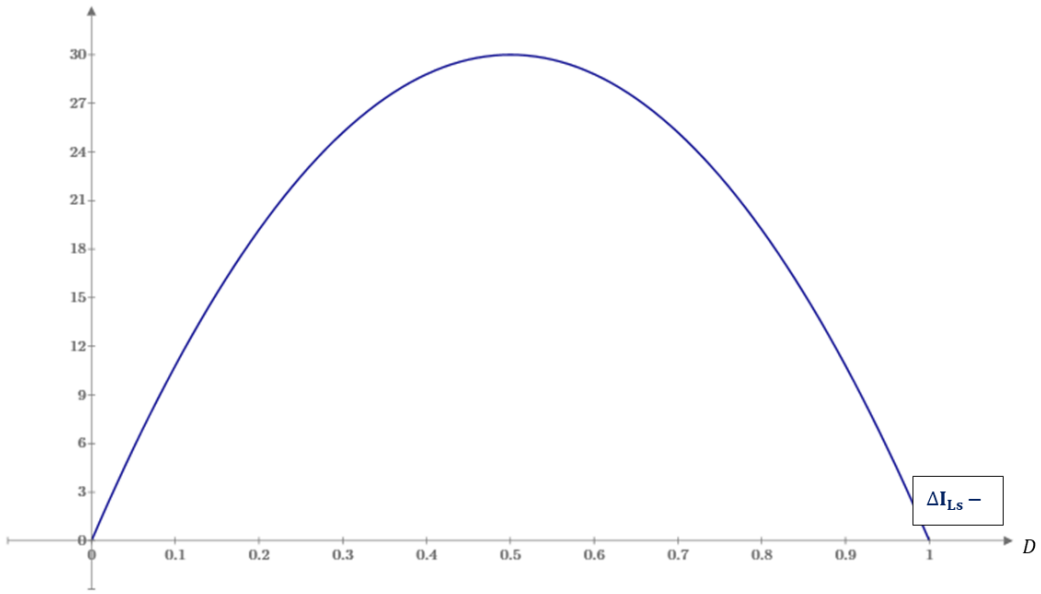

Figure 3. 8. Peak to peak inductor current versus duty cycle.

This result can also be obtained by deriving equation 3.13 with respect to D setting the resulting equation equal to zero. This derivation can be seen in equation 3.14.

$$\frac{V_{DC}}{L_S} \cdot (1 - 2 \cdot D) \cdot T_S = 0 \ \rightarrow D = 0.5 \quad \textbf{(3.15)}$$

Introducing this duty value in to equation in 3.13, the value of the maximum current ripple in CCM is expresses as:

$$\Delta I_{Ls,max} = \frac{V_{DC}}{4 \cdot L_S} \cdot T_S \quad \textbf{(3.16)}$$

To guarantee that the converter operated in CCM, we can now relate the $\Delta I_{Ls,max}$ to the $\Delta I_{Ls}(\%)$ given by the specifications and solving for the inductor:

$$L_S \geq \frac{V_{DC}}{4 \cdot \Delta I_L} \cdot T_S \quad \textbf{(3.17)}$$

The minimum inductor value is at maximum input voltage because it gives the maximum ΔI_{Ls}. In order to decoupling the voltage ripple in the DC capacitor it can be supposed that the inductor need to store the pulsating current going to this. That is the RMS value of the current obtained in equation 3.10. We can now introduce this current in to equation 3.16 and with the rest of specifications the corresponding inductor value is:

$$L_S \geq \frac{400V}{4 \cdot 30\% \cdot 24.14A \cdot 70kHz} = 197.26\mu H \quad \textbf{(3.18)}$$

It is possible to check the mode of operation in boost mode for the dimensioned inductor, simulating the circuit of figure 3.1. The result of figure 3.9 show that the inductor current never become zero. Although the current values are not the used in the calculus, note the opposite direction of the current.

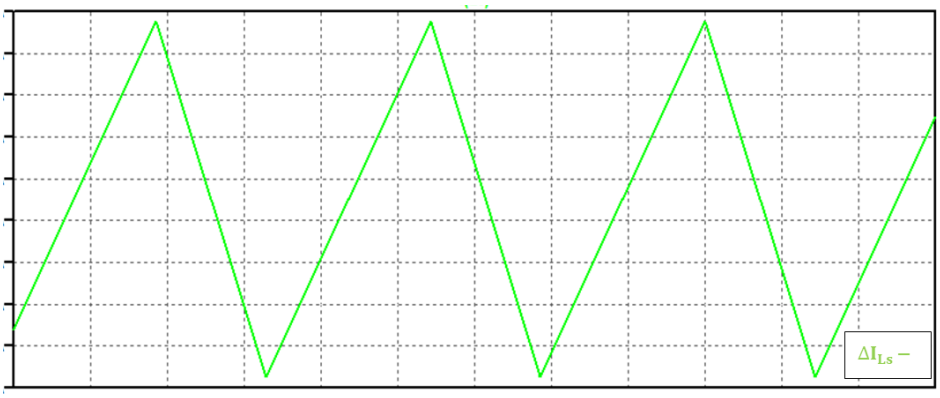

Figure 3. 9. Inductor Current in Boost mode of operation.

3.3.1. Peak Current.

The inductor must be able to sustain the following peak current:

$$I_{L\_P} = I_o + \frac{\Delta I_L}{2} = 27.8A \quad \textbf{(3.19)}$$

The allowed ripple current ΔI_L is specified as a percentage of the nominal output current, for example 30%.

3.3.2. Inductor's DC Resistance, R_L.

Due to the inductor's DC resistance the current through it causes power dissipation. There is also an additional power dissipation due to core loss. Anyway, the inductor must to maintain its inductance at the elevated operating temperature. Although the DCR value is usually given by the datasheet of a specific inductor, a limit for it can also be approximated from the output values assuming an acceptable power loss:

$$R_L = \frac{P_{DCR,loss}}{I_o^2} = \frac{5.6W}{(24.14A)^2} = 6.6m\Omega \quad \textbf{(3.20)}$$

3.4. Output Capacitor, C_S.

The output capacitor is used to store the energy coming from the ripple in the DC Link, thus the choice of this capacitor is an engagement with the C_{DC} capacitor value and the voltage ripple in the DC link, as the equation 3.8 shown.

Although the best way to choose the C_S capacitor is attending to the derivation in 3.2.3 there is other way when the converter work in buck mode. In this mode, the capacitor, C_s decrease the V_s voltage ripple due the inductor current ripple. Hence, the Buck circuit of figure 3.6 can be used to derivative alternative circuit.

The capacitor current can be estimated to be the same as the inductor current ripple, the AC inductor current, ΔI_L. The capacitor voltage ripple can then be related to the total charge contained in the positive portion of the waveform. Consider the circuit in figure 3.6, the inductor current has also a DC component, I_o, which must flow entirely through the battery. Figure 3.10 show the waveform of the capacitor, inductors and battery.

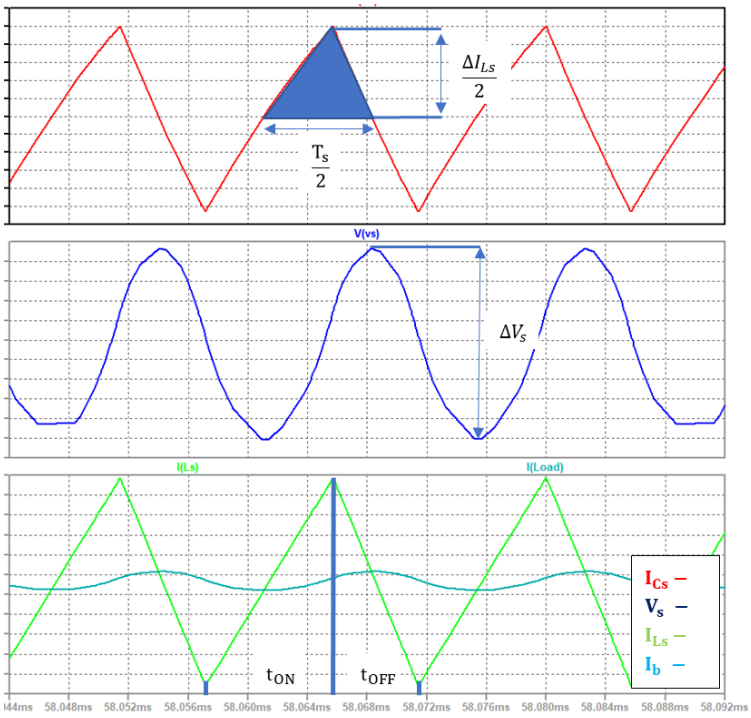

Figure 3. 10. Output Capacitor waveforms, load and inductor current.

The capacitor voltage increases from its minimum to its maximum when its current is positive, thus, the relations between charge Q and voltage for a capacitor is:

$$Q = C \cdot \Delta V_s \tag{3.21}$$

In addition, it is possible express the capacitor charge as the area of the positive portion of capacitor current, which is shown in blue triangle of figure 3.10.

$$Q = \frac{1}{2} \cdot \frac{T_s}{2} \cdot \frac{\Delta I_L}{2} \tag{3.22}$$

Combining equation 3.21 and 3.22, and rearranging, the C value is calculated as:

$$C = \frac{\Delta I_L}{8 \cdot f_s \cdot \Delta V_s} = \frac{30\% \cdot 24.14A}{8 \cdot 70kHz \cdot 0.25 \cdot 200V} = 0.3\ \mu F \tag{3.23}$$

3.4.1. RMS Current, $I_{Cs,RMS}$.

Ripple current flowing through a capacitor's equivalent series resistance causes power dissipation in the Capacitor and consequently a temperature increase which must be avoided as well as possible [32]. To control the temperature, the ripple current must to be know, that is the RMS value. For CCM output capacitor current waveform of figure 3.10.

$$\mathrm{I_{Cs,RMS}} = \Delta \mathrm{I_L} \cdot \frac{\sqrt{3}}{6} = 0.3 \cdot 24.14\mathrm{A} \cdot \frac{\sqrt{3}}{6} = 2\mathrm{A} \tag{3.24}$$

3.4.2. Equivalent Series Resistance, R_{Cs}.

Practical capacitors, as used in electric circuits, are not ideal components with only capacitance. They can be treated, to a very good degree of approximation, as being ideal capacitors in series with a resistance. This is the equivalent series resistance (ESR). Since it is a AC resistance, it can be calculated as:

$$\mathrm{R_{Cs}} \leq \frac{\Delta \mathrm{V_{Rcs}}}{\Delta \mathrm{I_L}} = \frac{0.05 \cdot 200\mathrm{V}}{0.3 \cdot 24.14\mathrm{A}} = 1.4\ \Omega \tag{3.25}$$

Note that the voltage ripple is split between the capacitor and its ESR to have a total ripple of 30%.

3.5. LCL Filter.

As it was introduced in section 2.5 of chapter 2 the LCL filter works as a low pass filter. Depending of the component values (capacitance and inductances) the cutting frequency will be in low or high.

Although there are different ways to design a LCL filter we will follow the energy flux as a design criterion to get a good efficiency. The components of a LCL filter are shown in the circuit of figure 3.11.

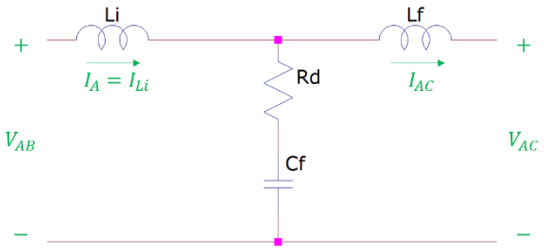

Figure 3. 11. LCL Filter

3.5.1. Capacitor C_f.

First of all, the capacitor $\mathrm{C_f}$ will consume reactive power, so its capacitance will be limited by the total in the inverter.

That means that the maximum current in the capacitor must be a portion of the nominal current (at full load). If we set this amount a 5% of the nominal load:

$$\mathrm{I_{Cf}} \leq 0.05 \cdot \frac{\mathrm{P_o}}{\mathrm{V_o}};\ \mathrm{I_{Cf}} = 0.05 \cdot \frac{7600\ \mathrm{Kw}}{230\ \mathrm{V}} = 1.652\ \mathrm{A} \tag{3.26}$$

Them the capacitor impedance will be the output AC voltage divided by the current in 3.22 since the capacitor is in parallel with the ac load.

$$\mathrm{Z_{Cf}} = \frac{\mathrm{I_{Cf}}}{\mathrm{V_o}};\ \mathrm{I_{Cf}} = \frac{230\ \mathrm{V}}{1.652\ \mathrm{A}} = 193.21\ \Omega \tag{3.27}$$

Once the capacitor impedance is known, it is easy solve the capacitance value from equation 3.24, where ω_1 is the fundamental frequency in rad/s of the load.

$$Z_{Cf} = \frac{1}{\omega_1 \cdot C_f};\ C_f = \frac{1}{\omega_1 \cdot Z_{Cf}} = \frac{1}{2 \cdot \pi \cdot 50\ \text{Hz} \cdot 193.21\ \Omega} = 22.865\ \mu\text{F} \quad \textbf{(3.28)}$$

The capacitor, C_f, also has an equivalent resistance whose value is critical since this works as a damping resistance. Although most of the time an additional series resistance is added.

The damping resistance, R_d increase the low amortiguation which come from the high-quality factor, Q_f. A high quality factor is a charatereistic in LC and LCL filters, this has low amortiguation at the resonant frequency which can instablilize the system.

A high resistance, R_d, value will decrease notability the oscillation at resonance frequency but will also decrease the efficiency of the system [22].

A good resistance value would be what keeps the attenuation in the current loop blow of 0dB, so different values of R_d are plot in figure 3.12 where $R_d = 50\ \Omega$ is chosen to have a good attenuation at the required frequency.

3.5.2. Inverter Side Inductance, L_i.

The inductance of the inductor at the inverter side, L_i, is calculated in similar way to the capacitor, but consider the inductor voltage when the inverter voltage at the output is the nominal voltage.

In the first place, we assume an impedance low or the same as the 5% of the load nominal impedance:

$$Z_{L_I} \leq 0.05 \cdot Z_{Load};\ Z_{L_I} = 0.05 \cdot \frac{{V_o}^2}{P_o} = 0.348\ \Omega \quad \textbf{(3.29)}$$

The impedance magnitude of an inductor is defined as 3.26.

$$Z_{L_I} = \omega_1 \cdot L_i \quad \textbf{(3.30)}$$

From where the inductance value can be easily solved:

$$L_i = \frac{Z_{L_I}}{\omega_1} = \frac{0.348\ \Omega}{2 \cdot \pi \cdot 50\ \text{Hz}} = 1.108\ \text{mH} \quad \textbf{(3.31)}$$

3.5.3. Load Side Inductance, L_f.

Lastly, the inductance at load side is selected from the resonance frequency equation.

$$\omega_{res} = \sqrt{\frac{L_i + L_f}{C_f \cdot L_i \cdot L_f}} \quad \textbf{(3.32)}$$

The resonance frequency should be located at less 10 times the load frequency and an halft of the switching frequency.

$$10 \cdot \omega_1 \leq \omega_{res} \leq \frac{\omega_s}{2} \quad \textbf{(3.33)}$$

With this criterion we avoid the resonance problems in the low and high frequency range of the harmonic spectrum.

If we set the resonance frequency at 10 KHz the inuctor value is:

$$\omega_{res} = \sqrt{\frac{L_i + L_f}{C_f \cdot L_i \cdot L_f}};\ L_f = \frac{1.108\ \text{mH}}{((2 \cdot \pi \cdot 10\ \text{KHz})^2 \cdot 1.108\ \text{mH} \cdot 22.865\ \mu\text{F}) - 1} = 11.19\mu\text{H} \quad \textbf{(3.34)}$$

Although in chapter 5 the harmonic spectrum is discuses as well as the output waveform, in figure 3.12 one can be see the frequency response obtained by LTspice.

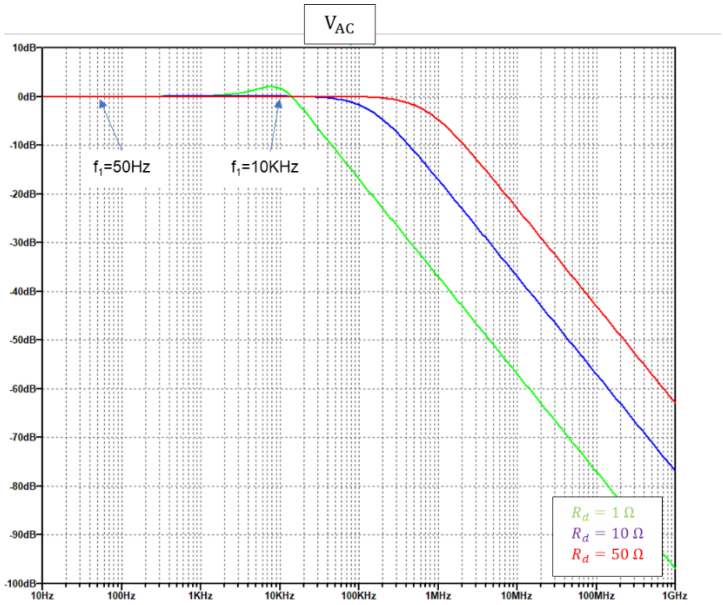

Figure 3. 12. LCL filter frequency response.

The simulation was done for 3 different values of R_d,where for the blue and red values (20 Ω and 50 Ω respectability) have a low response in despite the green value where the resonance frequency is higher. On another hand, the resonance frequency is situated at 10 kHz while the fundamental frequency of the load (50Hz) is not affected.

Chapter 4.

Modelling and Control Strategies

Chapter 4. Modelling and Control Strategies

4.1. Introduction.

This chapter 4 present various relevant control strategies and their analysis. For controlling the standalone PV system three independent control loops are used; DC-DC control, inverter input voltage control and output voltage control. Section 4.2 describes the details about the inverter modelling and its transfer functions, as well as the two control strategies purposed. Also, this section gives clear analysis of the transfer functions and their stability. Section 4.3 describes the bidirectional DC-DC converter control technique and the state-space averaging of the converter. Furthermore, this section includes stability analysis of the proposed converter control loop through bode diagrams. Section 4.4 introduce an alternative control strategy.

4.2. Single Phase Inverter Control.

In this work, a single phase VSI is used to convert DC power into AC power. To provide electrical power to any load or appliances, the inverter converts the DC bus voltage to a single-phase AC voltage with appropriate amplitude and frequency. To ensure a desired and stable input or output voltage, a control strategy is need in the inverter.

However, it would be extremely difficult to describe the numerous control strategy of the inverters, since the inverters are currently employed in very wide variety of cases in which different parameters to control are needed.

Here a current mode control is used Note that this is just the name of the control strategy which may not reflect the actual electrical value to control). There are two kinds of current control according to [34]:

- Linear Current Control: Multi loops with PI, PID…
- Nonlinear Current Control: Hysteresis Control.

In this project a linear current control is chosen where 2 loops are designed, an inner current loop and an outer voltage loop.

Although an input voltage control is briefly described at the end of this section (4.2.4), the inverter control is developed to control the output voltage.

The discussion of the controllers for the inverter can be divided into three parts: 1) average modelling and small signal modelling of the inverter, 2) the inner inductor current controller and 3) the outer output voltage controller. The purpose loops with the controllers can be seen in the block diagram of figure 4.1.

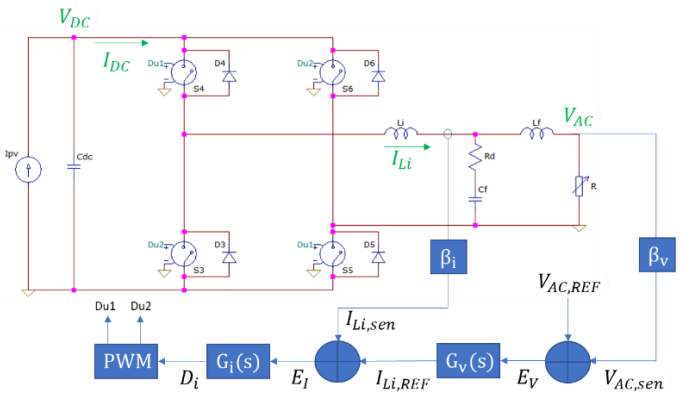

Figure 4. 1. Control strategy for single phase VSI.

Before designing the controller itself we must find a model which describes the inverter, preferably as a transfer function. To derive this transfer function, firstly an average circuit is developed, secondly the small signal circuit is derived and thirdly the transfer functions are calculated.

4.2.1. Inverter Average Model.

Due the behavior of the switched converters (DC/DC or AC/CD) is no-lineal, they should be linearized in an operation point before to apply linear control techniques. Although there are other techniques we will use the cycle by cycle averaging to linearize the inverter.

First of all, the switching functions are developing from the circuit in figure 4.2, a).

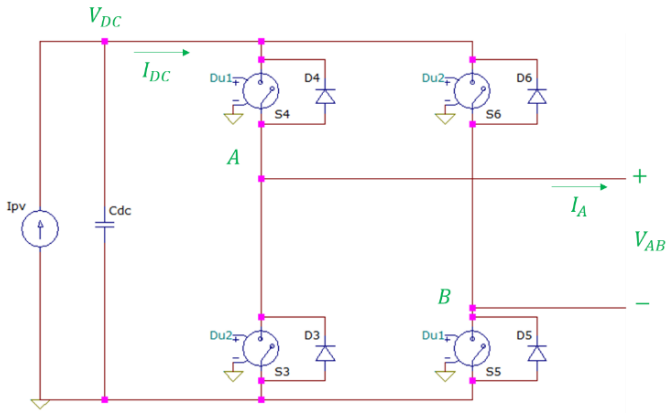

S_A	1	S4=1	S3=0
	0	S4=0	S3=1
S_B	1	S6=1	S5=0
	0	S6=0	S5=1

a) **b)**

Figure 4. 2. a) Inverter Switches circuit, b) Switching functions.

The two main switching rules were explained in section 3.4.2. Thus, the two switches of a same branch should not be open or closed at the same time. In this way the switching functions of each branch can be defined according to the table on figure 4.2, where the branch S_A is 1 when S4 switch ON and 0 when S4 is OFF. The S_B branch has the same functions. Therefore, one can define V_{AB} as:

$$V_{AB} = V_{DC} \cdot (S_A - S_B) \quad \textbf{(4.1)}$$

Similarly, the output current I_A

$$I_{DC} = (S_A - S_B) \cdot I_A \cdot \quad \textbf{(4.2)}$$

The above equations justify the inverter output voltage and current. If S4 is ON ($S_A = 1$) and the switch S5 is also ON ($S_B = 0$), then, the output voltage will be V_{DC} (from the

equation 4.1) since the branch S_A is 1 and S_B is 0. For the opposite situation the output voltage would be $-V_{DC}$ and analogous for the current (equation 4.2).

So, the circuit can be simplified as in figure 4.3, with only two switches. But this circuit is not yet a linear circuit.

To get a linear circuit the average model of the switching function is developing. By using cycle by cycle averaging the no-linear component, introduced by the switches, is removed.

If the switching frequency is much faster than the fundamental frequency ($f_s \gg f_1$), it can be assumed that the output waveform is constant.

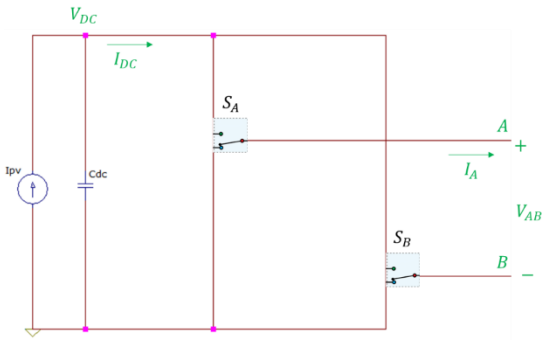

Figure 4. 3. Inverter with simplified switches.

Thus, studying on switching period, one can realise than from one switching period to another, the fundamental wave form does not change. This can be seen in figure 4.4 where V_{AO} is equal to V_{AB} if the B branch is connected to the same ground than V_{DC}.

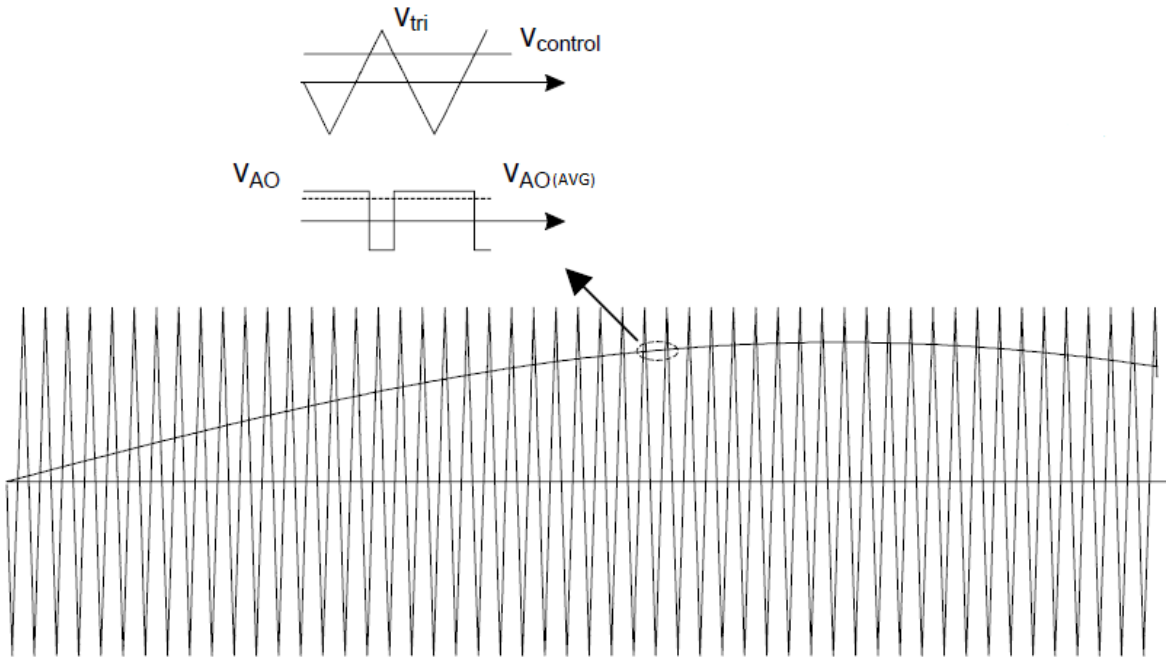

Figure 4. 4. Cycle by cycle averaging.

From figure 4.4 $V_{control}$ is the sinusoidal signal and V_{tri} the carrier triangular signal, according to the SPWM as explained in chapter 3. The average value of a switching function, A or B, is calculated:

$$d_k(t) = \frac{1}{T_s} \cdot \int_0^{d_k \cdot T_s} S(t) \cdot dt \quad (4.3)$$

Then, the average value of the switching functions is the duty cycle value (for one switching period). The duty cycle has the following expression:

$$d_k(t) = 0.5 + 0.5 \cdot m_a \cdot \sin(\omega_1 \cdot t) \quad (4.4)$$

Equation 4.4 follows the sinusoidal law (SPWM). The second term (+0.5) ensures only positive values of the duty cycle.

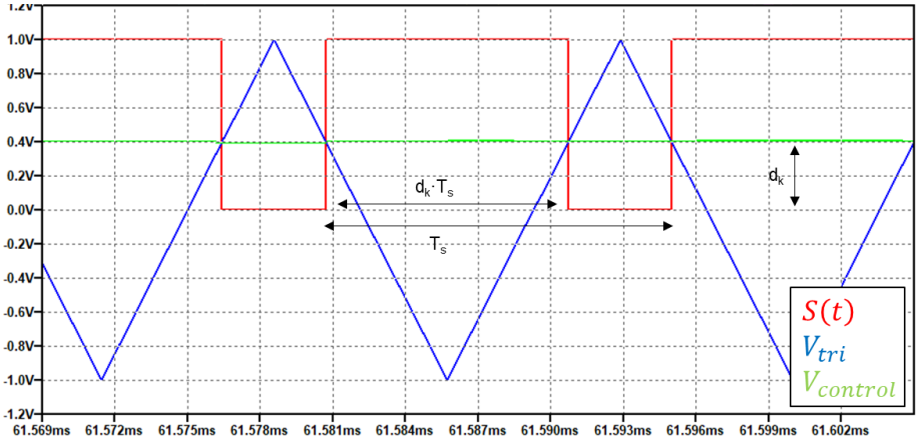

Figure 4. 5. Duty cycle waveform.

Now a linear circuit is obtained (figure 4.6.) where the switches are replaced by transforms with a ratio of $1: d_k$.

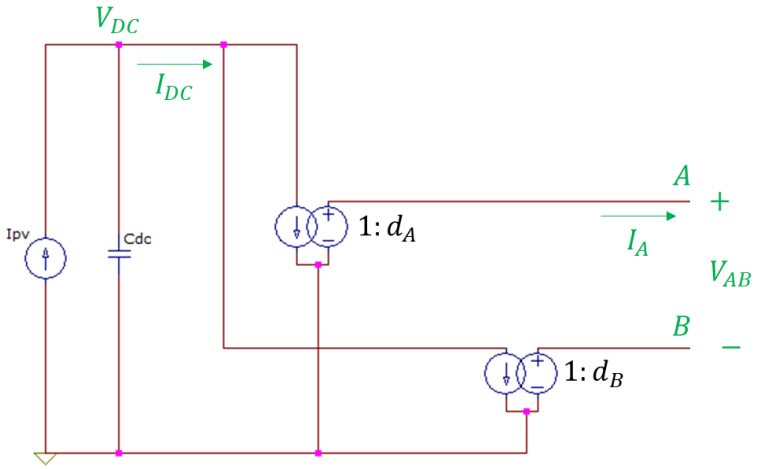

Figure 4. 6. Inverter with average switches.

After that, the output voltage (V_{AC}) can be developed as in equation 4.5:

$$\overline{V}_{AB}(t) = V_A(t) - V_B(t) = [d_A(t) - d_B(t)] \cdot V_{DC} \quad (4.5)$$

In bipolar modulation, each branch work complementary to the other and we can approximate the $d_B(t)$ function as:

$$d_{B,bip}(t) = [1 - d_A(t)] \quad (4.6)$$

For unipolar modulation $d_B(t)$ can be expressed as:

$$d_{B,unip}(t) = 0.5 + 0.5 \cdot m_a \cdot \sin(\omega_1 \cdot t - \pi) \quad (4.7)$$

Now by introducing equation 4.6 into 4.5, one gets:

$$\bar{V}_{AB}(t) = \left[d_A(t) - [1 - d_A(t)]\right] \cdot V_{DC} = [2 \cdot d_A(t) - 1] \cdot V_{DC} \quad (4.8)$$

Equation 4.8 is expresses with only the duty cycle of branch A, as the branches are complementary the equation is the same when this is rearranged for the duty of branch B. So, we can introduce a new duty cycle functions as:

$$D'_i(t) = [2 \cdot d_A(t) - 1] \quad (4.9)$$

Where the subscript "i" means the inverter duty cycle because another duty cycle will be developed for the DC-DC converter.

The current relation conversion can also be expressed as in equation 4.10, which shows the DC side current as function of the duty cycle:

$$\bar{I}_{DC}(t) = [2 \cdot d_A(t) - 1] \cdot I_A \quad (4.10)$$

In this way the circuit on figure 4.6 can be further reduced to only include one ratio $(2 \cdot d_k(t) - 1)$. The final average circuit of the inverter is shown in figure 4.7:

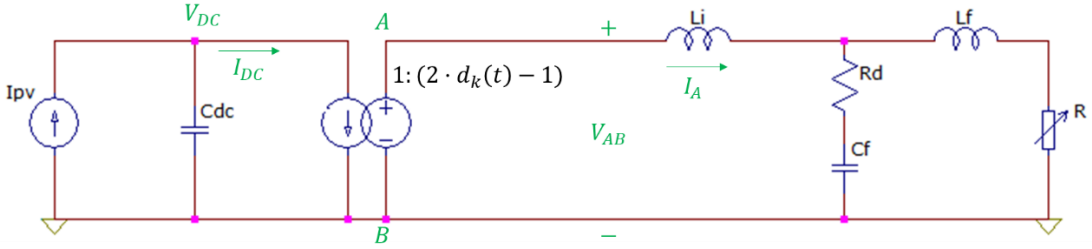

Figure 4. 7. Final average circuit model of the inverter.

Seeing the above circuit, one realizes that this is similar to a buck converter circuit (when the filter is added) but with a DC operation point which is a time varying signal.

The circuit in figure 4.7 can be checked by comparing with the switching circuit in LTspice where it can be se that the outputs waveforms in the average model are the average value of the output waveforms in the switches model.

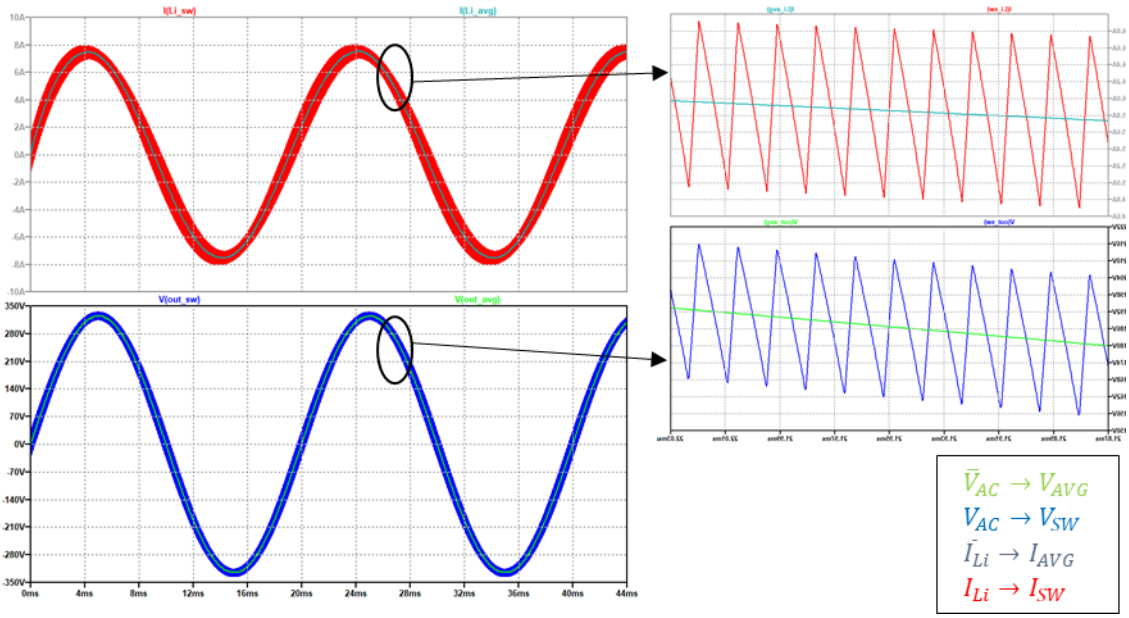

Figure 4. 8. Average waveforms compared to switches waveforms

In addition, the justification on figure 4.7 can also be done by an analytical way. By replacing equation 4.5 into 4.9, the average output voltage is:

$$\bar{V}_{AB}(t) = [2 \cdot (0.5 + 0.5 \cdot m_a \cdot \sin(\omega_1 \cdot t)) - 1] \cdot V_{DC} = V_{DC} \cdot m_a \cdot \sin(\omega_1 \cdot t) \quad \textbf{(4.11)}$$

It can be seen in equation 4.11 the output voltage is the same as the fundamental output voltage. It is important to note that equation 4.1 does not define the real output voltage, it only defines the average value when no other factors are considered.

For the current a similar derivation can be developed, replacing equation 4.12 and 4.4 into 4.10. The current, in the DC side and the AC side, depends on the load, if the load is linear the AC current will be sinusoidal with fundamental frequency and with amplitude and phase dependent of the load impedance. This output current (ac side) has the form of the equation 4.12:

$$\bar{I}_A(t) = I_A \cdot \sin(\omega_1 \cdot t - \varphi_1) \quad \textbf{(4.12)}$$

For the unipolar modulation the same equation is obtained when 4.4 and 4.7 are introduced into 4.5.

The average model can be used to get faster simulations, to see the frequency response and to design the control loops. However, it is not appropriate to simulate real behavior as power losses, switching noise and harmonic distortion.

4.2.2. Inverter Small Signal Model.

In order to get the plant transfer functions and the frequency response a small signal circuit model is developed.

We now need to perform perturbation and linearization and then the PWM switch model will be in the desired form, i.e., linearized about a given operating point.

The main idea of perturbation and linearization is assuming an operating point and introducing small variations about that operating point. For example, we assume that each averaged variable, x, can be represented as:

$$x = X + \hat{x} \quad \textbf{(4.13)}$$

where X is the value of the variable at the operation point (either a constant value or a value with the same fundamental frequency) and $\hat{x}$ is the small-signal variation around the operation point. Thus, the voltage and current equations (equations 4.8 and 4.10) can be rewritten as 4.14 and 4.15 respectively:

$$V_{AB} + \hat{v}_{AB} = \left[2 \cdot (D_i + \hat{d}_i) - 1\right] \cdot (V_{DC} + \hat{v}_{DC}) \quad \textbf{(4.14)}$$

$$I_{DC} + \hat{i}_{DC} = \left[2 \cdot (D_i + \hat{d}_i) - 1\right] \cdot (I_{Li} + \hat{i}_{Li}) \quad \textbf{(4.15)}$$

Where I_{Li} , the current through the inductor L_i is the same as I_A.

Now, separate steady-state quantities from ac quantities and also drop products of ac quantities because the variations are assumed to be small and products of two small quantities are assumed to be negligible. We arrive at the steady-state and ac relationships or, in other words, the dc and small signal model:

- *DC equations or operation point (OP)*

$$V_{Ab} = [2 \cdot D_i - 1] \cdot V_{DC} \quad \textbf{(4.16)}$$

$$I_{DC} = [2 \cdot D_i - 1] \cdot I_{Li} \quad \textbf{(4.17)}$$

- *Small signal equations.*

$$\hat{v}_{AC} = \hat{v}_{DC} \cdot (2 \cdot D_i - 1) + 2 \cdot V_{DC} \cdot \hat{d}_i \quad (4.18)$$

$$\hat{i}_{DC} = \hat{i}_{Li} \cdot (2 \cdot D_i - 1) + 2 \cdot I_{Li} \cdot \hat{d}_i \quad (4.19)$$

Finally, the small signal circuit can be built by replacing the transformer in figure 4.7 circuit with voltage and current sources which satisfy equations 4.18 and 4.19. This circuit is shown in figure 4.9.

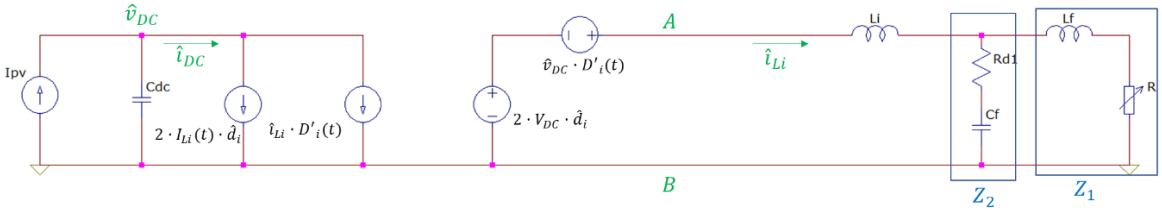

Figure 4. 9. Small signal inverter model.

4.2.3. Inverter transfer functions.

The transfer functions what is to be controlled to correct by the controller depends on the control strategy and how we configure the control loops. The control loops shown in figure 4.1 can be plotted in a block diagram form as shown in figure 4.10. Where, in addition, the gain of the PWM is added ($F_{m,i}$):

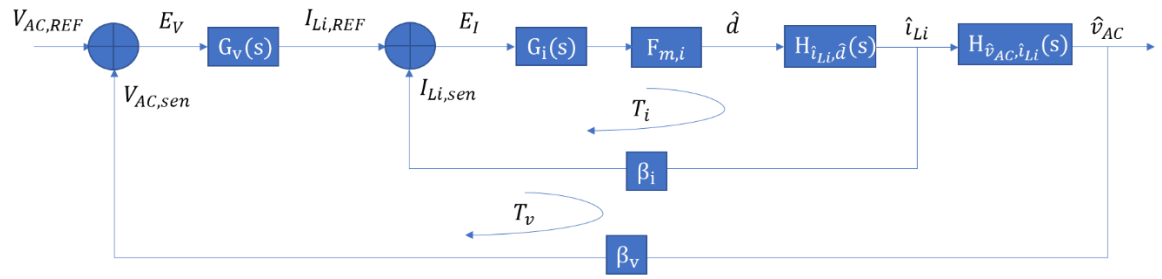

Figure 4. 10. Control block diagram for inverter.

There are two loops in figure 4.10, an inner current loop, T_i and an outer voltage loop T_v.

For the inner loop it is considered that the voltage controller will give a current reference. The current error (from comparing the current reference with the sensed current) will be compensated with a proportional integrator derivative (PID) controller which (with the F_m gain) gives the duty signal to the switches. So, the transfer function to be compensated in this inner loop is the Inductor current, $\hat{i}_{Li}$ to duty signal, $\hat{d}$. $H_{\hat{i}_{Li},\hat{d}}(s)$.

The outer transfer function depends on the output of the inner loop. Because $\hat{i}_{Li}$ is the output of the inner loop, the transfer function of the outer loop must be the output voltage $\hat{v}_{AC}$ to inductor current, $\hat{i}_{Li}$ transfer function, $H_{\hat{v}_{AC},\hat{i}_{Li}}(s)$. That is, the AC voltage at output of the final control loop.

To find the transfer functions we analyse the circuit in figure 4.9 for $\hat{v}_{DC} = 0$ since input voltage is supposed constant. Using Kirchhoff's laws, we get:

- *Output impedance.*

$$\hat{Z}_{O,i} = (Z_2 \| Z_1) + L_i;$$

$$\hat{Z}_{O,i} = \frac{s^3 \cdot C_f \cdot L_f \cdot L_i + s^2 \cdot C_f \cdot (L_i \cdot R + L_i \cdot R_d + L_f \cdot R_d) + s \cdot (L_i + L_f + C_f \cdot R_d \cdot R) + R}{s^2 \cdot C_f \cdot L_f + s \cdot C_f \cdot (R + R_d) + 1} \quad \textbf{(4.20)}$$

- *Inductor current- duty cycle transfer function.* $H_{\hat{\imath}_{Li},\hat{d}}(s)$

$$\frac{2 \cdot V_{DC} \cdot \hat{d}_i}{\hat{Z}_{O,i}} = \hat{\imath}_{Li};$$

$$H_{\hat{\imath}_{Li},\hat{d}}(s) = \frac{\hat{\imath}_{Li}}{\hat{d}_i}\bigg|_{\hat{v}_{DC}=0} = \frac{2 \cdot V_{DC}}{\hat{Z}_{O,i}} \quad \textbf{(4.21)}$$

- *Output voltage - Output current transfer function.* $H_{\hat{v}_{AC},\hat{\imath}_{Li}}(s)$

$$H_{\hat{v}_{AC},\hat{\imath}_{Li}}(s) = \frac{\hat{v}_{AC}}{\hat{\imath}_{Li}}\bigg|_{\hat{v}_{DC}=0} = \frac{R \cdot (Z_2 \| Z_1)}{Z_1} =$$

$$= \frac{s^2 \cdot C_f \cdot L_f \cdot R + s \cdot C_f \cdot (R^2 + R_d) + R}{s^2 \cdot C_f \cdot L_f \cdot R_d + s \cdot (L_f + \cdot C_f \cdot R_d \cdot R) + 1} \quad \textbf{(4.22)}$$

Once the plant transfer functions are found (equation 4.21 and 4.22), the bode diagram can be plotted by the values of C_f, L_f, L_i obtained in chapter 3 and in addition a load of $R = 50\Omega$ and a $V_{DC} = 400V$. It is possible also to check the bode diagram with the one obtained by simulation as figure 4.11 shows.

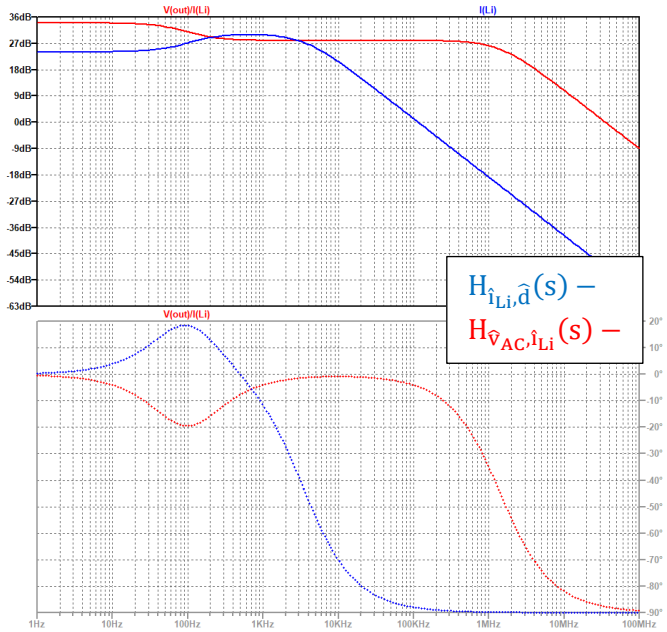

Figure 4. 11. $H_{\hat{\imath}_{Li},\hat{d}}$ obtained from simulation of the small signal circuit in LTspice

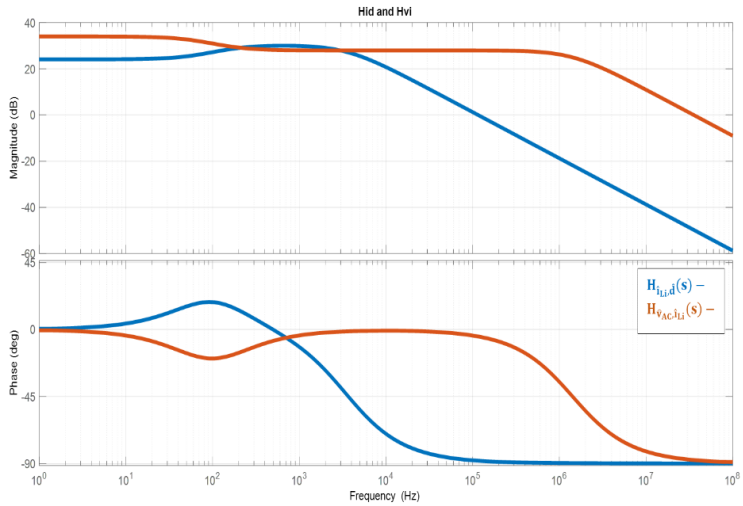

Figure 4. 12. Obtained from the equations.

The bode diagrams in figure 4.11 have an initial gain of 24.08 dB for $\mathrm{H}_{\hat{\imath}_{\mathrm{Li}},\hat{d}}(s)$ and 33.97dB for $\mathrm{H}_{\hat{v}_{\mathrm{AC}},\hat{\imath}_{\mathrm{Li}}}(s)$, whereas the bode diagrams in figure 4.12 have an initial gain of 24.1dB and 34dB for $\mathrm{H}_{\hat{\imath}_{\mathrm{Li}},\hat{d}}(s)$ and $\mathrm{H}_{\hat{v}_{\mathrm{AC}},\hat{\imath}_{\mathrm{Li}}}(s)$ correspondingly. The cutting frequencies are 114.32KHz and 35.33 MHz for $\mathrm{H}_{\hat{\imath}_{\mathrm{Li}},\hat{d}}(s)$ and $\mathrm{H}_{\hat{v}_{\mathrm{AC}},\hat{\imath}_{\mathrm{Li}}}(s)$ respectively in simulated bode diagrams, as well as, in the calculated bode diagram are 115 KHz and 35.5 MHz. Therefore, the loops can be designed since the transfer functions correctly describe the system dynamics.

4.2.4. Inner current loops.

Since the current loop is the inner loop we need to calculate it first, before we analyze the outer voltage loop.

To tune the PID regulator constants, we will analyze the transfer function from equation 4.21. Inserting parameters values, simplifying and rearranging in pole-zero form, we get the equation shown in 4.23:

$$\mathrm{H}_{\hat{\imath}_{\mathrm{Li}},\hat{d}}(s) = \frac{7.273 \cdot 10^5\ (s + 437.4)}{(s + 2.222 \cdot 10^4)(s + 892.6)} = \frac{16.041\ (2.286 \cdot 10^{-3} \cdot s + 1)}{(4.5 \cdot 10^{-5} \cdot s + 1)(1.12 \cdot 10^{-3} \cdot s + 1)} \quad \textbf{(4.23)}$$

Now, by using the IMC method of [35], one can compare the transfer function in 4.23 with the correspondently on table 11.1 of reference [35]:

$$\tilde{\mathrm{G}}(s) = \frac{\mathrm{K} \cdot\ (\tau_3 \cdot s + 1) \cdot e^{-\theta \cdot s}}{(\tau_1 \cdot s + 1) \cdot (\tau_2 \cdot s + 1)} \quad \textbf{(4.24)}$$

According to the table and neglecting the term $e^{-\theta \cdot s}$,because this only represent the time delay, the values of equation 3.25 are:

$\mathbf{K}$	$\mathbf{16.041}$
$\boldsymbol{\tau_1}$	$4.5 \cdot 10^{-5}$
$\boldsymbol{\tau_2}$	$1.12 \cdot 10^{-3}$
$\boldsymbol{\tau_3}$	$2.29 \cdot 10^{-3}$

Table 4. 1.Transfer function gain, poles and zero constants.

The PID regulator has the following transfer functions:

$$\mathrm{PID}(s) = K_p \cdot \left(1 + \frac{1}{\tau_I \cdot s} + \tau_D \cdot s\right) \tag{4.25}$$

Where if we use the IMC tuning method the parameters should be set to [35]:

$$K_p = \frac{\tau_1 + \tau_2 - \tau_3}{K \cdot (\tau_C + \theta)} \tag{4.26}$$

$$\tau_I = \tau_1 + \tau_2 - \tau_3 \tag{4.27}$$

$$\tau_D = \frac{\tau_1 \cdot \tau_2 - (\tau_1 + \tau_2 - \tau_3) \cdot \tau_3}{\tau_1 + \tau_2 - \tau_3} \tag{4.28}$$

For the proportional constant equation 4.26 τ_C is the desired time response, as a rule of thumb we can chose this constant as:

$$\frac{\tau_{dom}}{5} \leq \tau_C \leq \frac{\tau_{dom}}{2} \tag{4.29}$$

Where τ_{dom} is the dominating time constant which decides the response time of the process $\tilde{G}(s)$ and $H_{\hat{i}_{Li},\hat{d}}(s)$ is relatively safe since its phase only goes to -90º, we can therefore try a quite aggressive controller:

$$\tau_C = \frac{\tau_{dom}}{4} = \frac{\tau_2}{4} = 2.8 \cdot 10^{-4} \tag{4.30}$$

That $\tau_C = 2.8 \cdot 10^{-4}$ means that the controller is designed to give a response time of 280 µs.

So, K_p is:

$$K_p = \frac{4.5 \cdot 10^{-5} + 1.120 \cdot 10^{-3} - 2.286 \cdot 10^{-3}}{16.041 \cdot (2.8 \cdot 10^{-4})} = -0.25 \tag{4.31}$$

We get a negative K_p, which we know it cannot be since overall loop gain must be positive.

The method failed because the zero time constant τ_3 is dominating. The system with a dominating zero leads to a faster response and overshot to step response. Figure 4.13 compares the two systems, the true one (with the zero) and the one without the zero.

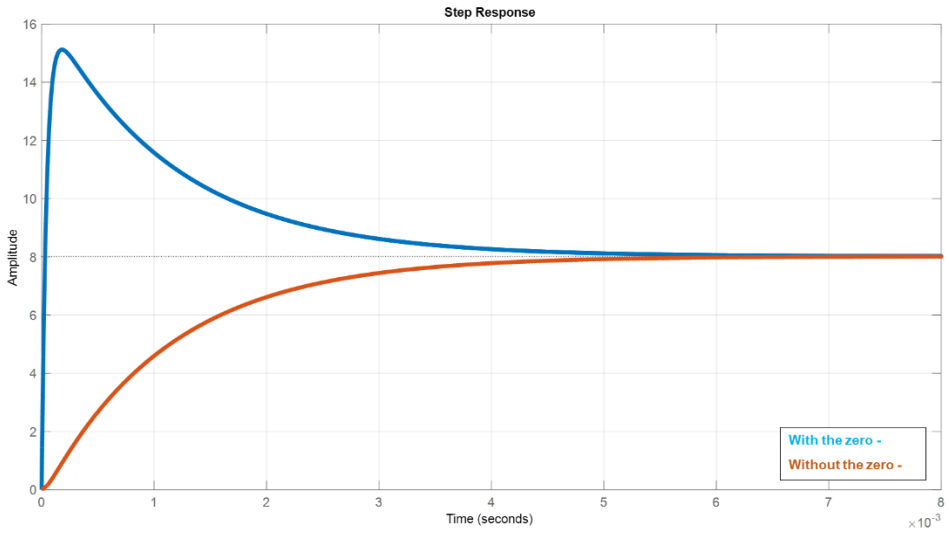

Figure 4. 13. Step response of $H_{\hat{i}_{Li},\hat{d}}(s)$ with (blue) and without (red) the dominant zero.

As the IMC method failed for our process function we will try to disregard the dominant zero in the transfer function. This should give a functional controller, but it may be a bit too aggressive; but we can adjust that based on simulations afterwards. Thus, the transfer functions to compensate is expressed in equation 4.32.

$$H_{\hat{i}_{Li},\tilde{d}}^{new}(s) = \frac{16.041}{(4.5 \cdot 10^{-5} \cdot s + 1)(1.120 \cdot 10^{-3} \cdot s + 1)} \quad (4.32)$$

Comparing the new plant transfer functions with the one found in table 11.1 of reference [35]:

$$\tilde{G}(s) = \frac{K}{(\tau_1 \cdot s + 1) \cdot (\tau_2 \cdot s + 1)} \quad (4.33)$$

The new parameters of the PID regulator are now:

$$K_p = \frac{\tau_1 + \tau_2}{\tau_C} \quad (4.34)$$

$$\tau_I = \tau_1 + \tau_2 \quad (4.35)$$

$$\tau_D = \frac{\tau_1 \cdot \tau_2}{\tau_1 + \tau_2} \quad (4.36)$$

Although the zero has been avoided to set the PID constant, it is always there in the true transfer function, so the controller should not be aggressive. Thus, the response time constant is settled to:

$$\tau_C = \tau_2 \quad (4.37)$$

The parameters of the PID regulator are then:

$$K_p = 0.065 \quad (4.38)$$

$$\tau_I = 1.2 \cdot 10^{-3} \quad (4.39)$$

$$\tau_D = 43.27 \cdot 10^{-6} \quad (4.40)$$

The open loop of the inner current loop, T_i is calculated from the block diagram in figure 4.10 as:

$$T_{i,OL} = G_{i,i}(s) \cdot H_{\hat{v}_{AC},\hat{i}_{Li}}(s) \cdot F_m \quad (4.41)$$

Where the F_m has the following expression:

$$F_m = \frac{1}{V_{PP,tri}} \quad (4.42)$$

We suppose a $V_{PP,tri}$ of 1V.

Finally, the closed loop of the current loop is described as:

$$T_{i,CL}(s) = \frac{T_{i,OL}}{1 + T_{i,OL}} \quad (4.43)$$

Simplifying and rearranging to zero-pole form the current closed loop has the following transfer functions and bode diagram:

$$T_{i,CL}(s) = \frac{0.671\ (s + 437.4)}{(s + 293.5)} = \frac{(2.286 \cdot 10^{-3} \cdot s + 1)}{(3.407 \cdot 10^{-3} \cdot s + 1)} \quad (4.44)$$

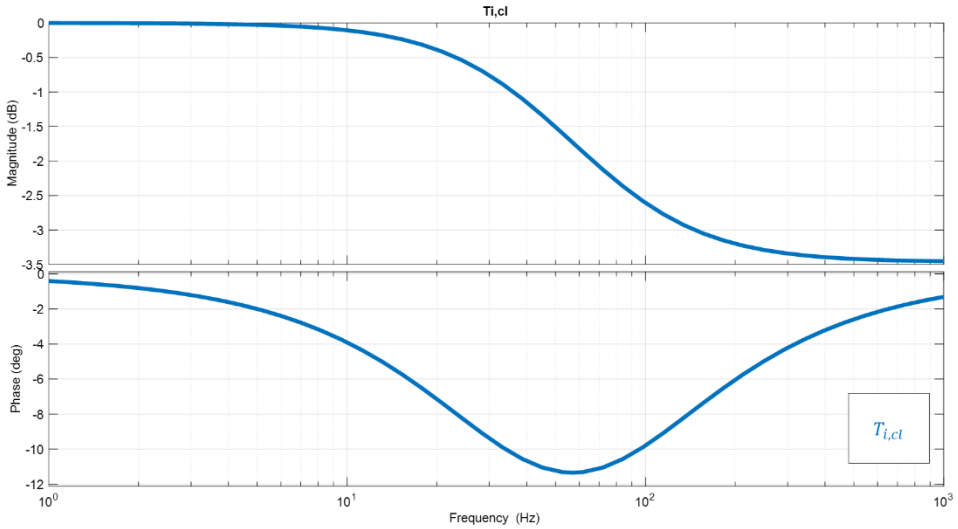

Figure 4. 14. Frequency response of the inner closed loop.

The closed loop transfer function (equation 4.44) becomes a lead-lag function with a slight dominating lag, $\tau_p > \tau_z$.

If the K_p of the PI controller increase the transfer function becomes theoretically 1 when $K_p \to \infty$ because of $\tau_p = \tau_z$. See the following table and figure.

$\mathbf{K_p}$	$\mathbf{T_{i,CL}(s)}$
$\mathbf{2 \cdot K_p}$	$\frac{(2.286 \cdot 10^{-3} \cdot s + 1)}{(2.846 \cdot 10^{-3} \cdot s + 1)}$
$\mathbf{5 \cdot K_p}$	$\frac{(2.286 \cdot 10^{-3} \cdot s + 1)}{(2.5 \cdot 10^{-3} \cdot s + 1)}$
$\mathbf{100 \cdot K_p}$	0.99512

Table 4. 2. Closed Loop transfer functions for increments of K_p

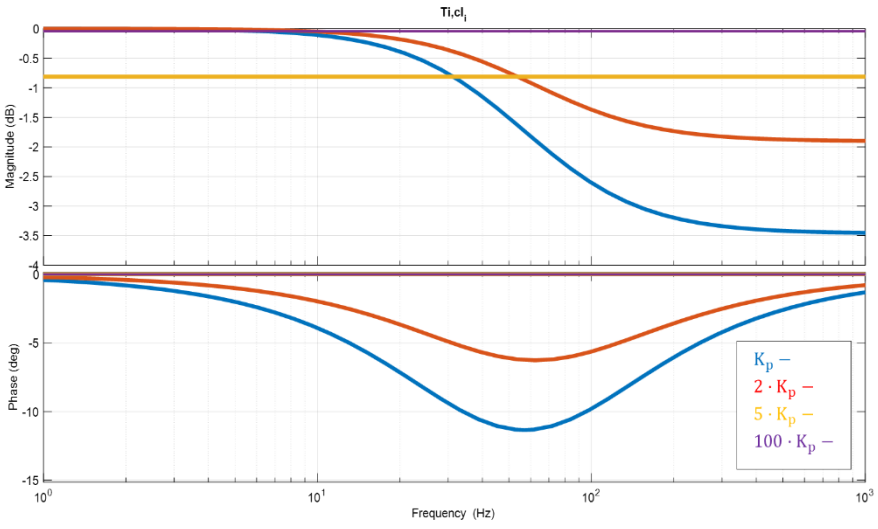

Figure 4. 15. Closed Loop frequency response for increments of K_p.

4.2.5. Outer voltage loop.

Once the inner current closed loop is known the voltage controller can be designed. The outer controller must compensate the closed inner loop together with the AC voltage - Inductor current transfer function.

So, this transfer function is:

$$\mathrm{H_P(s)} = \mathrm{T_{i,CL}(s)} \cdot \mathrm{H_{\hat{v}_{AC},\hat{i}_{Li}}(s)} = \frac{1.498 \cdot 10^8 \cdot (s + 874.7)}{(s + 293.5) \cdot (s + 8.928 \cdot 10^6)} = \\ = \frac{50 \cdot (1.143 \cdot 10^{-3} \cdot s + 1)}{(3.407 \cdot 10^{-3} \cdot s + 1) \cdot (1.12 \cdot 10^{-7} \cdot s + 1)} \quad \textbf{(4.45)}$$

Again, we use the IMC method and compare the equation 4.45 with the corresponding process in table 11.1 of reference [35]:

$$\widetilde{\mathrm{G}}(\mathrm{s}) = \frac{\mathrm{K} \cdot \ (\tau_3 \cdot \mathrm{s} + 1) \cdot \mathrm{e}^{-\theta \cdot \mathrm{s}}}{(\tau_1 \cdot \mathrm{s} + 1) \cdot (\tau_2 \cdot \mathrm{s} + 1)} \quad \textbf{(4.46)}$$

The constants are collected in table 4.3, neglecting the term $e^{-\theta \cdot s}$:

$\mathbf{K_V}$	$\mathbf{50}$
$\boldsymbol{\tau_{1,V}}$	$3.41 \cdot 10^{-3}$
$\boldsymbol{\tau_{2,V}}$	$1.12 \cdot 10^{-7}$
$\boldsymbol{\tau_{3,V}}$	$1.14 \cdot 10^{-3}$

Table 4. 3. $\mathrm{H_P(s)}$ transfer function gain, poles and zero constants.

The largest time constant is $\tau_{1,V}$, as this is larger than the zero time constant, the IMC method can now probably be used directly. Using the same rule as in 4.29, τ_C is first chosen as:

$$\tau_C = \frac{\tau_{dom}}{4} = \frac{\tau_1}{4} = 0.29 \cdot 10^{-3} \quad \textbf{(4.47)}$$

Introducing the value in table 4.3 in equation 4.26-4.28. The time constant of the PID outer controller are:

$\mathbf{K_{P,V}}$	$\mathbf{1.617 \cdot 10^{-3}}$
$\boldsymbol{\tau_{I,V}}$	$2.264 \cdot 10^{-7}$
$\boldsymbol{\tau_{D,V}}$	$-1.143 \cdot 10^{-3}$

Table 4. 4. Constants PID voltage regulator.

Because of the negative value in the $\tau_{D,V}$, the derivative time constant is neglected and PI (proportional integrator) is used:

$$\mathrm{PI(s)} = \mathrm{K_p} \cdot \left(1 + \frac{1}{\tau_I \cdot \mathrm{s}}\right) \quad \textbf{(4.48)}$$

Simplifying and rearranging to zero-pole form the final closed loop of the system in figure 4.10 has the following transfer functions and bode diagram:

$$\mathrm{T_{v,CL}(s)} = \frac{2.42 \cdot 10^{11}}{(\mathrm{s} + 2.42 \cdot 10^{11})} = \frac{0.99}{(4.13 \cdot 10^{-12} \cdot \mathrm{s} + 1)} \quad \textbf{(4.49)}$$

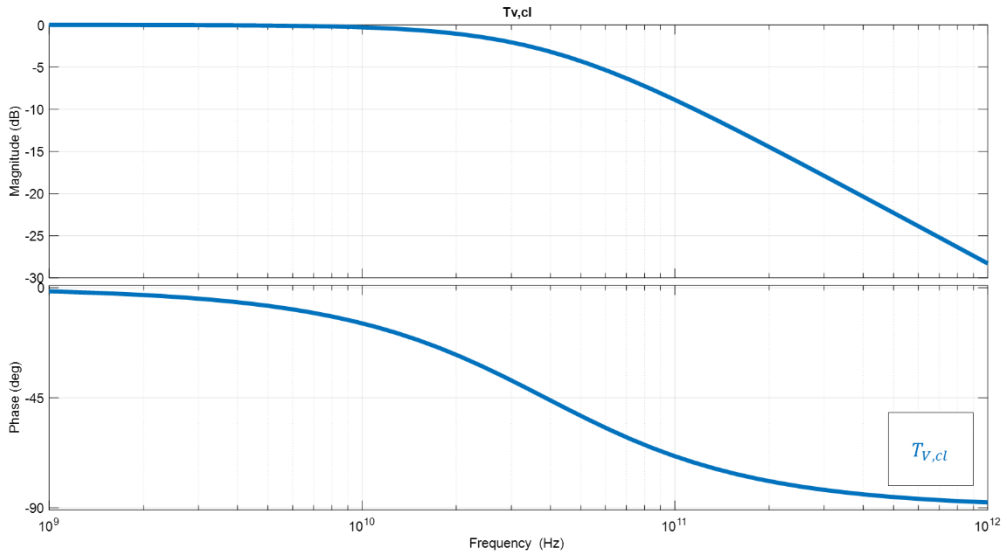

Figure 4. 16. Outer closed loop bode diagram.

4.2.6. Inverter input voltage control.

We have now developed a controlled for the output voltage of the inverter. However, control the input voltage of an inverter is usually the control strategy adopted when the inverter is connected to the grid or when it works as a rectified since the gird voltage will set the output voltage. The current should be in phase with the AC voltage, working as a power factor correction (PFC) because of that a phase locked loop (PLL) is used. This control strategy is shown in figure 4.17:

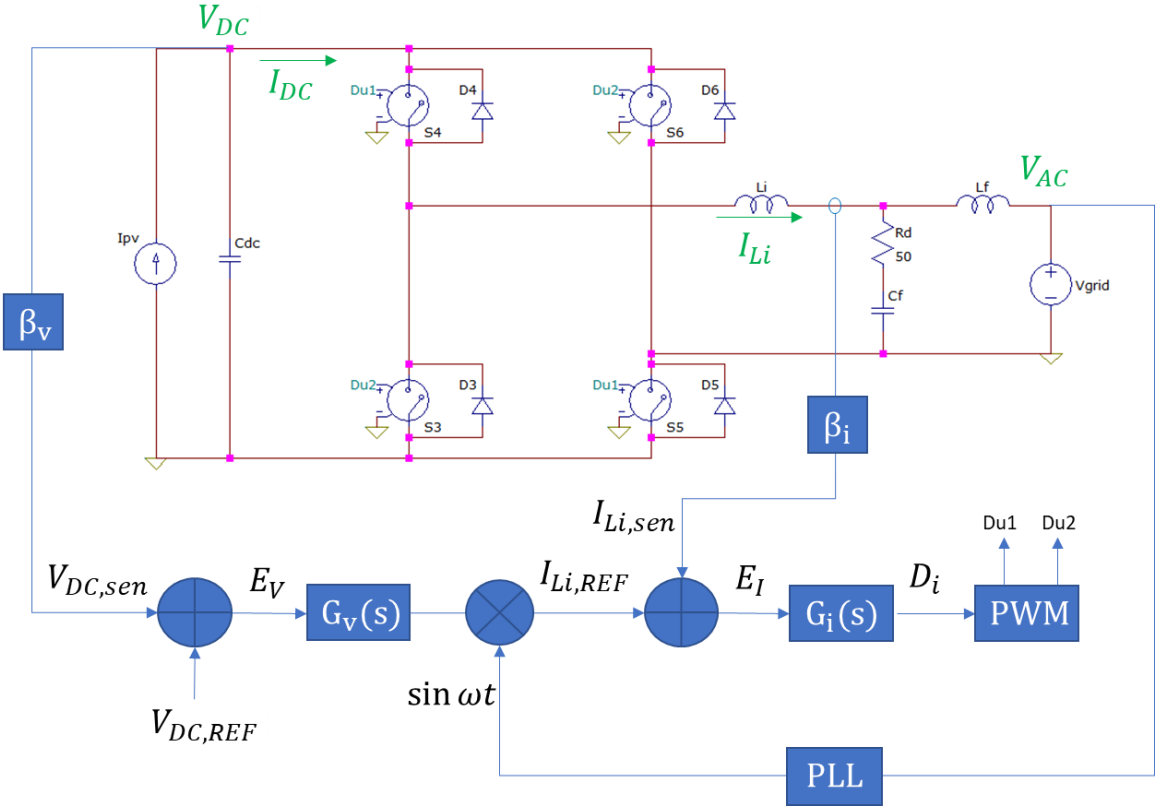

Figure 4. 17. Input voltage inverter control.

This control strategy is shown in block diagram form as figure 4.18. Where the two transfer functions are the inductor current- duty cycle for the inner loop and the DC voltage- Inductor current for the outer loop.

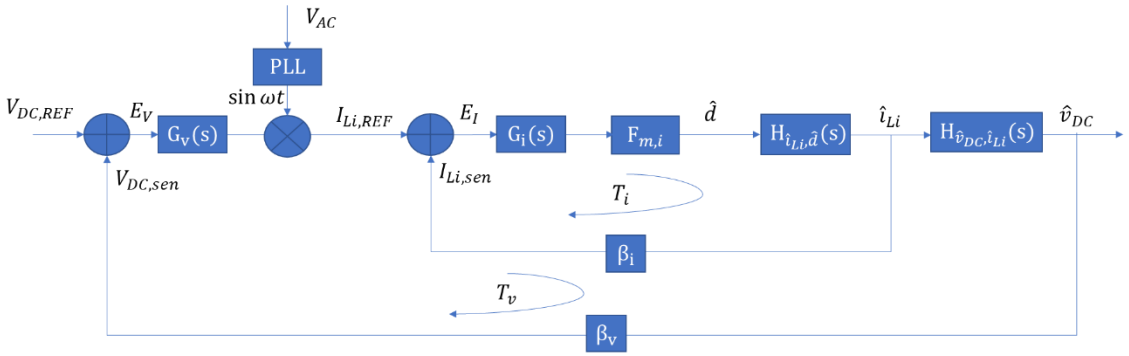

Figure 4. 18. Block diagram form input voltage control strategy.

However, note that during grid-tied mode, the dynamics of the ac capacitor can be ignored, just as the dynamics of the dc capacitor can be ignored during stand-alone mode. That mean that to control the input voltage $\hat{v}_{AC} = 0$ instead of $\hat{v}_{DC}$.

The same as the single-phase boost power factor correction (PFC) circuit presented in [36], for grid connected mode, there is no small-signal model. Any small signal circuit can cover its operation from dc up to half of the switching frequency due to the time-variant nature of the converter which is never in steady state per se.

Anyway, the inner loop can be controlled with the same regulator as reference [37] and [5] demonstrate. The frequency response of the transfer function $H_{\hat{i}_{Li},\hat{d}}(s)$ also, does not differed so much as the calculated in section 4.2.3. The equation and bode plots of the different transfer functions can be found also in [37]. Although other authors study the inverter in other way and other transfer function is developing as reference [2],[39] show.

The voltage controller should compensate for the closed current loop and the transfer function, $H_{\hat{v}_{DC},\hat{I}_{Li}}(s)$. This loop must be slower than the double-line frequency ripple in the DC voltage. Different ways to find the transfer function are also developed in [2 -5], [36-37]. For this loop a PI controller is also calculated by online tuning in simulation. The constants of the PI are collected in table 4.5.

$\mathbf{K_{P,V}}$	**3**
$\boldsymbol{\tau_{I,V}}$	40

Table 4. 5. PI controller for input voltage loop.

The PLL is implemented as a unitary sine factor with the same fundamental frequency since this is no the goal of the project. This will be leaved as further work.

Both control strategies are tested for several load conditions and work property. In chapter 5 the time response and stability of the two control strategies are shown.

4.3. Bidirectional DC-DC converter.

The bidirectional converter and storage capacitor will store energy which coming from the voltage ripple of the DC link in the battery or capacitor. The battery is mainly used to provide a steady power to the local load irrespective of source or load power variation. In this PV system the battery operates in two modes. When the DC voltage is above of its average value, the battery is charged storing the excess energy from

voltage ripple and when the DC voltage is below its average value the battery is discharged to supply the needed energy. The primary objective of the battery converter is to maintain a stable common DC bus voltage [38]. A bidirectional buck-boost DC-DC converter is used to maintain continuous power flow between the DC bus and battery or storage capacitor. A constant DC-link voltage is maintained by charging or discharging the battery depending on the sign in the voltage ripple. So, regardless of whether the battery is charging or discharging, the DC-link voltage should be stable and regulated throughout this operation.

Although several control strategies exist, the control strategy developed is based on the control of the DC link voltage with a single loop where a PID controller controls the converter to follow the reference. The control strategy can be seen in figure 4.19.

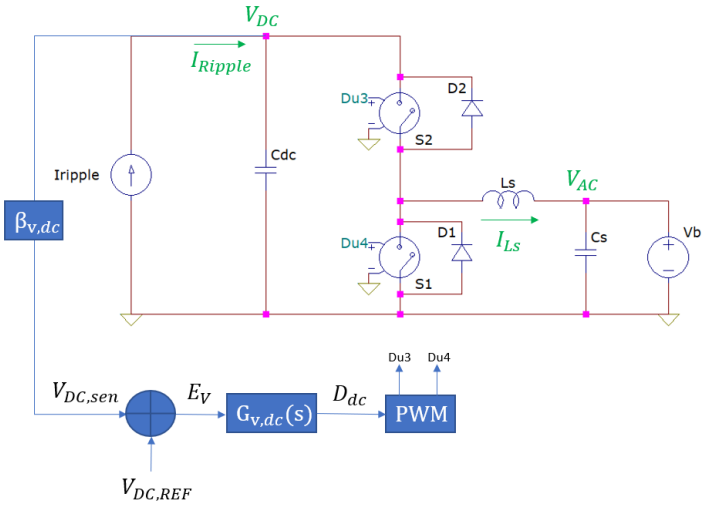

Figure 4. 19. Control strategies Bidirectional DC-DC converter

Where the load or disturbance to this converter is the ripple from the inverter, which is modelled as a sinusoidal current source. V_b is the voltage of the battery or large storage capacitor. As it is not a main point of this project it is simply modelled as a voltage source plus a series resistor.

Similarly, to the inverter procedure, before designing the converter the transfer functions of the plant should be known. For this converter we found the transfer functions by State Space Modelling instead of using average circuit model. Thus, firstly the steady state modelling is carried out, secondly the tree possible transfer functions are found and thirdly, the controller is designed [20], [21].

4.3.1. Bidirectional converter State Space Modelling.

This technique is commonly applied to develop models for switched mode power supplies (SMPS).

From reference [39], the energy storage elements are chosen as the state of the system, which is current for inductors and voltage for capacitors. The converter work as boost or buck according to the switches S1 and S2 respectively. The switches work in complimentary way, so only two sub-intervals are considered. Boost mode 1 (S1 on S2 off) and Buck mode 2(S1 off, S2 on). Therefore, a common model can be developed for both the modes of power flow.

Bidirectional Converter State Selection.

Seeing the circuit in figure 4.19, state $x(t)$, input $u(t)$ and output $y(t)$ vectors are chosen as follows:

$$x(t) = \begin{bmatrix} \text{DC link Capacitor Voltage} \\ \text{Stoarge Capacitor Voltage} \\ \text{Storage Inductor Current} \end{bmatrix} = \begin{bmatrix} v_{Cdc}(t) \\ v_{Cs}(t) \\ i_{Ls}(t) \end{bmatrix} \quad (4.50)$$

$$u(t) = \begin{bmatrix} \text{Current Ripple} \\ \text{Battery Voltage} \end{bmatrix} = \begin{bmatrix} i_{ripple}(t) \\ v_b(t) \end{bmatrix} \quad (4.51)$$

$$y(t) = \begin{bmatrix} \text{Battery Current} \\ \text{Storage Inductor Current} \\ \text{DC link Capacitor Voltage} \end{bmatrix} = \begin{bmatrix} i_b(t) \\ i_{Ls}(t) \\ v_{dc}(t) \end{bmatrix} \quad (4.52)$$

The derivative of the state vector is a vector whose elements are equal to the derivatives of the corresponding elements of the state vector. Regarding the output vector, we are free to place any dependent signal in the vector $y(t)$, regardless of whether the signal is actually a physical output.

From equation 4.50-4.52, the energy storage elements are chosen as states (voltage of the capacitor and current in the inductor). The current ripple coming from the inverter and battery voltage are considered as the inputs. The dc link voltage, battery current and the inductor current are chosen as the controlled variables.

Boost mode 1 (S1 ON S2 OFF).

In this mode the battery is discharged and the current flow through its internal resistance R_b to the C_s capacitor and L_s inductor. Using KCL and KVL equations in the resulting circuit shown in figure 4.20. The follow equations can be written:

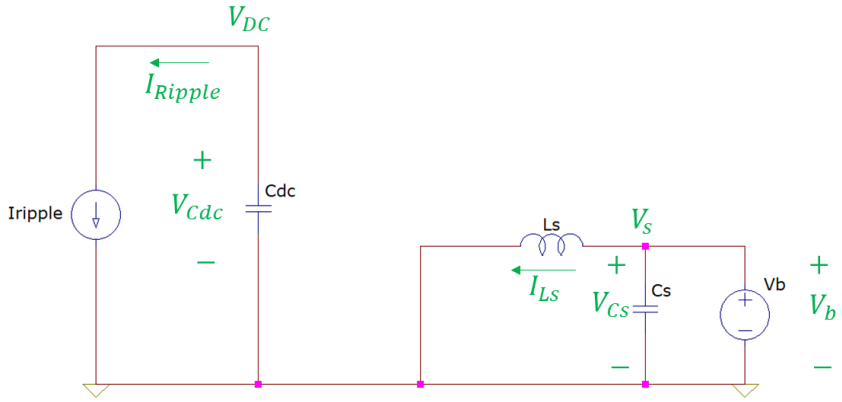

Figure 4. 20. Mode 1, S1 on S2 off.

$$C_{dc} \cdot \frac{dv_{Cdc}}{dt} = -i_{ripple} \quad (4.53)$$

$$i_b = i_{Ls} + i_{Cs} \quad (4.54)$$

$$v_b - i_b \cdot R_b - i_{Cs} \cdot R_{Cs} - v_{Cs} = 0 \quad (4.55)$$

$$v_{Cs} + i_{Cs} \cdot R_{Cs} - i_{Ls} \cdot R_{Ls} - L_s \cdot \frac{di_{Ls}}{dt} = 0 \quad (4.56)$$

$$C_s \cdot \frac{dv_{Cs}}{dt} = i_{Cs} \quad (4.57)$$

Where R_b, R_{Cdc} R_{Cs}, R_{Ls}, are the serie resistances of input voltage source(battery), DC link capacitor, storage capacitor and storage inductor, respectively.

According the steady state modelling in reference [39], the above equations can be rearranged and written in the following vector form for equation 4.50-4.52

$$K \cdot \frac{dx(t)}{dt} = A_1^* \cdot x(t) + B_1^* \cdot u(t) \quad (4.58)$$

$$y(t) = C_1 \cdot x(t) + E_1 \cdot u(t) \quad (4.59)$$

Where K is a matrix containing the values of capacitance and inductance, and the matrices A_K, B_K, C_K, D_K contain constants of proportionality. Thus, to have two similar equations, we can rewrite A_K and B_K as the same terms but divided by K.

$$\frac{A_1^*}{K} = A_1 \quad (4.60)$$

$$\frac{B_1^*}{K} = B_1 \quad (4.61)$$

So, the next vectors can be expressed:

$$\frac{dx(t)}{dt} = A_1 \cdot x(t) + B_1 \cdot u(t) = A_1 \cdot \begin{bmatrix} v_{Cdc} \\ v_{Cs} \\ i_{Ls} \end{bmatrix} + B_1 \cdot \begin{bmatrix} i_{ripple} \\ V_b \end{bmatrix} \quad (4.62)$$

$$A_1 = \begin{bmatrix} 0 & 0 & 0 \\ 0 & \frac{-1}{C_s \cdot (R_b + R_{Cs})} & \frac{-R_b}{C_s \cdot (R_b + R_{Cs})} \\ 0 & \frac{R_b}{L_s \cdot (R_b + R_{Cs})} & -\frac{(R_{Ls} \cdot R_b + R_{Ls} \cdot R_{Cs} + R_b \cdot R_{Cs})}{L_s \cdot (R_b + R_{Cs})} \end{bmatrix} \quad (4.63)$$

$$B_1 = \begin{bmatrix} \frac{-1}{C_{dc}} & 0 \\ 0 & \frac{1}{C_s \cdot (R_b + R_{Cs})} \\ 0 & \frac{R_{Cs}}{L_s \cdot (R_b + R_{Cs})} \end{bmatrix} \quad (4.64)$$

$$y(t) = C_1 \cdot x(t) + E_1 \cdot u(t) = C_1 \cdot \begin{bmatrix} v_{Cdc} \\ v_{Cs} \\ i_{Ls} \end{bmatrix} + E_1 \cdot \begin{bmatrix} i_{ripple} \\ V_b \end{bmatrix} \quad (4.65)$$

$$C_1 = \begin{bmatrix} 0 & \frac{-1}{(R_b + R_{Cs})} & \frac{R_{Cs}}{(R_b + R_{Cs})} \\ 0 & 0 & 1 \\ 1 & 0 & 0 \end{bmatrix} \quad (4.66)$$

$$E_1 = \begin{bmatrix} 0 & \frac{1}{(R_b + R_{Cs})} \\ 0 & 0 \\ -R_{Cdc} & 0 \end{bmatrix} \quad (4.67)$$

Buck mode 2 (S1 OFF, S2 ON).

Analogous mode 1, the equations of the circuit shown in figure 4.21 are written.

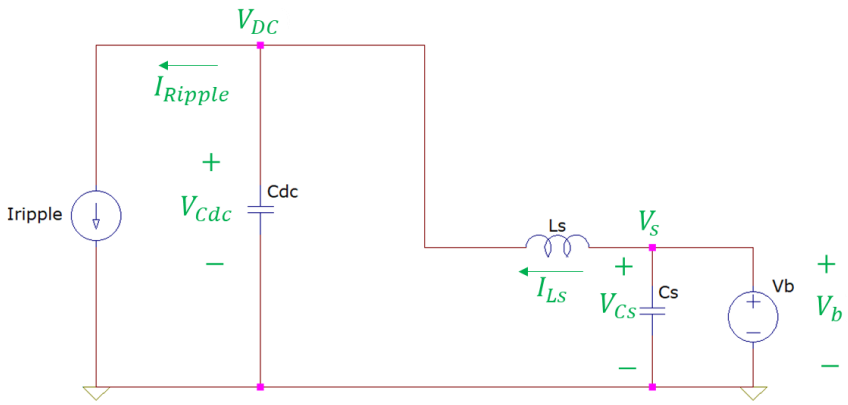

Figure 4. 21. Buck mode 2 (S1 off, S2 on).

$$i_{ripple} = i_{Ls} - C_{dc} \cdot \frac{dv_{Cdc}}{dt} \tag{4.68}$$

$$i_b = i_{Ls} + i_{Cs} \tag{4.69}$$

$$v_b - i_b \cdot R_b - i_{Cs} \cdot R_{Cs} - v_{Cs} = 0 \tag{4.70}$$

$$i_{Cs} = C_s \cdot \frac{dv_{Cs}}{dt} \tag{4.71}$$

$$v_b - i_b \cdot R_b - i_{Ls} \cdot R_{Ls} - L_s \cdot \frac{di_{Ls}}{dt} - i_{Cdc} \cdot R_{Cdc} - v_{Cdc} = 0 \tag{4.72}$$

The states of the system and the output state equations can be expressed in the same way as for the previous mode, as shown:

$$\frac{dx(t)}{dt} = A_2 \cdot x(t) + B_2 \cdot u(t) = A_2 \cdot \begin{bmatrix} v_{Cdc} \\ v_{Cs} \\ i_{Ls} \end{bmatrix} + B_2 \cdot \begin{bmatrix} i_{ripple} \\ V_b \end{bmatrix} \tag{4.73}$$

$$A_2 = \begin{bmatrix} 0 & 0 & \frac{1}{C_{dc}} \\ 0 & \frac{-1}{C_s \cdot (R_b + R_{Cs})} & \frac{-R_b}{C_s \cdot (R_b + R_{Cs})} \\ \frac{-1}{L_s} & \frac{R_b}{L_s \cdot (R_b + R_{Cs})} & -\frac{(R_{Ls} \cdot R_b + R_{Ls} \cdot R_{Cs} + R_b \cdot R_{Cs} + R_b \cdot R_{Cdc} + R_{Cdc} \cdot R_{Cs})}{L_s \cdot (R_b + R_{Cs})} \end{bmatrix} \tag{4.74}$$

$$B_2 = \begin{bmatrix} -\frac{1}{C_{dc}} & 0 \\ 0 & \frac{1}{C_s \cdot (R_b + R_{Cs})} \\ \frac{R_{Cdc}}{L_s} & \frac{R_{Cs}}{L_s \cdot (R_b + R_{Cs})} \end{bmatrix} \tag{4.75}$$

$$y(t) = C_2 \cdot x(t) + E_2 \cdot u(t) = C_2 \cdot \begin{bmatrix} v_{Cdc} \\ v_{Cs} \\ i_{Ls} \end{bmatrix} + E_2 \cdot \begin{bmatrix} i_{ripple} \\ V_b \end{bmatrix} \tag{4.76}$$

$$C_2 = \begin{bmatrix} 0 & \frac{-1}{(R_b + R_{Cs})} & \frac{R_{Cs}}{(R_b + R_{Cs})} \\ 0 & 0 & 1 \\ 1 & 0 & R_{Cdc} \end{bmatrix} \tag{4.77}$$

$$E_2 = \begin{bmatrix} 0 & \frac{1}{(R_b + R_{Cs})} \\ 0 & 0 \\ -R_{Cdc} & 0 \end{bmatrix} \quad (4.78)$$

Bidirectional Converter State-Space Averaged Model.

In order to get an average model, we consider now that the converter operates in continuous conduction mode. The converter has 2 subintervals where in each of the circuit elements are connected differently. Therefore, the respective state equation A_1, B_1, C_1, D_1 and A_2, B_2, C_2, D_2 matrices may also differ. Provided that the natural frequencies of the converter, as well as the frequencies of variations in the converter inputs, are much slower than the switching frequency, then according to [39], the state-space averaged model that describes the converter in equilibrium is

$$0 = A \cdot X + B \cdot U \quad (4.79)$$

$$Y = C \cdot X + E \cdot U \quad (4.80)$$

where the averaged matrices are:

$$A = D \cdot A_1 + (1 - D) \cdot A_2 \quad (4.81)$$

$$B = D \cdot B_1 + (1 - D) \cdot B_2 \quad (4.82)$$

$$C = D \cdot C_1 + (1 - D) \cdot C_2 \quad (4.83)$$

$$E = D \cdot E_1 + (1 - D) \cdot E_2 \quad (4.84)$$

The matrix form of the equation 4.72 and 4.73 are:

$$0 = A \cdot X + B \cdot U = A \cdot \begin{bmatrix} v_{Cdc} \\ v_{Cs} \\ i_{Ls} \end{bmatrix} + B \cdot \begin{bmatrix} i_{ripple} \\ V_b \end{bmatrix} \quad (4.85)$$

$$A = \begin{bmatrix} 0 & 0 & \frac{(1-D)}{C_{dc}} \\ 0 & \frac{-1}{C_s(R_b + R_{Cs})} & \frac{-R_b}{C_s \cdot (R_b + R_{Cs})} \\ \frac{-(1-D)}{L_s} & \frac{R_b}{L_s(R_b + R_{Cs})} & -\frac{(R_{Ls}R_b + R_{Ls}R_{Cs} + R_bR_{Cs} + ((1-D)(R_bR_{Cdc} + R_{Cdc}R_{Cs}))}{L_s \cdot (R_b + R_{Cs})} \end{bmatrix} \quad (4.86)$$

$$B = \begin{bmatrix} -\frac{1}{C_{dc}} & 0 \\ 0 & \frac{1}{C_s(R_b + R_{Cs})} \\ (1-D)\frac{R_{Cdc}}{L_s} & \frac{R_{Cs}}{L_s(R_b + R_{Cs})} \end{bmatrix} \quad (4.87)$$

$$y(t) = C \cdot X + E \cdot U = C \cdot \begin{bmatrix} v_{Cdc} \\ v_{Cs} \\ i_{Ls} \end{bmatrix} + E \cdot \begin{bmatrix} i_{ripple} \\ V_b \end{bmatrix} \quad (4.88)$$

$$C = \begin{bmatrix} 0 & \frac{-1}{(R_b + R_{Cs})} & \frac{R_{Cs}}{(R_b + R_{Cs})} \\ 0 & 0 & 1 \\ 1 & 0 & (1-D)R_{Cdc} \end{bmatrix} \quad (4.89)$$

$$E = \begin{bmatrix} 0 & \frac{1}{(R_b + R_{Cs})} \\ 0 & 0 \\ -R_{Cdc} & 0 \end{bmatrix} \quad (4.90)$$

DC equations or operation point (OP).

The quantities X, U, Y and D represent the equilibrium values of the averaged vectors in equations 4.79 and 4.80. These equations can be solved to find the equilibrium state and output vectors:

$$X = -A^{-1} \cdot B \cdot U \quad (4.91)$$

$$Y = (-CA^{-1}B + E)U \quad (4.92)$$

Small signal equations.

Now by perturbation and linearization, the same as done in equation 4.13 the state equations of the small-signal ac model are:

$$\frac{d\hat{x}(t)}{dt} = A \cdot \hat{x}(t) + B \cdot \hat{u}(t) + [(A_1 - A_2) \cdot X + (B_1 - B_2) \cdot U] \cdot \hat{d}(t) \quad (4.93)$$

$$\hat{y}(t) = C \cdot \hat{x}(t) + E \cdot \hat{u}(t) + [(C_1 - C_2) \cdot X + (E_1 - E_2) \cdot U] \cdot \hat{d}(t) \quad (4.94)$$

Finally, assuming the only applied disturbance is the duty cycle perturbation and taking Laplace Transform of 4.93 and 4.94:

$$\frac{\hat{x}(s)}{\hat{d}(s)} = (s - A)^{-1} \cdot [(A_1 - A_2) \cdot X + (B_1 - B_2) \cdot U] \quad (4.95)$$

$$\hat{y} = C \cdot \hat{x}(s) + [(C_1 - C_2) \cdot X + (E_1 - E_2) \cdot U] \cdot \hat{d}(s) \quad (4.96)$$

Bidirectional converter transfer functions.

Although the only transfer functions needed is the DC voltage - duty cycle, all the transfer functions for each output variable control are derived. The block diagram of the control strategy is shown in figure 4.22 where the transfer function $H_{\hat{v}_{DC},\hat{d}_{dc}}(s)$ is compensated by a PID regulator. The sensor $\beta_{v,dc}$ and PWM modulator $F_{m,dc}$ gains are assumed to be 1.

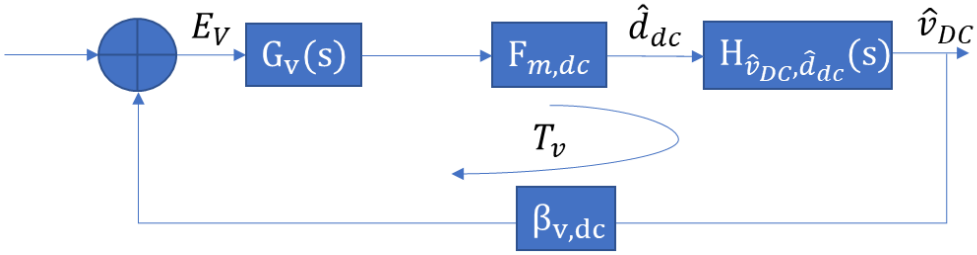

Figure 4. 22. Block diagram DC-DC converter loop.

Inductor Current - Duty Transfer Function.

To find the transfer functions based in the inductor current. We set $C_1 = C_2 = [0\ 0\ 1]$ and $E_1 = E_2 = [0\ 0]$.

$$\frac{\hat{i}_{Ls}(s)}{\hat{d}(s)} = C\frac{\hat{x}(s)}{\hat{d}(s)} = C \cdot ((s - A)^{-1} \cdot [(A_1 - A_2) \cdot X + (B_1 - B_2) \cdot U]) \quad (4.97)$$

$$\frac{\hat{\imath}_{Ls}(s)}{\hat{d}(s)} = \frac{1}{L_s}\left[\frac{V_b}{1-D} - \frac{i_{ripple}(R_b + R_{Ls})}{(1-D)^2}\right] \cdot \tag{4.98}$$

$$\cdot\left[\frac{\left(s + \frac{1}{C_s R_2}\right)\left(s + \frac{i_{ripple}}{C_{dc}\left(\frac{V_b}{(1-D)} - \frac{i_{ripple}(R_b + R_{Ls})}{(1-D)^2}\right)}\right)}{s^3 + s^2\left(\frac{R_1}{L_s} + \frac{1}{C_s R_2}\right) + s\left(\frac{R_1}{L_s C_s R_2} + \frac{R_b^2}{L_s C_s {R_2}^2} + \frac{(1-D)^2}{L_s C_{dc}}\right) + \frac{(1-D)^2}{L_s C_{dc} C_s R_2}}\right]$$

$$R_1 = R_{Ls} + (1-D)R_{Cdc} + \frac{R_b R_{Cs}}{R_b + R_{Cs}} \tag{4.99}$$

$$R_2 = R_b + R_{Cs} \tag{4.100}$$

Remember that in this small signal model i_{ripple} is assumed to be a steady state constant average value.

Battery current - Duty Transfer Function.

For the current ripple the matrixes are setting as equations 4.101 and 4.102 the transfer function is expressed in 4.104.

$$C_1 = C_2 = \begin{bmatrix} 0 & -\frac{1}{R_b + R_{Cs}} & \frac{R_{Cs}}{R_b + R_{Cs}} \end{bmatrix} \tag{4.101}$$

$$E_1 = E_2 = \begin{bmatrix} 0 & \frac{R_{Cs}}{R_b + R_{Cs}} \end{bmatrix} \tag{4.102}$$

$$\frac{\hat{\imath}_b(s)}{\hat{d}(s)} = C\frac{\hat{x}(s)}{\hat{d}(s)} = C \cdot ((s - A)^{-1} \cdot [(A_1 - A_2) \cdot X + (B_1 - B_2) \cdot U]) \tag{4.103}$$

$$\frac{\hat{\imath}_b(s)}{\hat{d}(s)} = \frac{R_{Cs}}{R_2} \cdot \frac{\hat{\imath}_{Ls}(s)}{\hat{d}(s)} + \tag{4.104}$$

$$+\left[\frac{\frac{R_b}{L_s C_s {R_2}^2} \cdot \left(\frac{V_b}{(1-D)} - \frac{i_{ripple}(R_b + R_{Ls})}{(1-D)^2}\right)\left(s + \frac{i_{ripple}}{C_{dc}\left(\frac{V_b}{(1-D)} - \frac{i_{ripple}(R_b + R_{Ls})}{(1-D)^2}\right)}\right)}{s^3 + s^2\left(\frac{R_1}{L_s} + \frac{1}{C_s R_2}\right) + s\left(\frac{R_1}{L_s C_s R_2} + \frac{R_b^2}{L_s C_s {R_2}^2} + \frac{(1-D)^2}{L_s C_{dc}}\right) + \frac{(1-D)^2}{L_s C_{dc} C_s R_2}}\right]$$

Output Voltage - Duty Transfer Function.

Finally, the transfer functions that we need to control is found when $C_1 = [1\ 0\ 0], C_2 = [1\ 0\ R_{Cdc}]$ and $E_1 = E_2 = [R_{Cdc}\ 0\ 0]$. These equations are shown in equation 4.106.

$$\frac{\hat{v}_{dc}(s)}{\hat{d}(s)} = C\frac{\hat{x}(s)}{\hat{d}(s)} = C \cdot ((s - A)^{-1} \cdot [(A_1 - A_2) \cdot X + (B_1 - B_2) \cdot U]) + (C_1 - C_2) \cdot X \quad \textbf{(4.105)}$$

$$\frac{\hat{v}_{dc}(s)}{\hat{d}(s)} = \quad \textbf{(4.106)}$$

$$= \frac{\left(\left(-\frac{i_{ripple}}{(1-D)C_{dc}}\right)\left[\left(s+\frac{1}{C_sR_2}\right)\left(s+\frac{R_1}{L_s}\right)+\frac{R_b^2}{L_sC_sR_2{}^2}\right]+\frac{(1-D)}{C_{dc}}\left(\frac{V_b}{(1-D)}-\frac{i_{ripple}(R_b+R_{Ls})}{(1-D)^2}\right)\left(s+\frac{1}{C_sR_2}\right)\right)}{\left(s^3+s^2\left(\frac{R_1}{L_s}+\frac{1}{C_sR_2}\right)+s\left(\frac{R_1}{L_sC_sR_2}+\frac{R_b^2}{L_sC_sR_2{}^2}+\frac{(1-D)^2}{L_sC_{dc}}\right)+\frac{(1-D)^2}{L_sC_{dc}C_sR_2}\right)}+$$

$$+(1-D)R_{Cdc}\frac{\hat{i}_{Ls}(s)}{\hat{d}(s)}+V_{dc}-R_{Cdc}I_{Ls}$$

Note that i_{ripple} only appear in the gain and the zero for the three transfer functions.

Before to design the control loops, the bode diagrams are checked by simulations. The values in chapter 3 are used for $R_{Cs}, R_{Ls}, R_{Cdc}, C_{dc}, C_s, L_s$ and R_b. As initial condition $V_b = 200V$ and $i_{ripple} = 19A$. The input current i_{ripple} is set 19A since it will be the average value when the inverter is connected, but when the controller is designed, it is checked with a sinusoidal current which average value 0. Regarding the duty cycle value, D, although it is settled at 0.5, we will discuss about their critical values in the 4.3.2.

The equations before developed describe approximately the dynamic of the circuit as the following figures shown.

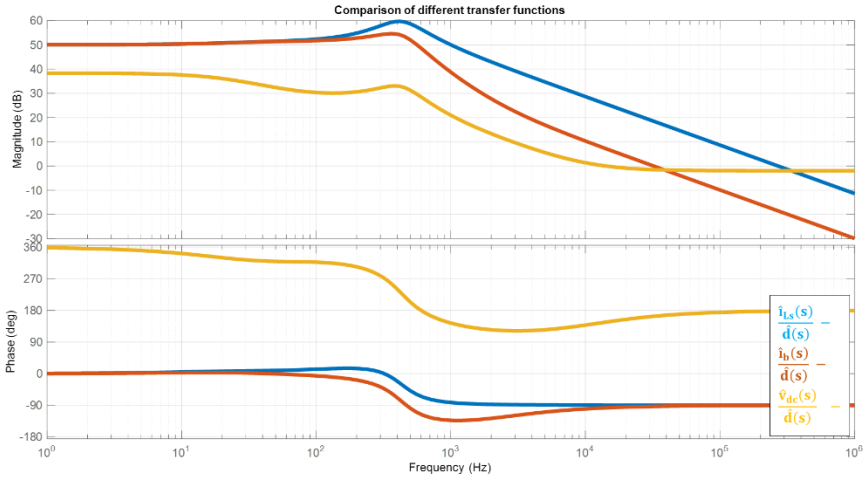

Figure 4. 23. Bode plots of transfer functions from equations.

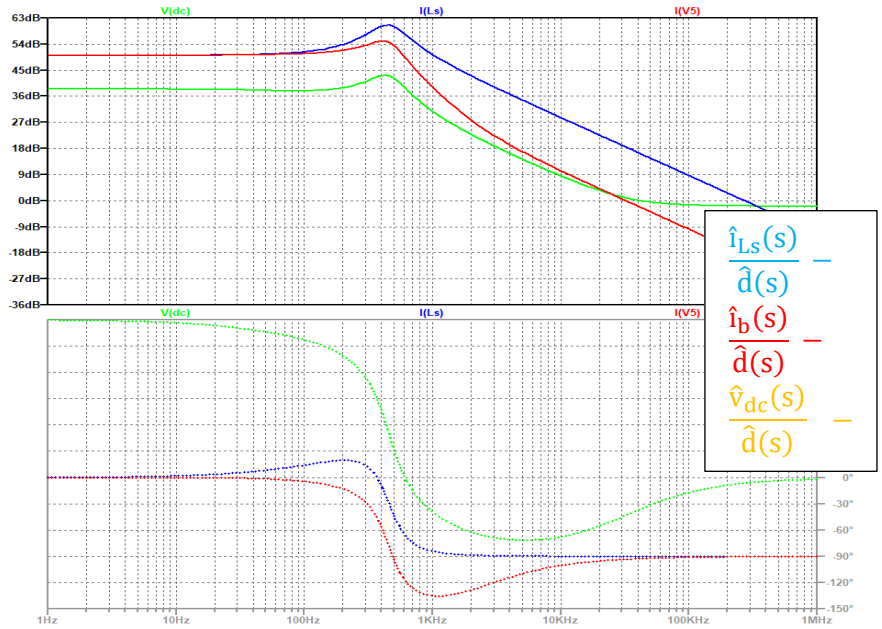

Figure 4. 24. Bode plots of transfer functions from LTspice.

4.3.2. Single Voltage Control Loop.

The control loop is designed with a PID controller were the PID parameters are chosen by online tuning. This method is based on the trial and error procedure. But to reduce the number of tries, we follow the technique of Ziegler and Nichols [35] for a first value of the constants.

First of all, the bode diagram of the transfer function, $H_{\hat{v}_{DC},\hat{d}_{dc}}(s)$ is analysed in order to know the gain margin. The bode diagram of this transfer function is shown in figure 4.23 for yellow curve. The gain margin is:

$$\left|H_{\hat{v}_{DC},\hat{d}_{dc}}(f_{180°})\right| = 10.2\text{dB} = 3.24 \tag{4.107}$$

Where the frequency at this point is:

$$f_{180°} = 677\text{Hz} \tag{4.108}$$

Now we can define the ultimate gain, K_{cu}, as the gain what will give a sustained oscillation with constant amplitude in the output. The period of this oscillation is called ultimate period, P_{cu}.

$$K_{cu} = \frac{1}{3.24} = 0.31 \tag{4.109}$$

$$P_{cu} = \frac{1}{677} = 1.5 \cdot 10^{-3} \tag{4.110}$$

Lastly, according to Ziegle Nichols tuning (table 11.4 on reference [35]) the time constants and gain of the PID can be chosen initially as summarized in equation 4.111-4.113 collect:

$$K_{p,dc} = 0.6 \cdot K_{cu} = 0.6 \cdot 0.31 = 0.18 \tag{4.111}$$

$$\tau_{i,dc} = \frac{P_{cu}}{2} = \frac{1.5 \cdot 10^{-3}}{2} = 0.75 \cdot 10^{-3} \tag{4.112}$$

$$\tau_{d,dc} = \frac{P_{cu}}{8} = \frac{1.5 \cdot 10^{-3}}{8} = 185 \cdot 10^{-6} \tag{4.113}$$

Before we simulate and fine tune the PID controller we have to take into account that only a limited set of duty values may be allowed as the output of the controller. This is because the duty cycle function of the converter is not an monotonic waveform. The duty cycle function was obtained by simulation and it is shown in figure 4.25.

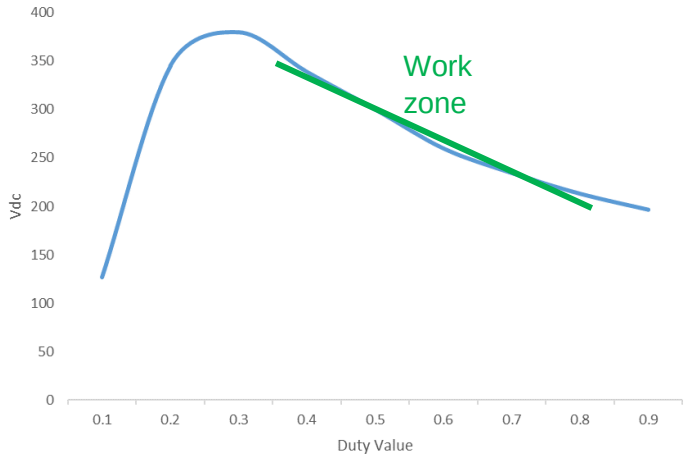

Figure 4. 25. Duty cycle-output voltage function.

It can be seen how before and after the value 0.3 the function decrease. This behaviour will cause the controller to become unstable. In addition, the maximum duty should be limited since this is compared with the triangular wave, so both must have the same amplitude range. The limited range is chosen from 0.3 to 0.8.

Finally, the PID constant are fine-tuned with trial and error procedure by simulations and the final controller is expressed in table 4.6.

$\mathbf{K_{P,V}}$	$\mathbf{-0.2 \cdot 0.18}$
$\boldsymbol{\tau}_{\mathbf{I,V}}$	$5 \cdot 0.75 \cdot 10^{-3}$
$\boldsymbol{\tau}_{\mathbf{D,V}}$	$185 \cdot 10^{-6}$

Table 4. 6. PID parameters for DC voltage control of the bidirectional converter.

It is possible compare the step response of the closed loop transfer functions and the simulated controller circuit in LTspice. Figure 4.26 show the step response of the circuit. This has a time response of 20ms and an overshot of 1.73 (17.3%) when the reference is changed in a step from 400V to 410V approximately.

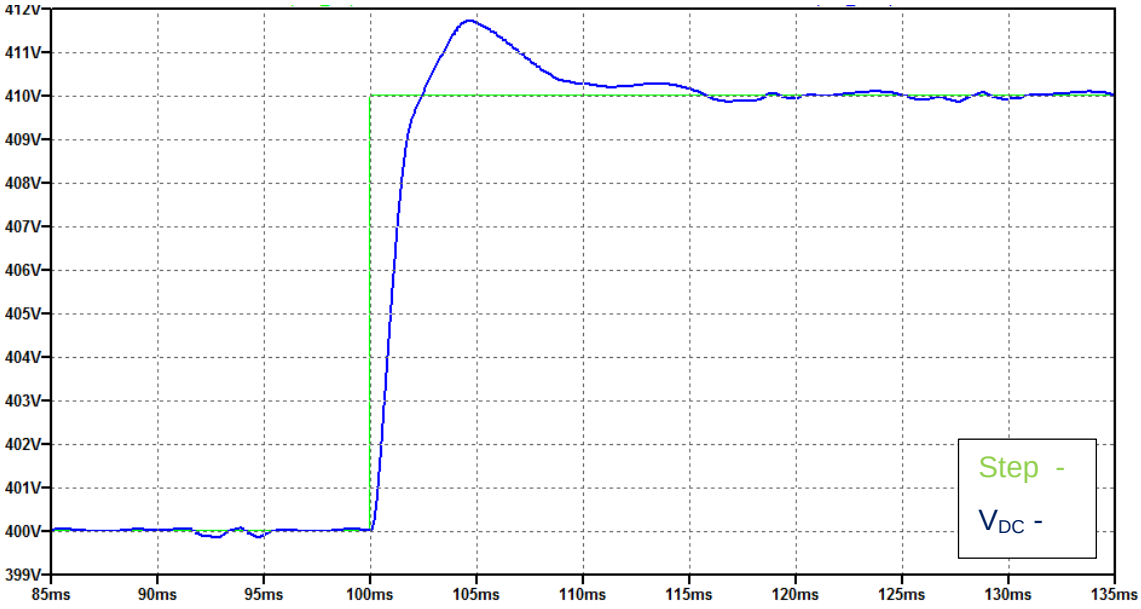

Figure 4. 26. Step response of the circuit closed loop.

Whereas the step response of the transfer function has a time response of 24ms and an overshot of 0.032 (32%) over 1.1 approximately.

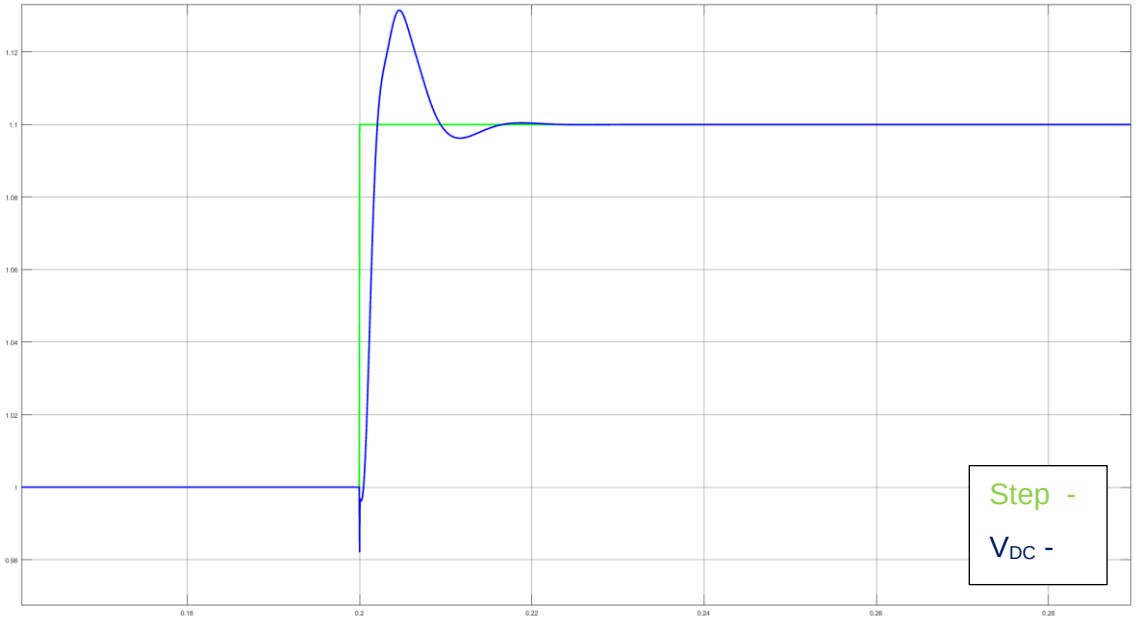

Figure 4. 27. Step response of the transfer function closed loop.

4.4. Other control strategies.

To lead with the ripple in the DC link capacitor other control strategies were studied in which the parameters of the regulators were tuned by trial and error method. These control strategies are introduced and only the control loops are explained.

Power flux control.

Another control strategy is to use a single current control loop to set the reference average current in the inductor. The fact is that the reference current can be expressed by equation 4.114 where the power storage in the auxiliary capacitor V_s and battery unit is the difference between the input power and the output power, this is the ripple

power, as developed in equations 2.5-2.7. The control loop of this strategy is shown in figure 4.29. A PI controller is added in order to force the inductor current to follow the reference.

$$I_{Ls,ref} = \frac{P_{DC} - P_{AC}}{V_{Cs,AVG}} \tag{4.114}$$

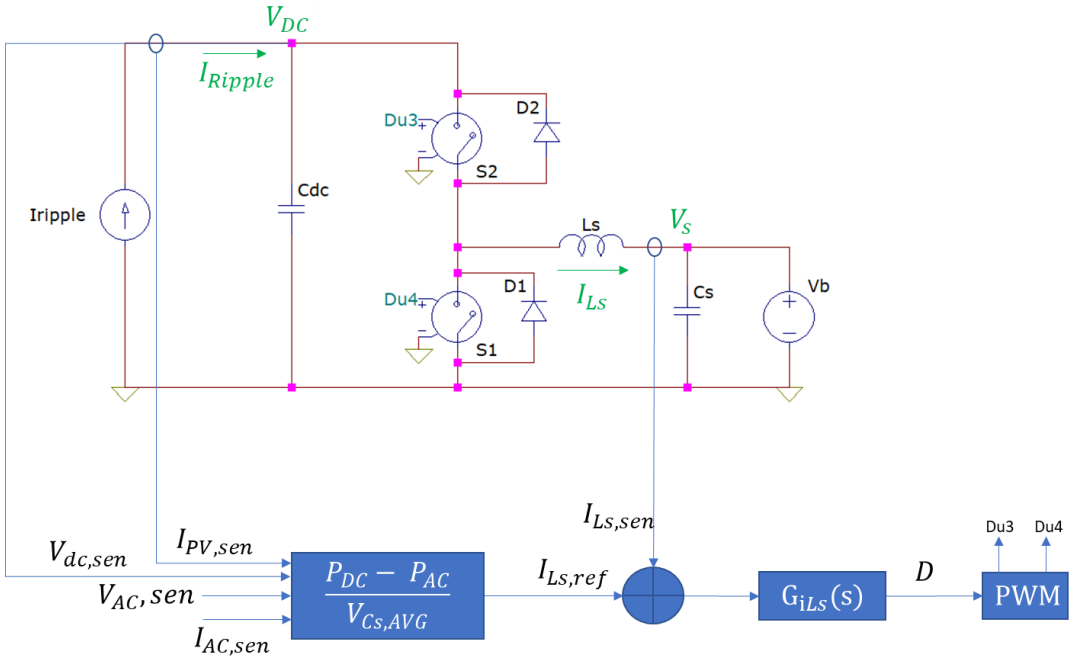

Figure 4. 28. Power flux. Control strategy.

More control strategies can be found in the literature, [27] and [28]. Where even a steady state strategy is developed to store energy coming from the ripple [28].

The above control strategies are tested and simulated in the time domain. The results of these simulations are shown in chapter 5 together with the control strategies developed.

Chapter 5.

Simulations and Results

Chapter 5. Simulations and Results.

5.1. Introduction.

Chapter 5 contains the simulation results of the system and discussion about it. The system is simulated with the different control strategies which were introduced in chapter 4. Also, each power stage is simulated under several conditions. In addiction a spectrum analysis is executed in order to study the harmonics.

The PV system is first simulated with inverter in standalone mode, and with grid connected mode when no DC-DC converter is added. In a similar way the DC-DC converter is simulated without the inverter, here the input current is fixed at the same value as delivered by the inverter.

Then the system is simulated with all part includes, i.e. the full system. We study all the different control strategies for the bidirectional converter introduced in section 4.3. Where the input or output voltage of the inverter were controlled depending of the control strategy of the bidirectional converter.

The simulations were done in LTspice, a free software of SPICE simulations, schematic capture and waveform viewer from Linear Technology. The total time of simulations was 2s with a timestep of 10ms.

Finally, the spectrum of the output voltage and current in the inverter was analyzed for both operation modes. With a simple resistive load, and when the inverter is connected to the grid. For this last one a LISN (Line Impedance Stabilization Network) was used to decouple the grid signal.

The parameters used for the simulations are collected in table 5.1. Where the switches, as well as the diodes were fixed as ideals.

DC-Link Capacitor	$\mathbf{C_{DC}}$	**3 mF**
LCL Filter inductor (inverter side)	$\mathbf{L_i}$	1.1 mH
LCL Filter inductor	$\mathbf{L_f}$	11.2 µH
LCL Filter capacitor	$\mathbf{C_f}$	22.86 µF
LCL Filter damping resistor	$\mathbf{R_d}$	50 Ω
Bidirectional DC-DC inductor	$\mathbf{L_S}$	130 µH
Bidirectional DC-DC capacitor	$\mathbf{C_S}$	1 mF
Bidirectional DC-DC battery voltage	$\mathbf{V_b}$	200V
DC-Link voltage	$\mathbf{V_{DC}}$	400V
Resistive load	$\mathbf{R_{Load}}$	50 Ω 1KW @230v

Table 5. 1. Component values used for simulations.

5.2. Single phase inverter.

First let us assume that the inverter is working without the dc-dc converter. The inverter is simulated for both control strategies. These depend of the outer voltage loop, if it controls the output (AC) or for the input voltage (DC).

For the input voltage control the inverter is supposed connected to the grid whereas for the output voltage control a resistor of 50 Ω is chosen as a load and a 400V voltage source is add to the input to have constant voltage.

For the output voltage control the source described on chapter 2 is used as dependent current source (PV cell) and a sinusoidal voltage source of 230v and 50Hz is selected as the grid.

At this condition the PV system is simulated for steady state, load steps, input power variations and different references.

5.2.1. Controlling the AC voltage.

The inverter was simulated first, for an outer voltage loop which control the load voltage. The reference was a sine wave with amplitude 230V RMS and frequency 50Hz. The circuit which was simulated is shown in figure 5.1. Where the inductor L_i current is measured with a voltage probe (B2) as well as its reference is a voltage value, that is why every current reference is a voltage value in every simulation. In addiction low pass filters were added to the measured current and voltage, and to the derivative PID current regulator. The filters remove the switching components of the waveforms.

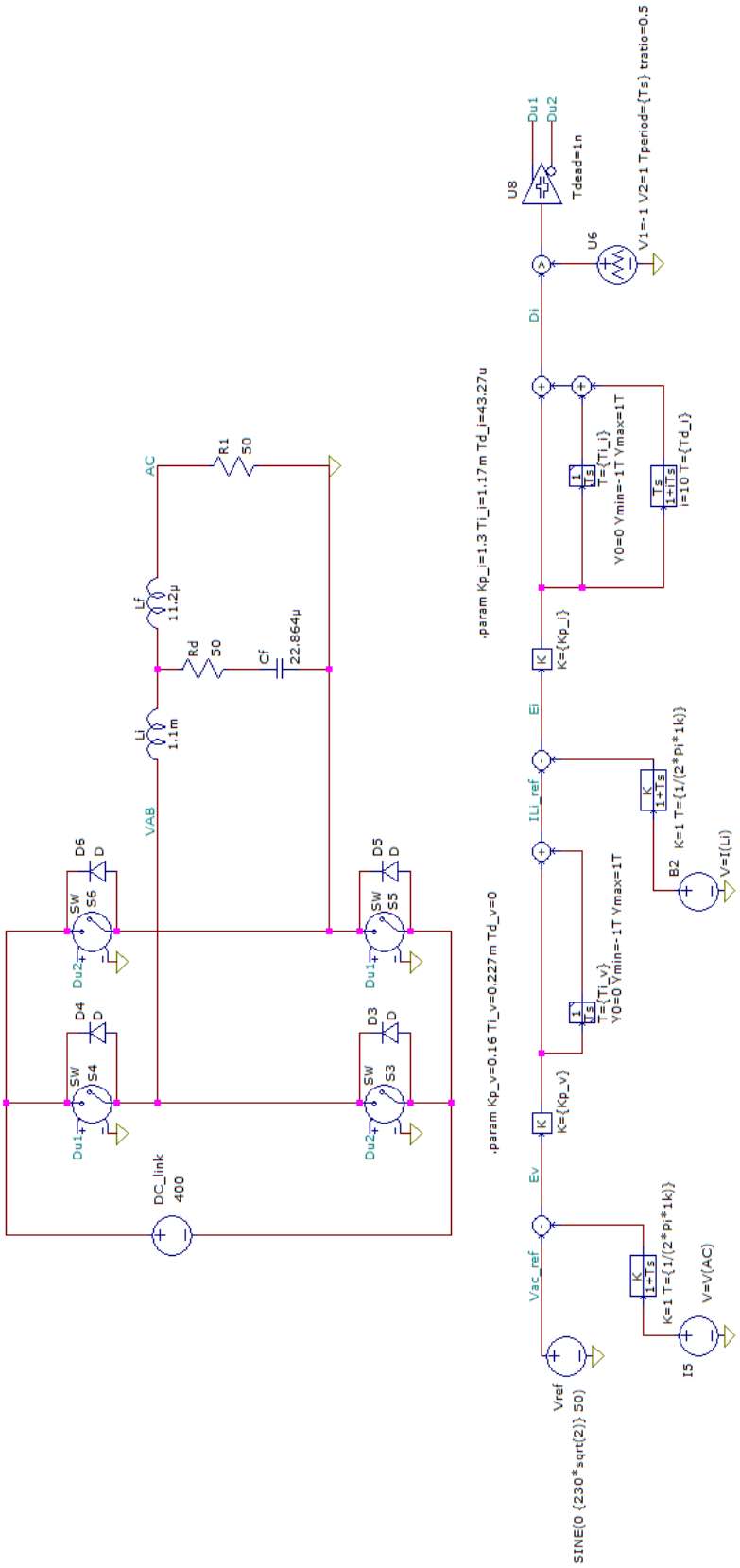

Figure 5. 1. Simulated inverter circuit for output voltage control.

The result of the tracking of the reference can be seen in figure 5.2. Where the “A” plot panel shows the inductor current value (I_{Li}) and the reference coming from the voltage loop, and the “B” plot panel shows the AC voltage and the sine reference detailed before.

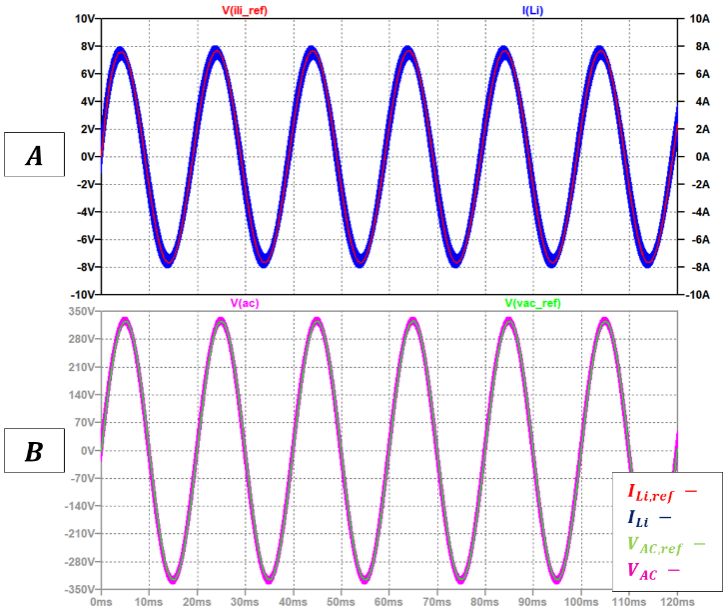

Figure 5. 2. AC voltage and Inductor L_i current control of the inverter.

From figure 5.3 one can see the response of the inverter when steps of load were added to check the robustness and stability under disturbances. Although the step has a variation from 0 to 1 in figure, this change from 50Ω to 100Ω respectably in the simulation circuit. The “A” panel show the steps which have a rise/fall time of 20ms, “B” panel shows the inductor current and its reference and the “C” panel shows the stable output voltage (tracking its reference) against the load variations.

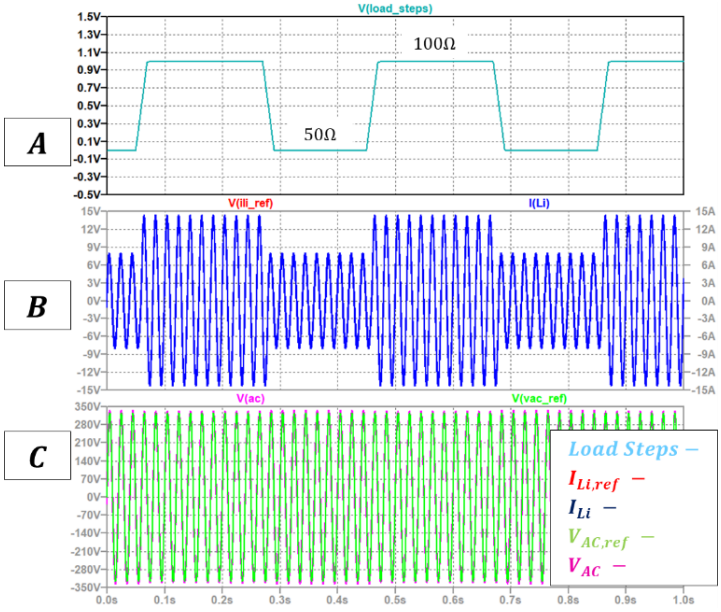

Figure 5. 3. Inverter loop response to steps of load.

In third part, the system was tested under different voltage reference amplitude. As figure 5.4 show the control loop correctly follow the reference. The “A” panel show the steps of voltage references which change from 230V RMS (1) to 110V RMS (0.5) with

rise and fall time of 25ms. The “B” panel shows the inductor current loop follow the current reference from the voltage loop. The “C” panel show the voltage response following the different voltage references. The time of response is 40ms.

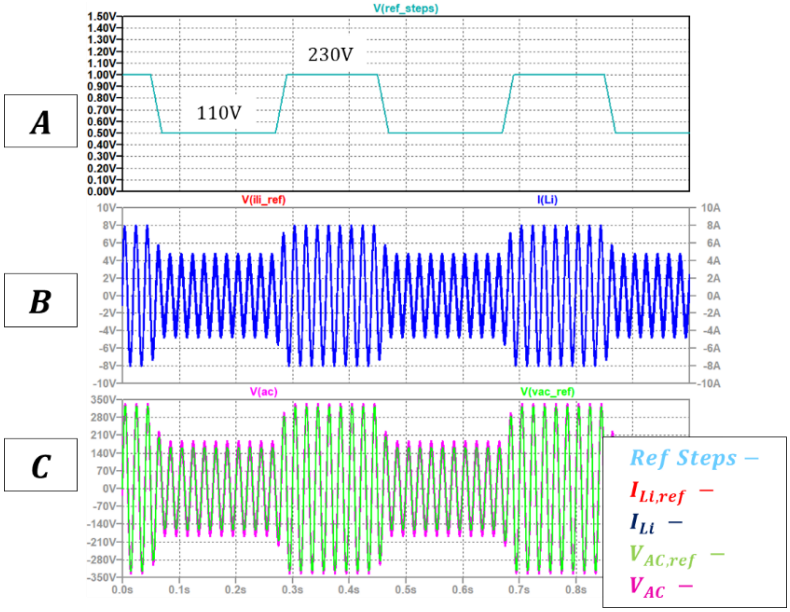

Figure 5. 4. Amplitude variations in the voltage reference. Inverter DC voltage control.

5.2.2. Controlling the DC voltage.

Now the input voltage of the inverter is controlled. The circuit simulated is shown in figure 5.5. Where the voltage controller is tuned by online method. In addiction low pass filters are used to remove the switching components.

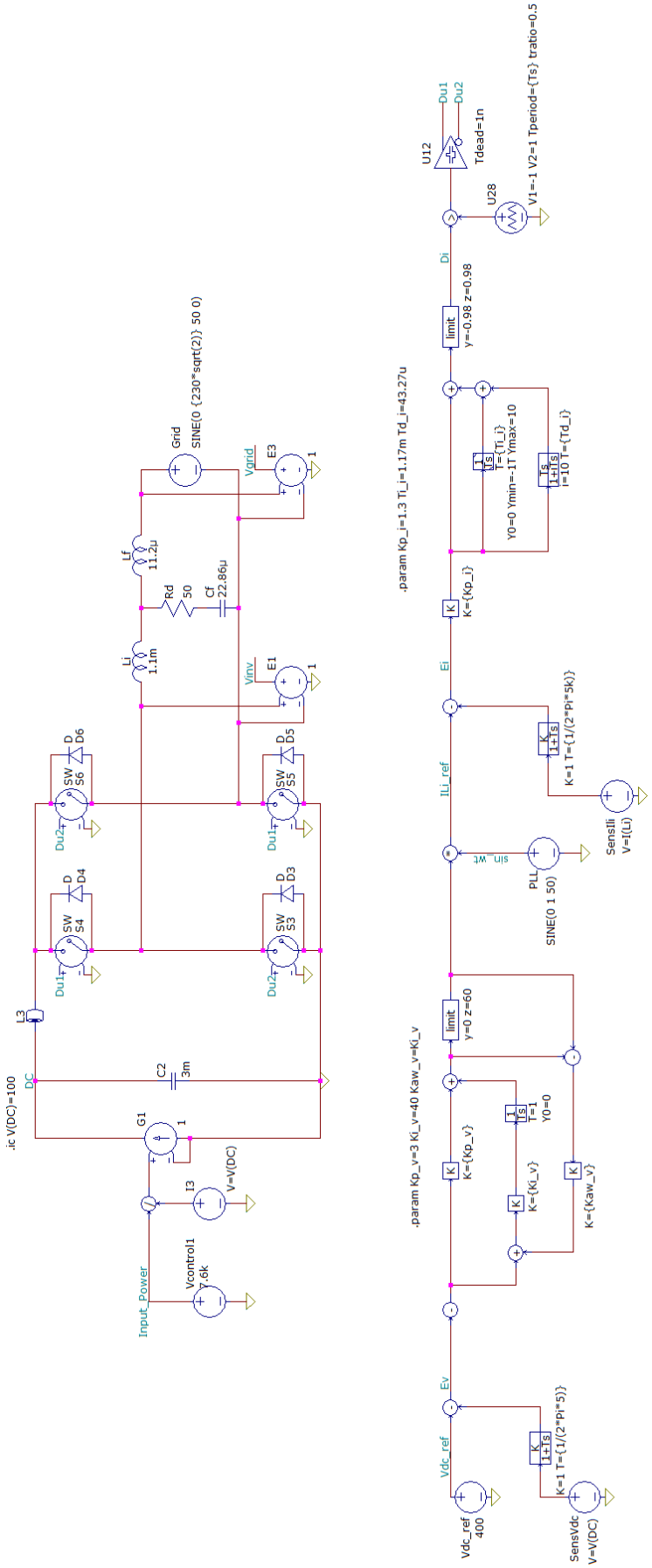

Figure 5. 5. Simulated inverter circuit for input voltage control.

Figure 5.6 the steady state of the DC link voltage (input voltage of the inverter) and the current by the inductor L_i are shown in panel B and A respectively. The response time is 250ms and the voltage has an overshot of 60%. The overshot can be decrease precharging the DC capacitor which is fixed at 100V in the simulation.

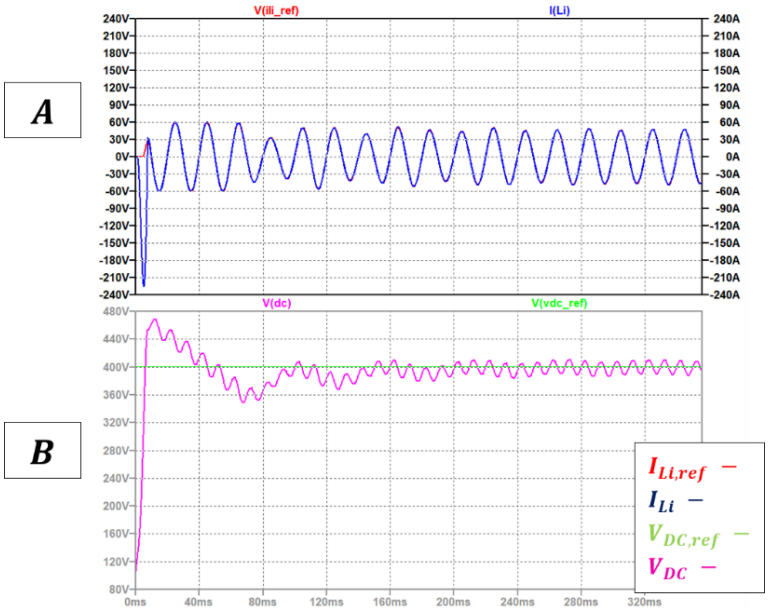

Figure 5. 6. Inductor current, inductor L_i (blue waveform) and V_{dc} voltage (pink waveform).

The controlling action of the inverter can be checked too. Where the DC-link voltage follows its reference value, 400V. The current through the inverter side inductor also follow the reference which comes from the voltage controller plus the PLL.

Form figure 5.7 the ripple in the DC link capacitor can be seen, it is the same as the specification requirement that was used for the DC link capacitor design. The ripple in the DC link is 0.05% since the variation of the average value (400V) is $\Delta V_{DC} = 20V$.

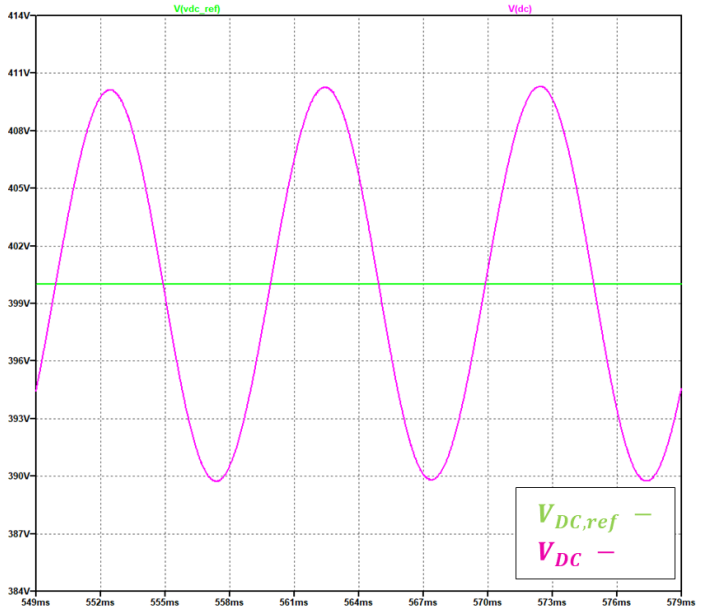

Figure 5. 7. Ripple in the DC link voltage.

The solar power is intermittent in nature, and can not thus provide a steady power to the load connected. Due to the variation in solar power generation a MPPT algorithm is

needed which gives the voltage reference of the maximum power point to the voltage loops. This reference will change with the solar irradiance and temperature.

So, the circuit was simulated for two reference values on the DC link voltage as 800ms steps. The steps of amplitude 600V and 300V have a rise and fall time of 100ms. These changes in the reference will be the voltage values of the MPP if a MPPT algorithm is implemented further. We can see the DC voltage tracking of different references in the panel B of figure 5.8. Where the rise time is 350ms as well as the fall time is 260ms. The increase and decrease of the inductor current I_{Li} is also shown in panel B of figure 5.8.

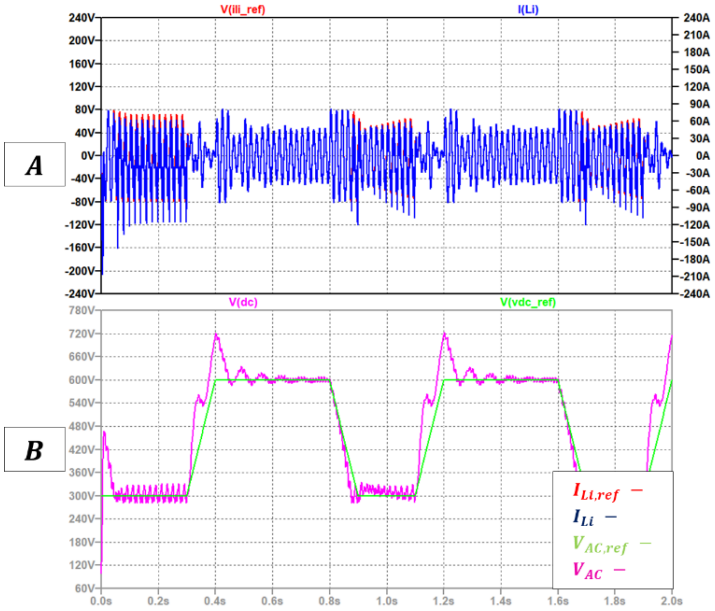

Figure 5. 8. Reference changes in the DC link voltage for inverter input voltage control.

In figure 5.9 the system was simulated under input power step. When small changes in the temperature or irradiance occur in the PV cell due to any unexpected factor, the MPP voltage reference is usually the same. The steps in the input current replicate these small changes in the photovoltaic panel. The 400ms steps have an amplitude of 6KW and 9KW. Its rise and fall time is 50ms. The steps have a voltage value because a voltage probe was used to measure these. The control loop correctly keeps a stable input voltage at 400V with a rise time of 80ms and a fall time of 100ms. This voltage (panel C), the power step (panel A) and the inductor current (panel B) can be seen in figure 5.9.

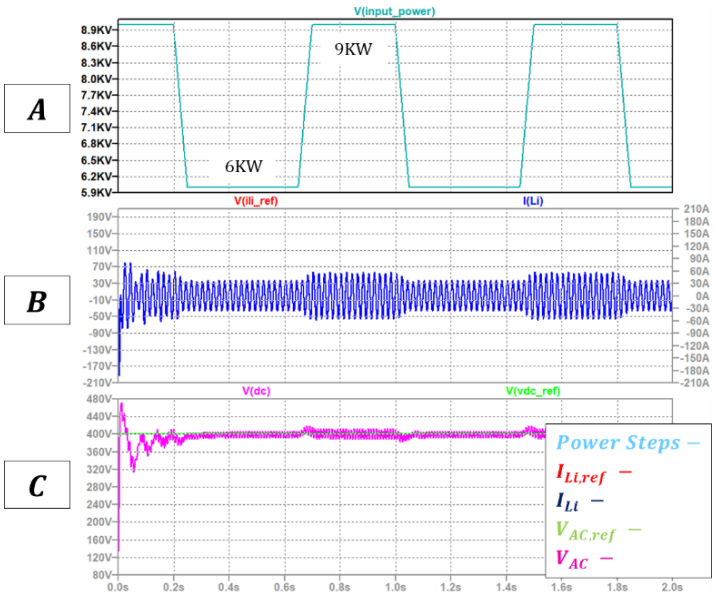

Figure 5. 9. Input power steps.

5.3. Bidirectional DC-DC converter.

The bidirectional converter was also simulated without the inverter. The input current was instead modelled as a sinusoidal current source with the same amplitude and frequency as the current which would have come from the inverter. We can see the waveform of the input current in figure 5.10.

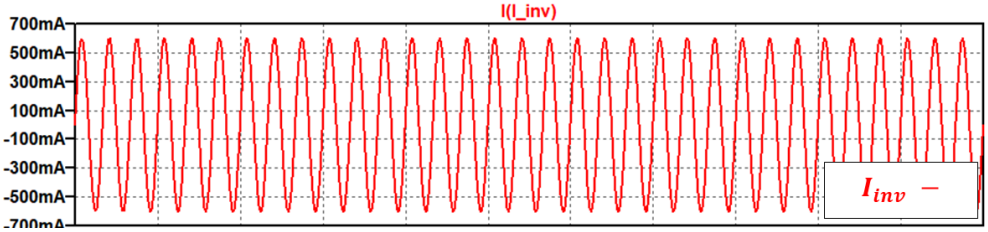

Figure 5. 10. Input current in bidirectional DC-DC converter.

The converter was tested under two control strategies, controlling the voltage V_{DC} and controlling the inductor current I_{Ls}. We simulated the bidirectional converter (in standalone mode) only under these two control loops because the control strategies introduced in chapter 4 are based on this two.

5.3.1. DC voltage control. Bidirectional converter.

The simulated circuit of the bidirectional DC-DC converter is shown in figure 5.11. The capacitor is precharged at 400v as well as the integrator time is initialised at 500ms. In addiction a low pass filter removes the switching components of the measured voltage.

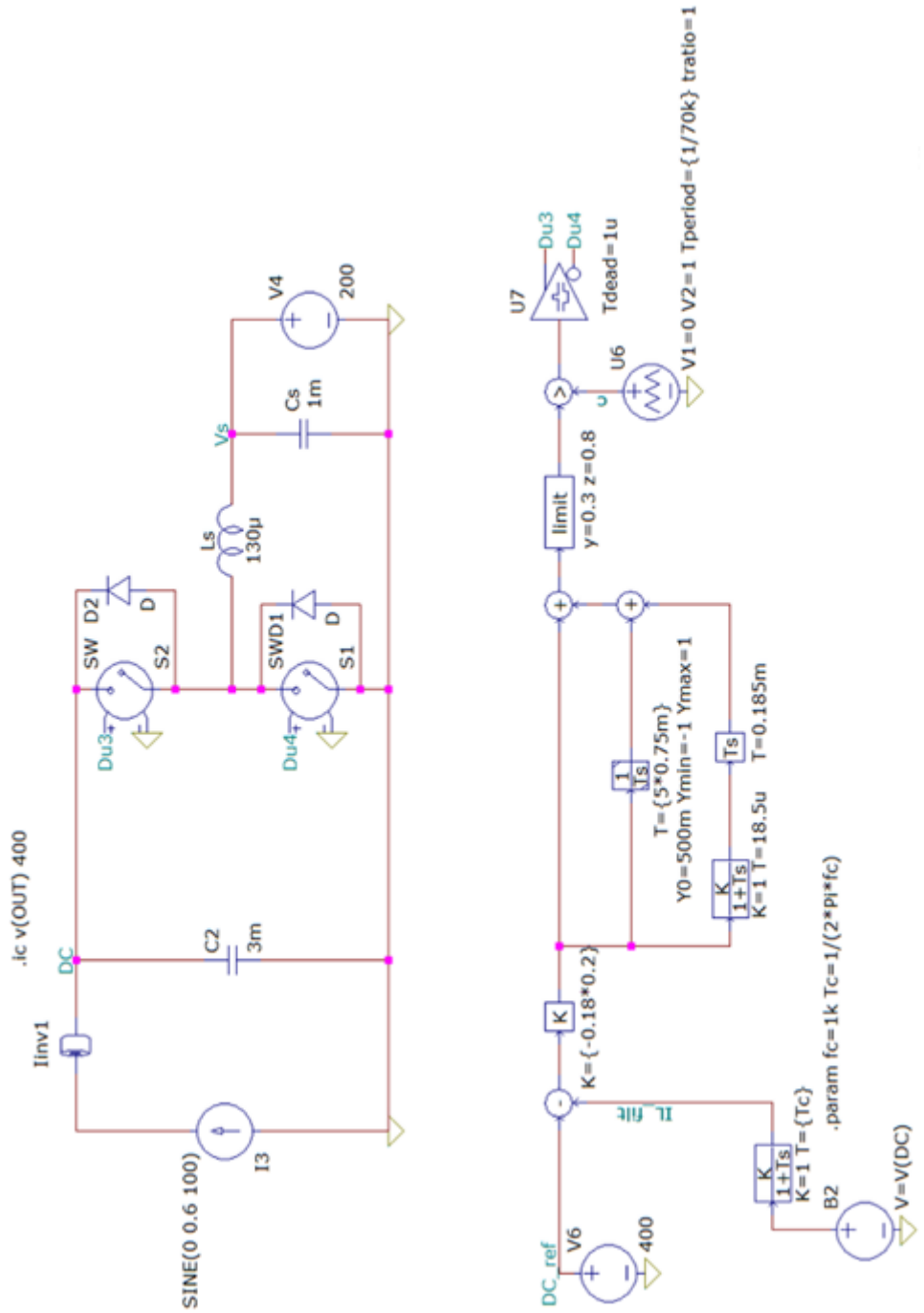

Figure 5. 11. Simulated Bidirectional converter circuit to control the DC voltage.

The result of the simulation is shown in figure 5.12 where one can see the steady state voltage in V_{DC} and the correct tracing of the reference at 400V (panel C). Also, the V_s voltage and I_{Ls} inductor current are shown (panels A and B) which charge and discharge the storage capacitor C_s and inductor L_s according to the voltage oscillation in V_{DC}.

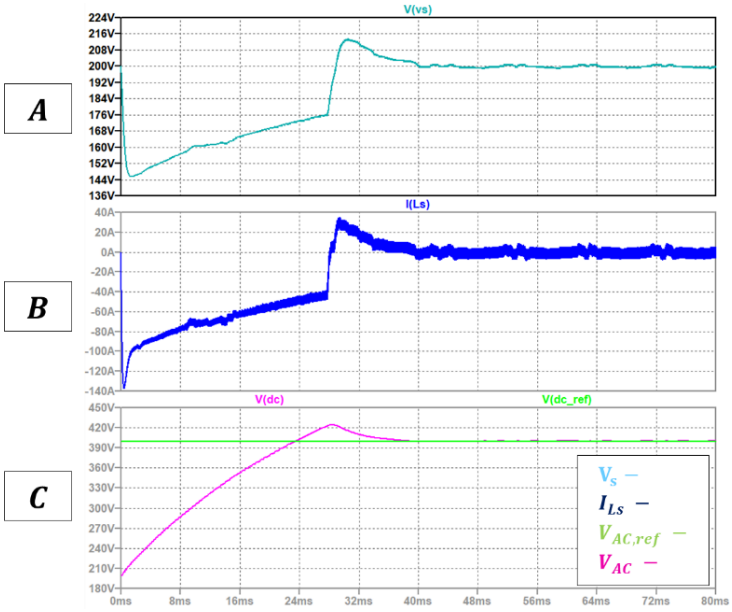

Figure 5. 12. Controlling the DC voltage in bidirectional DC-DC converter.

Moreover, changes in the input current (the current coming from the inverter) were add since the DC capacitor is shared with the inverter and any change in the inverter input current will affect to the bidirectional converter current.

The system was simulated under input current steps (panel A) of 200ms with rise and fall time of 20ms. The results are shown in figure 5.13 where the voltage in DC capacitor (panel D) is the stable even with these input steps.

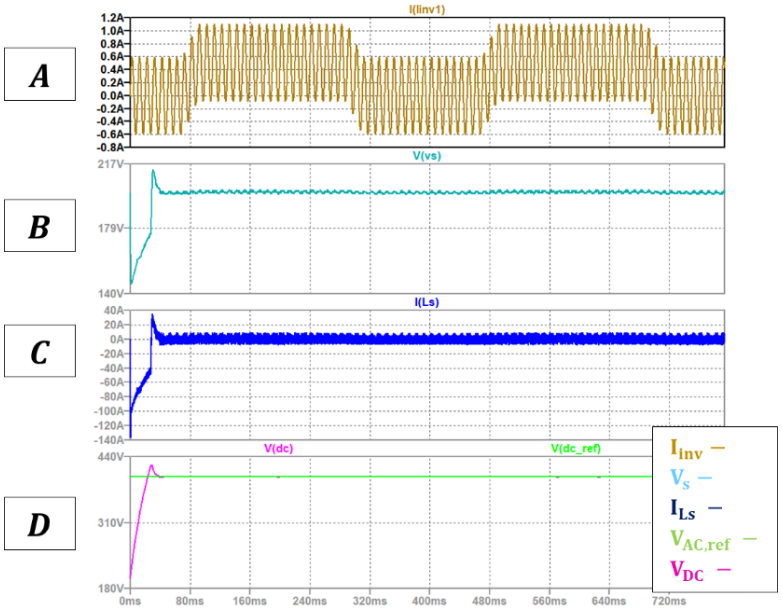

Figure 5. 13. Input current changes. Bidirectional DC-DC converter.

In addition, to test a future MPPT algorithm, the converter was simulated under several voltage references. The C_{DC} capacitor is shared with the inverter, so if the voltage reference change because the MPP change, then this new reference must to be also follow for the voltage loop of the bidirectional converter. A simulation for steps of references was done and it is shown in figure 5.14.

On the other hand, the system was tested for different voltage references. Step of the references were added for the same input and output; The steps from 380 to 420 have a ON time of 100ms and rise/fall time of 20ms. The result of this simulation can be seen in figure 5.14 (panel D). Where the inductor current (panel D) and V_s voltage increase or decrease with the opposite direction of the steps. This is to say, when the reference is increase the energy come from the battery and inductor to keep stable the DC voltage and vice versa.

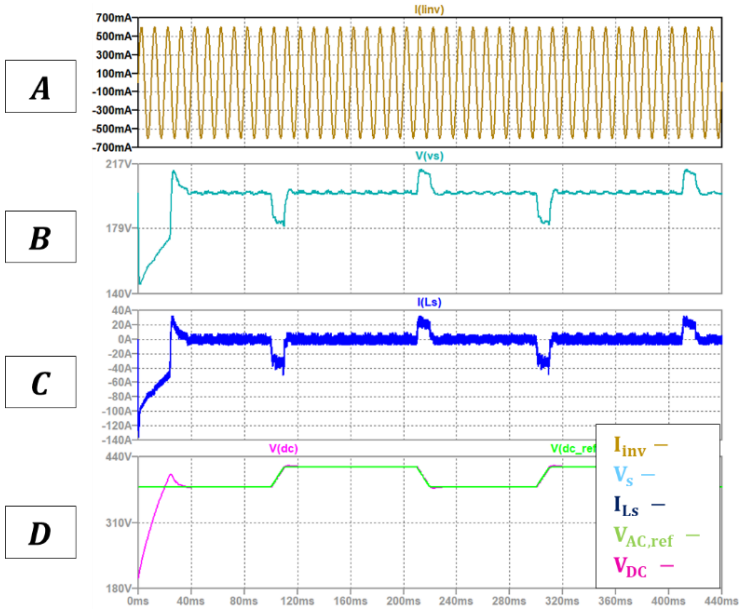

Figure 5. 14. Reference changes. Bidirectional converter voltage control.

5.3.2. Inductor current control. Bidirectional converter.

The control strategies proposed at the end of the of the chapter 4 were based in a final loop where the current through the inductor was controlled.

To test this loop before to add external controller or references which come from the inverter, the bidirectional converter was simulated when the inductor current control is controlled with a PID regulator. The simulated circuit is shown in figure 5.15 where it can be seen the inductor current is sensed with a voltage probe due to LTspice way.

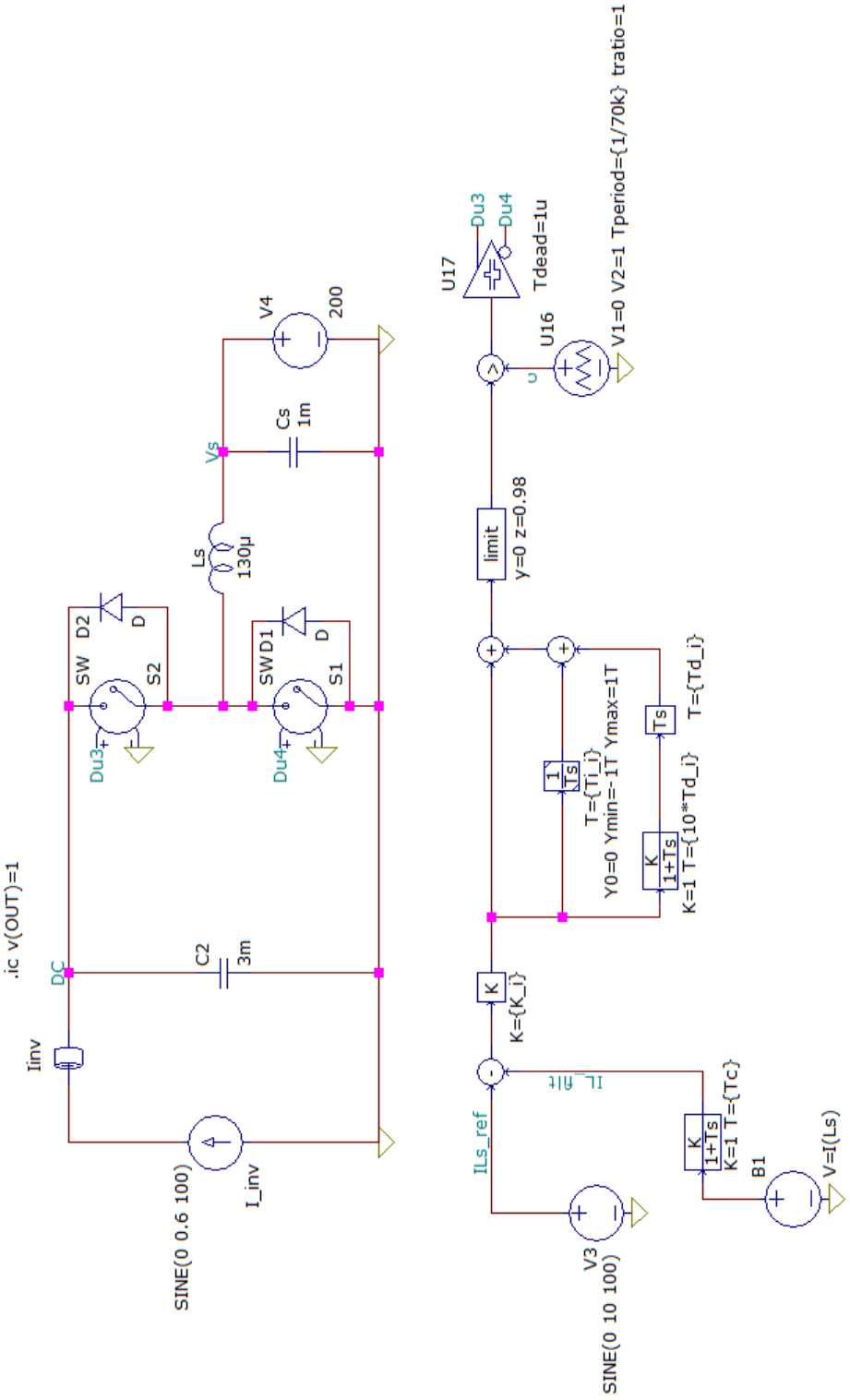

Figure 5. 15. Simulated bidirectional converter circuit for inductor current control.

In figure 5.15 it can be seen the correct behaviour of the current loop where this follow the sinusoidal reference, this have voltage units because of the probe used. In addiction in this figure the both conduction direction of the inductor can be checked since this go from -10A to 10A. The current from the inverter, the voltage V_S and the voltage V_{DC} are also shown in the panels A, B and D respectively.

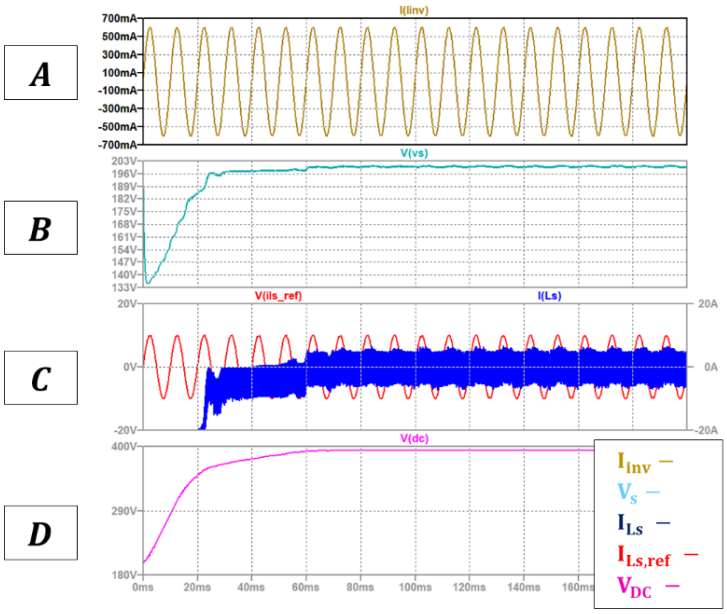

Figure 5. 16. Inductor current control of the bidirectional converter.

After that, steps of input current (panel A) were added like changed in the inverter current (solar voltage, load of the inverter, ect.). The robustness of the controller and the stability can be checked in figure 5.17 panel C. As the DC Capacitor is not controlled in this mode, its average voltage changes with the average current steps (panel D). The amplitude of the voltage V_S increase or decrease according to the average input current in order to keep stable the inductor current (panel B).

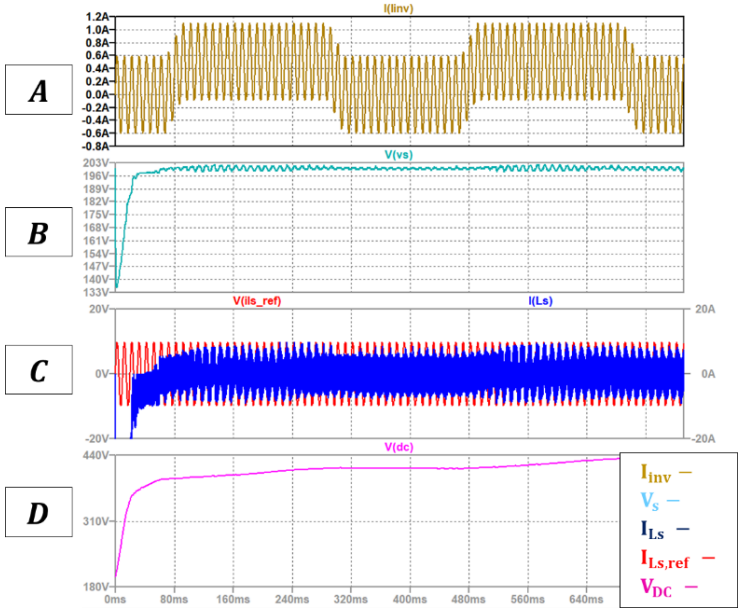

Figure 5. 17. Input current step in the bidirectional converter with inductor current control.

As well as step in the current reference to test the different references which will come from the equation 4.114. The result of the control loops for different references is shown in figure 5.18 were the loop follow correctly each current.

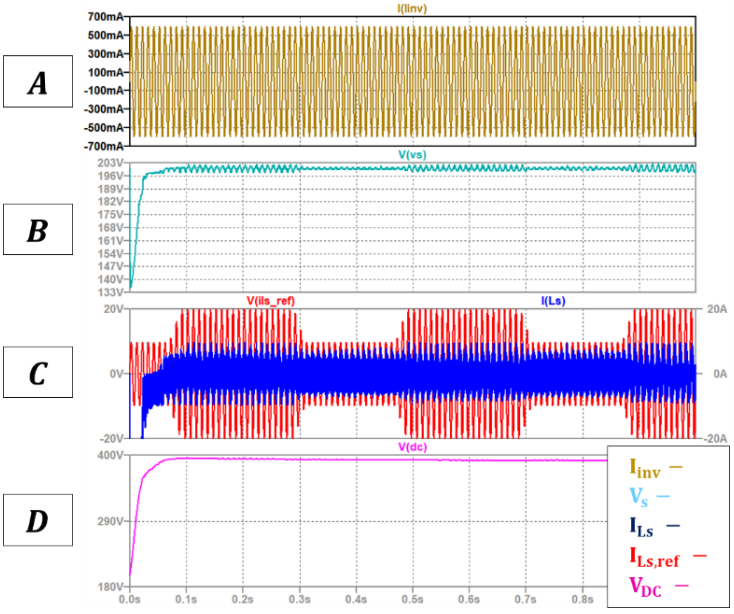

Figure 5. 18. Current reference changes in the bidirectional converter with inductor current control.

5.4. Single phase inverter with DC-DC bidirectional converter.

The inverter was simulated together with the bidirectional DC-DC converter to check the mitigation of the ripple in the DC capacitor. This is the both previous power stages together, the whole system.

Firstly, the system was tested when the inverter control loop keeps stable the AC voltage and the bidirectional converter control the DC voltage.

Secondly a different control strategy was simulated. When the inverter controls the DC voltage and the bidirectional converter controls its inductor current. Thus, according to the current reference the system was simulated for the control loops introduced in sections 4.4 of chapter 4.

5.4.1. DC voltage control.

When the inverter controls the output AC voltage, the bidirectional converter controls the input DC voltage. The bidirectional convert can stabilize the DC voltage as figure 5.20 shows. Where the V_{DC} is the voltage in the DC link capacitor and the V_S is the voltage in the storage capacitor and battery as the circuit on figure 5.19 shows. Because of the simulation time and switching components noise the full system was simulated in the equivalent average model.

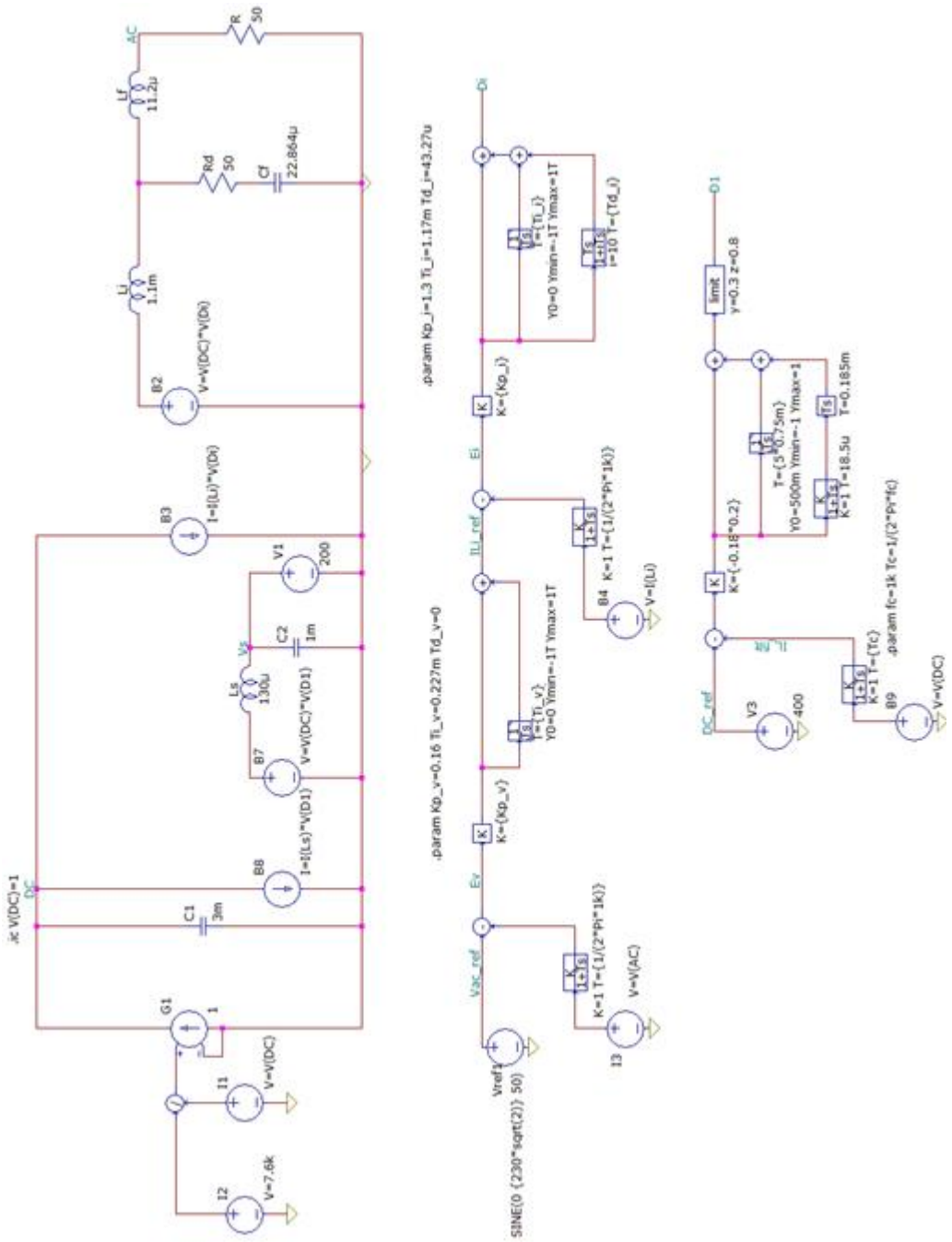

Figure 5. 19. Inverter with bidirectional converter for DC voltage control.

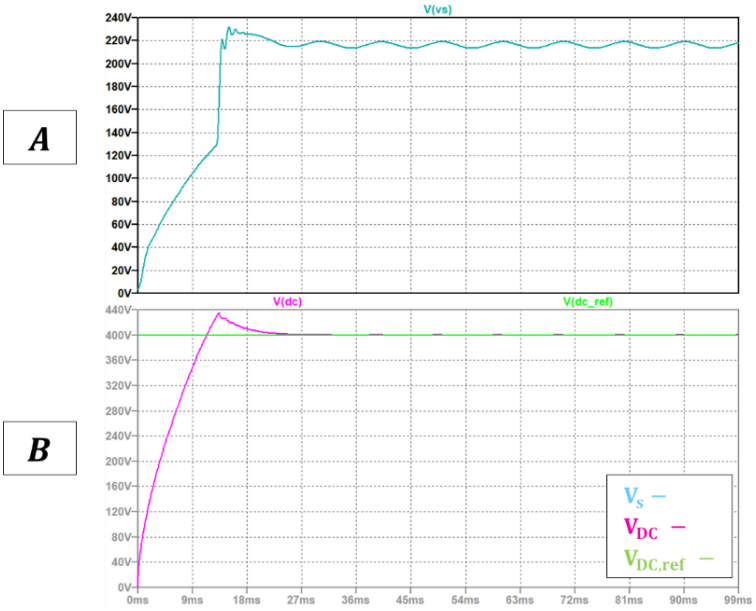

Figure 5. 20. Vs voltage versus DC voltage.

The DC link voltage is keep stable at 400V while the bidirectional converter reduces the ripple on this storing the energy in the C_S capacitor.

In figure 5.21 panel B, the C_{DC} capacitor has a ripple of $\Delta V_{DC} = 350mV$ whereas in the panel A, the C_S has a ripple of $\Delta V_S = 5V$ when the average value is settled at 200V. This mean that adding the DC-DC converter the voltage ripple in the DC link is reduced from $20V$ to $350mV$. That means that the ripple in the DC link decrease from 5% as it was initial designed to 0.08% when we add the bidirectional DC-DC converter. The following figure show the waveform of V_{DC} and V_S voltages.

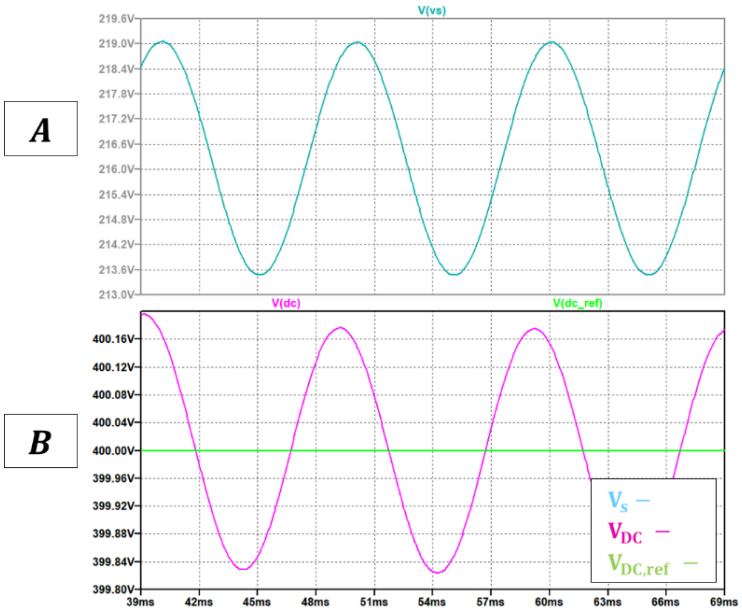

Figure 5. 21. Voltage ripple in DC link with bidirectional converter.

The current through the inductor increase when the DC voltage is higher than the average value, 400V. In this semi-period the inductor is charged with the over voltage and the bidirectional converter is working as a buck mode. In the next semi-period the inductor discharges its power in the C_S capacitor and this capacitor raises the voltage in

the DC side, thus the bidirectional converter work as a boost mode. The waveforms of the V_{AC}, I_{Ls}, V_S and V_{DC} can be seen in figure 5.22.

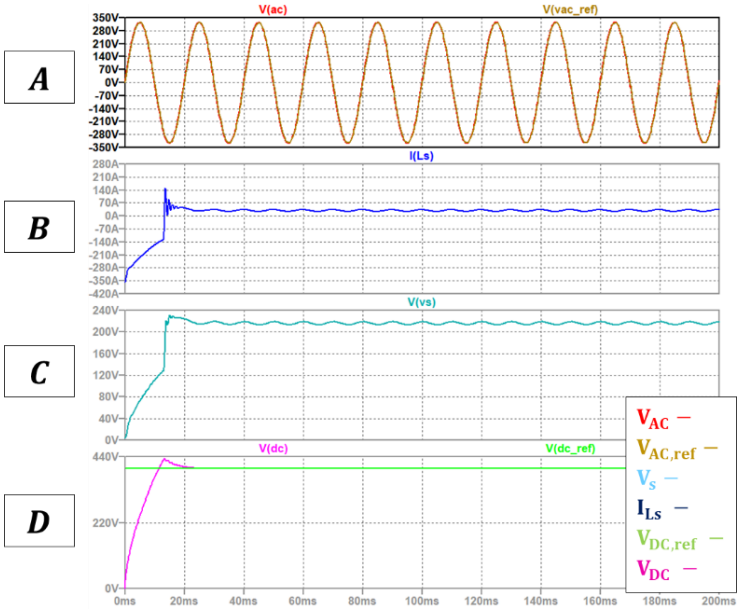

Figure 5. 22. V_{DC}, V_S and I_{Ls} waveforms of the inverter with the bidirectional converter.

5.4.2. Power flow control.

The inductor current was controlled in the bidirectional converter were the reference of the loop was the current which coming from the powers balance equation 4.103. Figure shows the DC link voltage in comparation with the Vs voltage.

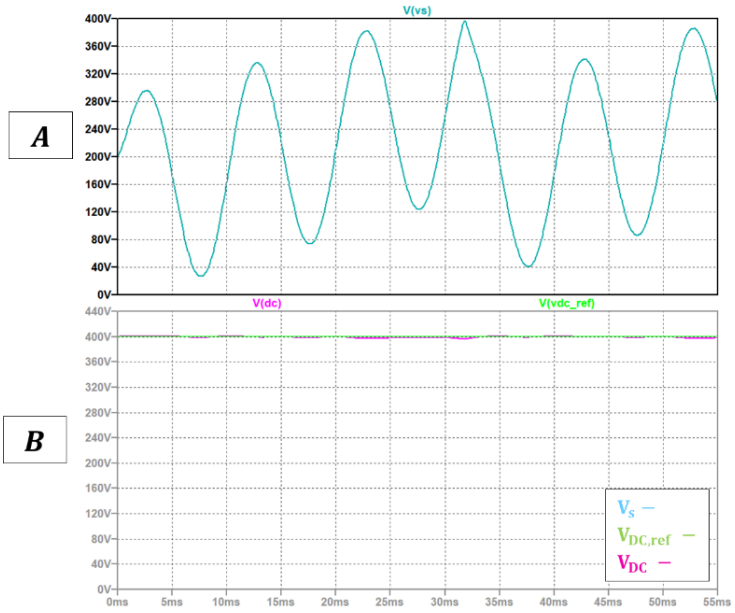

Figure 5. 23. System simulation for power flux control strategy.

Although the system has a tiny oscillation it can be considered stable. The ripple in the DC link voltage can be checked in figure 5.24.

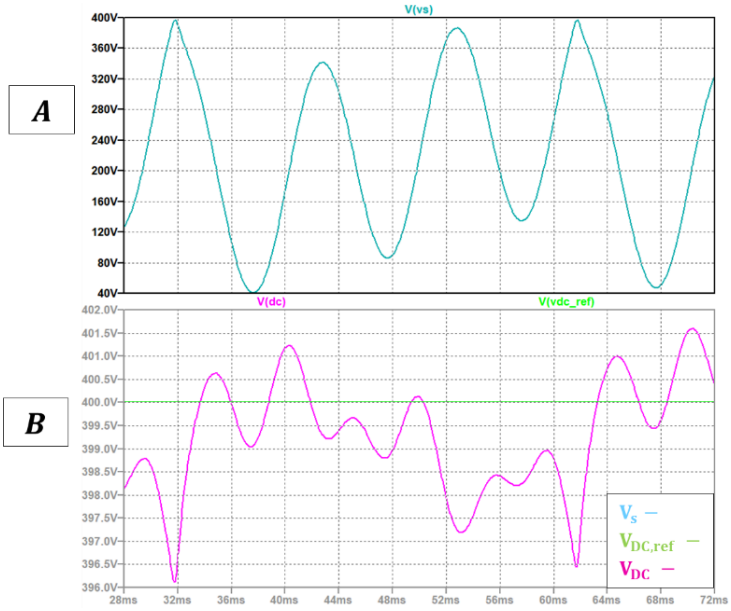

Figure 5. 24. DC link voltage ripple for power flux control strategy

From figure 5.24 the ripple in the DC link is $\Delta V_{DC} = 760mV$ this means that the ripple is now 0.19% instead 5% without bidirectional converter.

5.5. Output spectrums analysis.

An analysis of the spectrum was done in order to see the main harmonics. The performance of the LCL output filter is also checked and its performance.

When the inverter is connected to the grid, a LISN is needed to decouple the grid signal. A LISN is a device placed between the element under test and a power source, this introduce a known impedance and to provide a radio frequency noise measurement port. The equivalent model of the LISN as found in reference [40] and is presented in figure 5.25

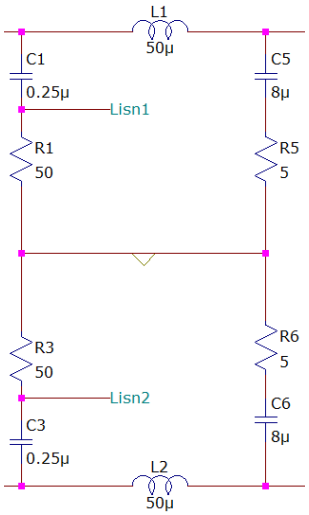

Figure 5. 25. LISN equivalent model from [29].

The LISN circuit mode can be also used to measure the EMI (electromagnetic interference) however, EMI are not studied in this thesis.

5.5.1. Standalone inverter with resistive load.

The spectrum of the output current when the inverter is working in standalone mode with a resistive load is shown in figure 5.27. The main harmonic is at the fundamental frequency, 50Hz and the first order harmonic due to the switching frequency, at 70KHz the magnitude of this harmonic is 19dB.

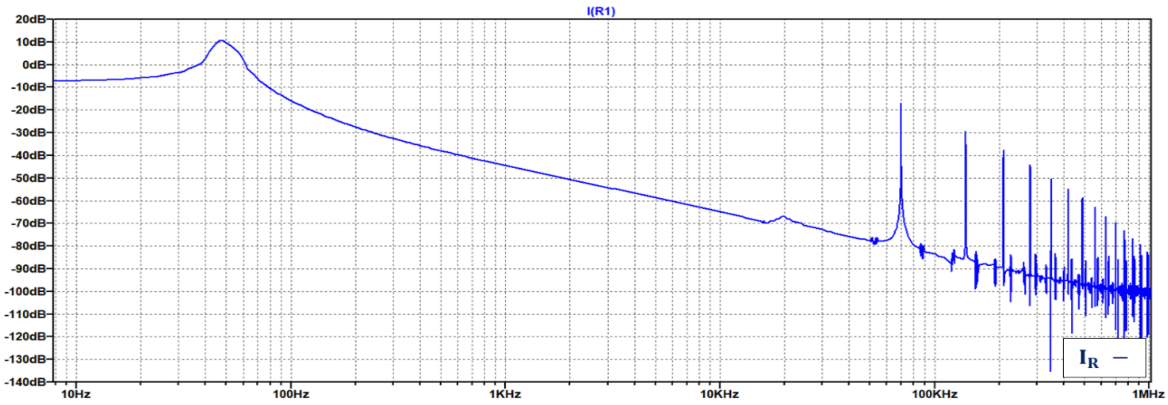

Figure 5. 26. Output current spectrum for resistive load.

5.5.2. Grid connected inverter.

When the inverter is connected to the grid, this inject a current which has a spectrum as the one shown in figure 5.27. This has a magnitude of -6 dB in the first order harmonic and -28 dB in the second order harmonic. So, one can predict that the filter work correctly.

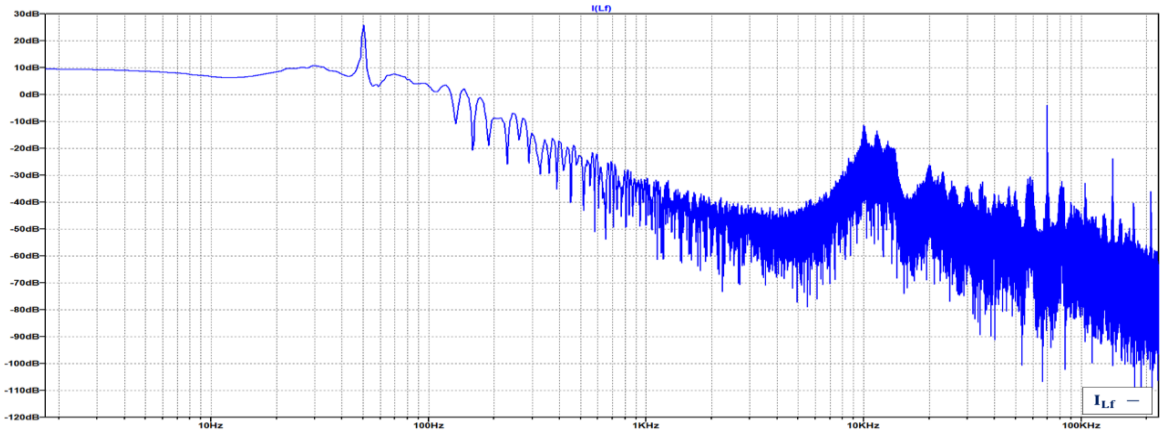

Figure 5. 27.Output current spectrum when the inverter is connected to the grid.

Note that any component before to the 70KHz, may be introduced by the LISN and they are not considered.

5.6. Summarize.

Although two control strategies are introduced to mitigate the voltage ripple in the DC link capacitor, the DC voltage control method offers more stability and robustness. In addition, this method reduces the voltage ripple until 0.08% despite the control flow strategy which reduces until 0.19%.

In future work the DC control strategy will be used to develop the circuit until the experimental phase. Where only three sensors are needed, this fact decrease the price and the complex of the circuit.

Chapter 6.

Conclusion and Future Work.

Chapter 6. Conclusion and Future Work

6.1. Introduction.

A work done need a conclusion which gives an overall picture of the work and results achieved. As well as, the future work points which allow to the future reader to improve the research in this area.

This chapter is organised in two sections, section 6.2 gives a final conclusion of the results of this thesis and section 6.3 collects the future research lines.

6.2. Conclusion.

In this work, a single-phase inverter for photovoltaic application is studied, this inverter works together with a bidirectional buck and boost converter which is controlled to store the voltage ripple present in the DC link capacitor. The ripple storage system is used to make the DC bus power more stable and with less ripple.

By designing this bidirectional converter as the third leg of an inverter it is possible reduce the DC link capacitor and extend the life of the device. The pulsating power is store in the inductor and capacitor of the DC-DC converter instead of in a large and undesirable electrolytic capacitor. Because of the control of both power stages affect the performance of the full system the thesis is focused in the control strategy.

To feed the load and also to inject energy in the grid an inverter was design where a DC link capacitor was first dimensions by the traditional method. The inverter was modelled in its average model and small signal model in order to find the transfer functions. The transfer functions were validated by using the simulation software LTspice. After that two possible control strategies were studied, both of then based in an inner output current loop plus an outer voltage loop which was developed for the output voltage although the loop for input voltage was also introduced. A PI and PID controller were designed used the IMC method.

In addition, since the output current and voltage of the inverter is not a pure sine, a LCL low pass filter was designed. The behaviour of the filter was tested with the analysis of the output spectrums. When the inverter is connected to the grid a LISN have to be used to decouple the grid signal, so a spice model of this device was found.

The bidirectional converter was analysed in steady state and then its transfer functions were developed using the space state technique. The transfer functions were also validated with simulations. The control strategy proposed to store the ripple coming from the inverter was based on the goal to keep the DC link voltage stable and without ripple. Furthermore, an alternative control strategy based in the current through the inductor was also introduced and tested with simulations.

Finally, the full system was simulated under different variations in order to validate all the operations point.

The simulations of the full system shown that it is possible choose a smaller capacitor in the DC link by using the bidirectional converter as decoupling circuit, that increase the power density. The DC link capacitor was designed for a voltage ripple of 5% and by using the bidirectional converter controlling the DC link voltage, the voltage ripple in this capacitor is reduced until 0.08%. The control of the DC link voltage by a external circuit does not interfere in the behaviour of the inverter which correctly keep a desirable voltage an current in the AC side.

Adding this DC-DC converter gives the advantage to the inverter to work as a three-phase inverter as well as single-phase inverter.

These two reasons give two important advantages compared with to the conventional inverters.

6.3. Future works.

To extend the reach of this project some points should be covered, these are the follows:

- Using commercial switches and improve their losses by adding snubber circuits. In this way an efficiency study can be done.
- Design a new control strategy which can convert the inverter in a three-phase inverter using the bidirectional DC-DC converter as a third leg.
- Study the harmonic normative regulations and improve the filter based on this.
- Design an EMI filter to minimize the electromagnetic interference.
- Test the system for rectifier mode when the photovoltaic is replace by a battery and the energy flow in the opposite direction.
- Add some advanced control strategies like islanding mode which detect any failure in the grid and change to the standalone mode.
- To build an experimental prototype to validate the effectiveness of the system.

Bibliography.

[1] *"Snapshot of Global Photovoltaic Markets 2017,"* Report from International Energy Agency. 19 April 2017. Retrieved 11 July 2017.

[2] C.L. Trujillo. "*Concepción de controladores reconfigurables para microinversores fotovoltaicos operando como unidades autónomas de generación de energía en microrredes,"* Ph.D. Thesis, Universidad Politécnica de Valencia, Spain, 2011.

[3] S. Kjaer, J. Pedersen, and F. Blaabjerg, "*A review of single-phase grid-connected inverters for photovoltaic modules*," Industry Applications, IEEE Transactions on, vol. 41, no. 5, pp. 1292 – 1306, sept.-oct. 2005.

[4] X. Zong. "*A Single-Phase Grid Connected DC/AC Inverter with Reactive Power Control for Residential PV Application"* M.A. Thesis, University of Toronto, Canada, 2011.

[5] D. Dong, T. Thacker, I. Cvetkovic, R. Burgos, D. Boroyevich, F. Wang, G. Skutt "*Modes of Operation and System-Level Control of Single-Phase Bidirectional PWM Converter for Microgrid Systems,*" in IEEE Transactions on Smart Grid, vol. 3, Issue: 1, March 2012.

[6] D. M. Brod and D. W. Novotny, "*Current control of vsi-pwm inverters,"* Industry Applications, IEEE Transactions on, vol. IA-21, no. 3, pp. 562 –570, may 1985.

[7] T. Kato and K. Miyao, *"Modified hysteresis control with minor loops for singlephase full-bridge inverters,"* in Industry Applications Society Annual Meeting, 1988., Conference Record of the 1988 IEEE, oct 1988, pp. 689 –693 vol.1.

[8] T.-F. Wu, K.-H. Sun, C.-L. Kuo, and C.-H. Chang, *"Predictive current controlled 5-kw single-phase bidirectional inverter with wide inductance variation for dc microgrid applications,"* Power Electronics, IEEE Transactions on, vol. 25, no. 12, pp. 3076 –3084, dec. 2010.

[9] N. Mohan, T. M. Undel and W. P. Robbins. *"Power Electronics: Converters, Applications, and Design,"* U.S.A: Wiley, 2002.

[10] J. M. A. Myrzik and M. Calais, *"String and module integrated inverters for single-phase grid connected photovoltaic systems - a review,"* 2003 IEEE Bologna Power Tech Conference Proceedings, 2003, pp. 8 pp. Vol.2.

[11] P. Shaw. *"Modeling and Control of a Battery Connected Standalone Photovoltaic System,"* M.Sc. Thesis, National Institute of Technology Rourkela, India, 2015.

[12] P. T. KREIN AND R. S. BALOG, *"COST-EFFECTIVE HUNDRED-YEAR LIFE FOR SINGLE-PHASE INVERTERS AND RECTIFIERS IN SOLAR AND LED LIGHTING APPLICATIONS BASED ON MINIMUM CAPACITANCE REQUIREMENTS AND A RIPPLE POWER PORT,"* 2009 TWENTY-FOURTH ANNUAL IEEE APPLIED POWER ELECTRONICS CONFERENCE AND EXPOSITION, WASHINGTON, DC, 2009, PP. 620-625.

[13] A. LAHYANI, P. VENET, G. GRELLET, AND P.-J. VIVERGE, *"FAILURE PREDICTION OF ELECTROLYTIC CAPACITORS DURING OPERATION OF A SWITCH MODE POWER SUPPLY,"* IEEE TRANS. POWER ELECTRON., VOL. 13, NO. 6, PP. 1199–1206, NOV. 1998.

[14] S. LI, A. T. L. LEE, S. C. TAN AND S. Y. R. HUI, *"PLUG-AND-PLAY VOLTAGE RIPPLE MITIGATOR FOR DC LINKS IN HYBRID AC–DC POWER GRIDS WITH LOCAL BUS-VOLTAGE CONTROL,"* IN IEEE TRANSACTIONS ON INDUSTRIAL ELECTRONICS, VOL. 65, NO. 1, PP. 687-698, JAN. 2018.

[15] S. FAN, Y. XUE AND K. ZHANG, *"A NOVEL ACTIVE POWER DECOUPLING METHOD FOR SINGLE-PHASE PHOTOVOLTAIC OR ENERGY STORAGE APPLICATIONS,"* 2012 IEEE ENERGY CONVERSION CONGRESS AND EXPOSITION (ECCE), RALEIGH, NC, 2012, PP. 2439-2446.

[16] A. K. ADAPA AND V. JOHN, *"SINGLE PHASE TO THREE PHASE POWER CONVERSION USING REDUCED RATED INVERTERS,"* 2015 IEEE INTERNATIONAL CONFERENCE ON SIGNAL PROCESSING, INFORMATICS, COMMUNICATION AND ENERGY SYSTEMS (SPICES), KOZHIKODE, 2015, PP. 1-6.

[17] L. PAN, AND C. ZHANG, *"AN INTEGRATED MULTIFUNCTIONAL BIDIRECTIONAL AC/DC AND DC/DC CONVERTER FOR ELECTRIC VEHICLES APPLICATIONS,"* ENERGIES, VOL. 9, NO. 7, PP. 493, 2016.

[18] Y. TANG, Z. QIN, F. BLAABJERG AND P. C. LOH, *"A DUAL VOLTAGE CONTROL STRATEGY FOR SINGLE-PHASE PWM CONVERTERS WITH POWER DECOUPLING FUNCTION,"* IN IEEE TRANSACTIONS ON POWER ELECTRONICS, VOL. 30, NO. 12, PP. 7060-7071, DEC. 2015.

[19] A. F. RESTREPO, C. A. RAMOS-PAJA AND E. FRANCO, *"POWER CONTROL OF A BIDIRECTIONAL DC BUS FOR FUEL CELLS APPLICATIONS,"* REVISTA EIA, ISSN 1794-1237 N. 18, P. 159-170. DEC. 2012.

[20] M. BHARDWAJ, *"MODELING BI-DIRECTIONAL BUCK/BOOST CONVERTER FOR DIGITAL CONTROL USING C2000 MICROCONTROLLERS".* TEXAS INSTRUMENTS. JANUARY 2015.

[21] L. SOLERO, A. LIDOZZI, J.A. POMILIO, "*DESIGN OF MULTIPLE-INPUT POWER CONVERTER FOR HYBRID VEHICLES".* IEEE TRANS ON POWER ELECTRONICS, VOL. 20 NO. 5, PP. 1007-1016, SEP 2005.

[22] M. LISERRE, F. BLAABJERG AND S. HANSEN, *"DESIGN AND CONTROL OF AN LCL-FILTER-BASED THREE-PHASE ACTIVE RECTIFIER,"* IN IEEE TRANSACTIONS ON INDUSTRY APPLICATIONS, VOL. 41, NO. 5, PP. 1281-1291, SEPT.-OCT. 2005.

[23] FLORIDA SOLAR ENERGY CENTER. *"HOW A SOLAR CELLS WORK."* INTERNET: http://www.fsec.ucf.edu/en/consumer/solar_electricity/basics/how_pv_cells_work.htm, [DEC. 7, 2017].

[24] K. ZIPP. *"WHAT ARE THE COMPONENTS OF A SOLAR ENERGY STORAGE SYSTEM?"* INTERNET: https://www.solarpowerworldonline.com/2017/08/components-solar-energy-storage-system/, AUG. 13, 2017 [DEC. 7, 2017].

[25] JIAWEI EUROPE, "JW-S100" DATA SHEET [REVISED DEC. 7, 2017].

[26] M. GRADELLA, E. RUPPERT. *"DYNAMIC ANALYSIS OF THE INPUT-CONTROLLED BUCK CONVERTER FED BY A PHOTOVOLTAIC ARRAY."* UNIVERSITY OF CAMPINAS (UNICAMP). BRAZIL.

[27] E. BRACO. *"DESIGN AND SIMULATION OF A SINGLE-PHASE INVERTER WITH DIGITAL PWM,"* BACHELOR FINAL THESIS. UNIVERSITY OF APPLIED SCIENCES – HOCHSCHULE NIEDERRHEIN, GERMANY, JULY, 2016.

[28] J. ZHANG. *"BIDIRECTIONAL DC-DC POWER CONVERTER DESIGN OPTIMIZATION, MODELING AND CONTROL,"* PHD THESIS. VIRGINIA POLYTECHNIC INSTITUTE, U.S.A, JAN. 30, 2008.

[29] E. ROGERS. *"UNDERSTANDING BOOST POWER STAGES IN SWITCH MODE POWER SUPPLIES,"* APPLICATION REPORT. TEXAS INSTRUMENTS. MARCH 1999.

[30] R. WANG ET AL., *"A HIGH POWER DENSITY SINGLE-PHASE PWM RECTIFIER WITH ACTIVE RIPPLE ENERGY STORAGE,"* IN IEEE TRANSACTIONS ON POWER ELECTRONICS, VOL. 26, NO. 5, PP. 1430-1443, MAY 2011.

[31] F. RENKEN, *"THE DC-LINK CAPACITOR CURRENT IN PULSED SINGLE-PHASE H-BRIDGE INVERTERS,"* 2005 EUROPEAN CONFERENCE ON POWER ELECTRONICS AND APPLICATIONS, DRESDEN, 2005, PP. 10 PP.-P.10.

[32] E. ROGERS. *UNDERSTANDING BUCK POWER STAGES IN SWITCH MODE POWER SUPPLIES*. APPLICATION REPORT. TEXAS INSTRUMENTS. MARCH 1999.

[33] M. E. ORTÚZAR, *"DISEÑO Y CONSTRUCCIÓN DE CONVERSOR DC-DC PARA CONTROL DE ULTRACAPACITORES EN VEHÍCULO ELÉCTRICO,"* BACHELOR FINAL THESIS. PONTIFICIA UNIVERSIDAD CATOLICA DE CHILE, CHILE, 2002.

[34] S. BUSO AND P. MATTAVELLI, *"DIGITAL CONTROL IN POWER ELECTRONICS."* USA: MORGAN & CLAYPOOL, 2006.

[35] D. E. SEBORG, T. F. EDGAR, D. A. MELLICHAMP AND F. J. DOYLE, "*PROCESS DYNAMICS AND CONTROL."* HOBOKEN, N.J: WILEY, 2011.

[36] C. ZHOU, M. M. JOVANOVIC, *"DESIGN TRADE-OFFS IN CONTINUOUS CURRENT-MODE CONTROLLED BOOST POWER-FACTOR-CORRECTION CIRCUITS, PROCEEDINGS OF THE HIGH-FREQUENCY POWER CONVERSION CONFERENCE."* DELTA POWER ELECTRONIC LAB.

[37] D. DONG, T. THACKER, R. BURGOS, D. BOROYEVICH, F. WANG, AND B. GIEWONT, *"CONTROL DESIGN AND EXPERIMENTAL OF A MULTI-FUNCTION SINGLE-PHASE BIDIRECTIONAL PWM CONVERTER FOR RENEWABLE ENERGY SYSTEMS,"* IN PROC. 2009 EUR. CONF. POWER ELECTRON. APPL.

[38] S.-K. KIM, J.-H. JEON, C.-H. CHO, J.-B. AHN, AND S.-H. KWON. *"DYNAMIC MODELING AND CONTROL OF A GRID-CONNECTED HYBRID GENERATION SYSTEM WITH VERSATILE POWER TRANSFER".* IEEE TRANS. IND. ELECTRON. APR. 2008.

[39] R. ERICKSON. *"FUNDAMENTALS OF POWER ELECTRONICS."* U.S.A, KLUWER ACADEMIC PUBLISHERS, 2004.

[40] P. SMEETS. *SENTRIX DIFFERENTIAL MODE EMI SIMULATION.* INTERNET: http://www.zeonpowertec.com/Blog/files/a701c0c4f80d39b22568c3286d9761b4-6.html DEC. 28, 2014 [11/29/2017].